THE COMPOSITE RESPONSE ASSESSMENT OF THE STEEL BEAM-FRP DECK SYSTEM IN THE BOYER BRIDGE

by

Yupeng Luo

BE, Hubei Polytechnic University, 1999

Submitted to the Graduate Faculty of

the School of Engineering in partial fulfillment

of the requirements for the degree of

Master of Science in Civil Engineering

University of Pittsburgh

2003

UNIVERSITY OF PITTSBURGH

SCHOOL OF ENGINEERING

This thesis was presented

by

Yupeng Luo

It was defended on

December 20, 2002

and approved by

Dr. John F. Oyler, Adjunct Associate Professor,
Department of Civil and Environmental Engineering

Dr. Morteza A.M. Torkamani, Associate Professor,
Department of Civil and Environmental Engineering

Thesis Advisor: Dr. Christopher J. Earls, Associate Professor,
Department of Civil and Environmental Engineering

ABSTRACT

THE COMPOSITE RESPONSE ASSESSMENT OF THE STEEL BEAM-FRP DECK SYSTEM IN THE BOYER BRIDGE

Yupeng Luo, M.S.

University of Pittsburgh, 2002

Fiber Reinforced Polymer (FRP) composites have been considered as good alternatives for the repair and rehabilitation of damaged or deteriorating structures (e.g. highway bridges) recently. The present study reports on the field study of a steel beam-FRP deck composite bridge in Pennsylvania. The objective of the study is to assess the composite action between the steel beam-FRP deck system by evaluating the neutral axis location, the effective compression flange width and the distribution factors at service load conditions.

The research results reported herein support the notion of employing a design approach, for both interior and exterior beams of a composite floor system, which is consistent with current practice related to steel beams acting compositely with concrete decking. It appears from the results presented herein that FRP decks and floors acting compositely with underlying steel beams exhibit an effective width approaching 75% of the actual beam spacing "s" for interior beams, and 90% of the total distance, made up of one half the value "s" added to the deck overhang for exterior beams. In addition, the live load distribution factors (DFs) obtained from

the field tests show a very good agreement to the expected DFs for the case of steel beams with concrete decking.

DESCRIPTORS

Distribution Factors

FRP Deck

Effective Width

Neutral Axis Location

ACKNOWLEDGEMENTS

First I would like to thank my advisor, Dr. Christopher J. Earls, for his support, patience and invaluable guidance throughout my graduate studies. I also appreciate my committee members Dr. Morteza A.M. Torkamani and Dr. John F. Oyler for their feedback and suggestions.

Special thanks are due to Wahyu Yulismana and Chris Keelor for providing their priceless assistance in conducting the field tests on the Boyer Bridge.

I would also like to thank all of my officemates in 1121, both past and present, for their valuable friendship and support, as well as great help on my graduate study and thesis.

Finally, I want to express my deep gratitude to my family for their encouragement throughout the hard years away from home. This thesis is dedicated to them.

TABLE OF CONTENTS

LIST OF TABLES

LIST OF FIGURES

NOMENCLATURE

A	=	area of stringer, beam or girder (IN^2), truck location
B	=	truck location
B_E	=	the service load effective compression flange width (MM)
b	=	dimension, beam width (MM)
C	=	truck location
c	=	distance from the neutral axis of the composite cross section to the top of the bottom flange of beam (IN)
DF	=	distribution factor
h	=	dimension, depth of beam
E	=	modulus of elasticity (KSI, MPa)
E_B	=	modulus of elasticity of beam material (KSI)
E_D	=	modulus of elasticity of deck material (KSI)
E_{steel}	=	modulus of steel (MPa)
E_{frp}	=	modulus of FRP (MPa)
e_g	=	distance between the centers of gravity of the basic beam and deck (IN)
I	=	moment of inertia (IN^4)
K_g	=	longitudinal stiffness parameter (IN^4)
L	=	span of beam (FT)
M	=	bending moment (KIP*IN)
N_b	=	number of beams, stringers or girders
S	=	spacing of beams or webs (FT)
s	=	elastic section modulus (IN^3)

t_f = flange thickness (MM)

b_f = flange width (MM)

t_w = web thickness (MM)

t_{top} = thickness of the top facesheet of the FRP bridge deck (MM)

t_{btm} = thickness of the bottom facesheet of the FRP bridge deck (MM)

t_{haunch} = thickness of the haunch between the bridge deck and the steel beam (MM)

Y = distance from bottom of beam to the neutral axis of the cross section (MM)

$\bar{x}$, $\bar{y}$ = coordinates of x and y of the centroids for the composite areas, respectively.

η_1, η_2 = modular ratio

ε = normal strain

σ = normal stress (PSI)

1.0 INTRODUCTION

1.1 FRP Composites

Fiber Reinforced Polymer (FRP) composites have been the materials of choice in the aerospace industry since the 1960s. However, it is only recently that Glass-FRP composites have been gaining in popularity in civil, structural applications. One such popular civil structural application for GFRP is in bridge decking as a result of this material's high strength-to-weight ratio, corrosion resistance, and reduced installation time.

As the name implies, FRP composites are made of fiber reinforcing, surrounded by a polymer matrix (sometimes referred to as resin) that may also contain other bulk materials such as fillers and additives. The reinforcing fibers provide the primary stiffness and strength capacity of the FRP material. The resin affords the reinforcing fibers some degree of protection from mechanical and chemical environmental attack as well as helping to bind and maintain orientation of the fibers, and allow loads to be distributed among many of the individual fibers in the composite. The fillers serve to reduce shrinkage and the additives help to improve not only the mechanical and physical properties of the composites but also workability.

Among several possibilities, the fiber types that are typically used in the construction industry are carbon, glass, and aramid (not very common at present). Carbon fibers are the stiffest (strength exceeds 600ksi), most durable, and also most expensive fibers. However, carbon is a conductive fiber material. If it comes in contact with steel, it may accelerate corrosion of the steel. Glass fibers, which are the focus of the research discussed herein, have both lower strength (typically around 400ksi) and stiffness, but also a lower cost. At this time, one of the

concerns with these fibers is durability. Some research has shown that unprotected glass fibers tend to degrade, especially in hot/wet or highly alkaline environments.

1.2 Pultruded FRP Bridge Decking

FRP bridge decks frequently employ high strength, oriented fibers that are woven, twisted together, or simply placed side-by side in a lower strength polymeric matrix. In most bridge deck applications, FRP usually refers to a class of materials employing E-glass fibers, in either a woven matt, roving, stitched fabric, or a combination configuration. The glass fibers are impregnated with, and bonded together in, an iso-polyester based thermo-set resin matrix. As a result of this combination of composite material elements, the manufacturing technique most frequently employed in most composites bridge decks is pultrusion.

In the pultrusion process, spools of roving, strand, and fabric are pulled through a device that wets and impregnates the fibers with polyester resign so that when the fibers are oriented and subsequently pulled through a mandrel and heated die, the thermo-set matrix is formed, compressed, and hardened as a result of chemical reactions that take place in and around the fibers. The end result is a shaped FRP component that can be made to any length since what comes out of the heated die is a continuous stream of FRP material. A large saw is typically used to cut the FRP elements into discrete member lengths as dictated by a given deck geometry.

Due to the fact that to develop bulk strength properties, FRP tends to rely on the presence of very strong glass fibers bound together within a much weaker polymeric matrix, typical mechanical models predicated on isotropic material response are not directly applicable to FRP bridge deck design. Despite the fact that the fibers present within the pultruded section may be

oriented at various angles with respect to the axis of pultrusion (0, +/-45, 90 degrees most frequently), the FRP components themselves are best analyzed using orthotropic strength models. The orthotropy of the FRP product typically arises out of the geometry of the manufactured component itself. In the case of FRP deck, the deck components are typically pultruded in a honeycombed configuration and thus possess a latent directionality in the internal force resisting system. As a result of this orthotropy, it seems reasonable to assume that the approach to composite beam design using: 1) concrete deck-to-steel beam and 2) concrete filled steel grid deck-to-steel beam configurations are also somewhat applicable to FRP deck-to-steel beam composite flexural applications. In all cases, mechanical transfer of shear forces at the material interfaces is achieved through the application of headed shear studs welded to the steel beam and encased in either the concrete (in the case of the two more traditional applications) or grouted into the stud pockets which are sometime present in FRP bridge deck systems.

1.3 Research Project Overview

The Boyer bridge over the slippery rock creek in PennDOT Engineering District 10-0 has recently received a new FRP deck system as part of an overall bridge replacement project. The bridge employs a honeycombed FRP deck system that is attached to the five underlying steel beams through the use of headed shear studs spaced 610mm on center. Non-shrink grout is injected into stud pockets (or voids), coincident with the location of each stud, so as to create a composite FRP deck-steel beam system.

In support of a program of field monitoring, the Boyer Bridge is instrumented with 30 strain gages and monitored with a portable field data acquisition system. Three field tests were

conducted. The data are studied and used within standard transformed section calculations for the purpose of identifying appropriate effective widths for use with existing American bridge specification provisions related to live load deflections at service conditions (AASHTO 1998).

1.4 Earlier Research

While there are many papers in the literature related to the effective compression flange width present within steel beam – concrete deck composite flexural systems (ASCE 1979), there are currently no references available in the archival literature that relate to the specific case of steel beam – FRP deck composite designs; either at ultimate load or at service load. A single technical report was found that reports on the service load effective compression flange width in concrete filled steel grid deck acting compositely with underlying steel beams in a bridge in West Virginia (Ahmadi 1997). This technical thesis is relevant to the current research effort focusing on FRP decks since both FRP decks and concrete filled steel grid decks are best categorized as orthotropic plates whose strong direction is most frequently oriented normal to the underlying steel beam longitudinal axis.

Ahmadi's (1997) concrete filled grid deck research was carried out using a program of field testing on a bridge in West Virginia that had just received a new half-filled, flush fill, steel grid deck system. The grid deck was attached to the underlying steel beams through the use of headed shear studs that were encased in a haunch. The studs protruded into the plane of the grid deck and were subsequently encased in the concrete used to fill the deck. Ahmadi (1979) reported on: field measured and theoretical extreme fiber strains; field measured and theoretical neutral axis locations; field measured distribution factors; and field measured effective

compression flange widths. Ahmadi observed that at service loads the grid deck acted in a fully composite fashion with the underlying steel beams, and also ascertained that the service load effective compression flange width, for the case of concrete filled steel grid deck acting compositely with steel beams, was very close to the center-to-center spacing of the steel beams. Based on this earlier work, it seems logical to expect a similar result for the case of FRP-steel beam composite designs.

Since the present study employs field testing techniques for the purposes of monitoring neutral axis location in an FRP-steel beam composite bridge, it is necessary to demonstrate adequate interfacial shear transfer is present in the field installation so as to guarantee strain compatibility across the FRP-steel interface. A study of the connection detail employed in the subject bridge of the present study was found in the literature (Moon et al. 2002). Moon et al. (2002) tested the interfacial connection detail for fatigue and strength performance and concluded that the detail provided "approximately 60-70% of the [strength] capacity of a longitudinal connection in a continuous concrete deck" similarly attached (Ollgaard et al. 1971). Moon et al. also concluded that the fatigue performance exhibited by this same connection detail was adequate over the simulated 75 years of wear that the connection was subjected to in the laboratory. Furthermore, the differential interfacial displacements between the steel beam and FRP deck were observed to be extremely small at AASHTO service load levels and the resulting shear stiffness was approximately 140kN/mm (in a configuration with two studs across the flange each having a diameter of 22mm and a height of 150mm).

A series of push-off tests, incorporating the same deck profile used in the current research, were conducted at the University of South Carolina (Turner and Harries 2002) and the University of Delaware (Moon et al. 2002) where it was observed that the shear stiffness of an

individual shear plane was 236kN/mm (in a three stud configuration) and 140KN/mm (in a two stud configuration), respectively; with each stud having a diameter of 22mm and a height of 150mm). Both the Delaware and South Carolina tests employed shear stud sizes that are identical to what is used in the Boyer Bridge; the subject of the present field study. In addition, the shear studs tested at the University of Delaware and the University of South Carolina were welded to beam flanges with a thickness consistent with the flange thickness in the Boyer Bridge (the Boyer Bridge uses the two stud configuration across the flange). It is observed from the foregoing that the shear stiffness values for the FRP-steel interface are consistent with concrete-steel composite connection shear stiffness where metal decking is employed; a study by Jaya and Hossain (1987) measured stiffness values on the order of 50kN/mm in a two stud configuration with a shear stud size and spacing consistent with the earlier referenced FRP tests (Moon et al. 2002, Turner and Harries 2002). Based on this last point, it is concluded that full composite action may be considered at service loads in the FRP-steel composite installation under investigation. As a result, the current experimental testing program, focused on the field measurement of the neutral axis location, provides a sufficient basis to make recommendations on the effective compression flange width present in steel beam-FRP deck composite beam designs at service condition.

1.5 Objective

The objective of the research reported on herein, is to explore the composite action between the steel beam-FRP deck system in terms of the neutral axis location, the effective compression flange width and the distribution factors as obtained from field monitoring during a series of 27 load tests (9 tests per day during the course of three days of testing).

1.6 Organization of Thesis

This thesis begins with a discussion of the details related to the current research program and its supporting theoretical foundation. The test procedure and setup are then subsequently discussed. Test results are then presented along with a discussion of their implications. Particulars related to design recommendations emanating from the work are also presented. The thesis concludes with a discussion and summary of the findings from the research.

2.0 DESCRIPTION OF BRIDGE TESTED

2.1 Overview of the Boyer Bridge

The Boyer Bridge is a short span (12,649mm) simply supported composite structure located on a secondary road in PennDOT Engineering District 10-0. It consists of five galvanized W610x155 Gr.345 beams acting compositely with five FRP deck panels, as shown in Appendix A (Figure A-1). Each panel measures 7,772mm wide and 2,438mm long with the exception of the outer two panels, measuring 7,772mm by 2,540mm and 7,772mm by 2,743mm, respectively.

The bridge is easily closed to traffic and hence is an ideal platform for the testing program outlined herein.

2.2 Description of Deck System

The FRP deck system is a modular, closed-cell, cross-section manufactured by Martin-Marietta Composites (MMC) which goes by the trade name *DuraSpan*^{TM} (see Figure 1).

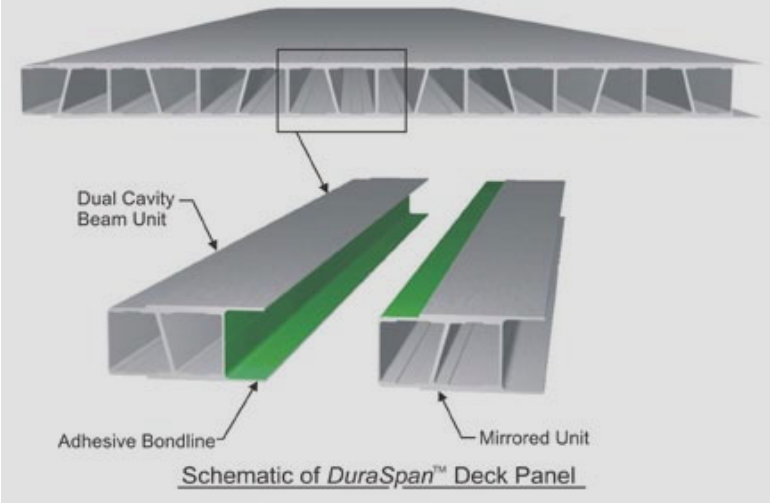

Figure 1 Schematic of DuraSpan^{TM} Deck Panel (MMC)

All MMC decks may utilize composite bending action with the underlying beams using either conventional shear studs (in the case of steel beams) or stirrups (in the case of pre-cast concrete beams). For the case of steel beams and headed shear studs, holes at the desired spacing for the connections are cut into the deck, foam inserts are placed inside the deck tubes to provide a closed cavity. Shear studs are field welded through the deck cut-outs after the deck panels are in place. Non-shrink grout is subsequently poured in the shear stud cavities.

In the case of the construction of the Boyer Bridge, headed shear stud groupings are installed through cut-outs in the FRP deck spaced at 610mm intervals along the longitudinal axis of the bridge. Each grouping consists of two studs welded side-by-side across the top flange

width. Non-shrink grout is then injected into the stud pockets (through the cut-outs) and allowed to flow into the beam haunches so as to fill the haunches and stud pockets, thus creating a composite system. Foam blocks are inserted in the stud pockets to limit the flow of grout out of the stud pockets (see Figure 2). A 102mm crowned layer of bituminous asphalt is placed over the top of the finished deck panels as a wearing surface.

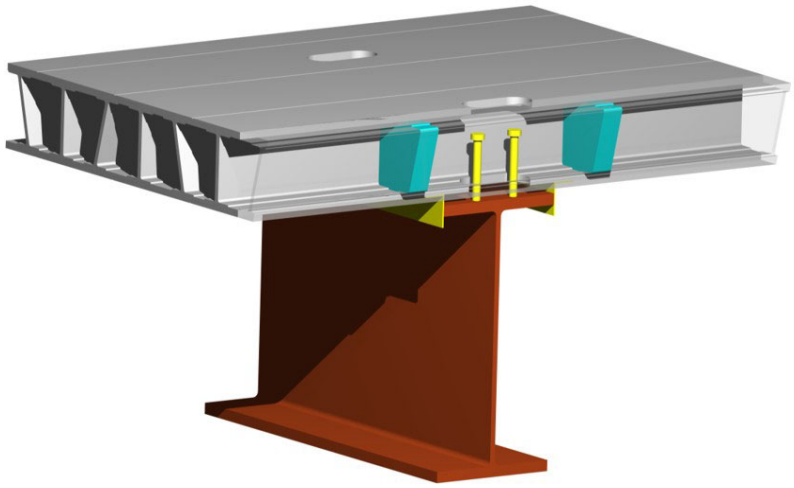

Figure 2 Typical Steel Beams to Deck Connection Detail (MMC)

2.3 Description of Steel Superstructure

The simply supported Boyer Bridge beams are 12,954mm in length and spaced 1,753mm O.C. Each beam rests on sole plates anchored to simple sleeper slab foundations with threaded steel rods. Guardrail posts are bolted to the two fascia beams with W460 steel sections. Diaphragms members, consisting of C310x37 steel sections, are bolted to connector plates, which are in turn welded to the beams. Overall cut-away views of the bridge are presented in Appendix C (Figure C-4 and C-5). Plan and section views of the steel superstructure are also

presented in Appendix A (Figure A-1 and A-2). Each beam is outfitted with light gauge, cold-formed angles welded to the outer tips of the top flange. The angles act as stay-in-place forms for the non-shrink grout haunches that are present between the FRP deck and the steel beams.

2.4 Design Principles

1. Using conservative as-fabricated material properties.
2. AASHTO HS25 design vehicle is considered.
3. A safety factor of 4 or greater against failure is used.
4. All strains at service condition are limited to below 20% of ultimate capacity.
5. Deck is designed to be fully composite and standard transformed section techniques are employed.
6. B_E = S & DF = 0.575 are assumed by Martin-Marietta Composites (MMC), where B_E is the effective width of the composite cross-section and DF refers to the corresponding distribution factor, which is defined as a fraction of wheel load distributed to each beam.
7. Design truck tire patch is taken as 254mm x 508mm.

3.0 LOAD TEST OF THE BOYER BRIDGE

Field testing of the Boyer Bridge over the slippery Rock Creek in PennDOT Engineering District 10-0 consists of a static load applied by a test vehicle to the deck; the response of the five galvanized rolled steel I-shape beams is concurrently monitored.

Three field tests were conducted on the Boyer Bridge. The first occurred on November 13, 2001, the second on February 15, 2002, and the last on March 21, 2002.

3.1 Description of Instrumentation and Data Acquisition System

On Oct. 6th, 2001, thirty, three-wire metal foil strain gages were applied to each of the five galvanized beams through the depth of the wide flange beam cross-sections at the following three installation positions:

1. On the top face of the bottom flange, 130mm from the outside flange tip.
2. On the web, at one half of the cross-sectional depth,
3. On the bottom face of the top flange, 130mm from the outside flange tip.

These installation locations are also shown schematically in Figure 3.

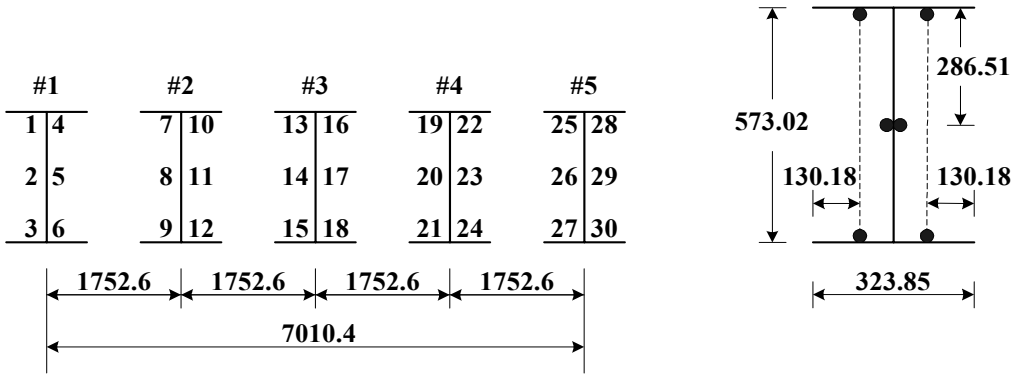

Figure 3 Schematic of Foil Strain Gage Installation Locations (mm)

All instrumented cross-sections are at a longitudinal position that is located 305mm from the mid-span of the bridge (i.e. slightly off-center to avoid a connector plate location). Since this is a multi-month field monitoring study, strain gages are duplicated at each installation position (i.e. two gages are placed at each installation location; one gage on either side of the web) so as to increase the probability that a coherent data set will be obtained despite inevitable instrumentation failures.

The strain gages are monitored with a Campbell Scientific *CR23x Micrologger* (*CR23x*) (see Figure C-11). A laptop computer is connected to the system through a serial connection to retrieve and store field test data.

3.2 Description of Load Testing

3.2.1 Test Vehicle

A tandem axle dump truck loaded with sand, and provided by PennDOT's Butler County Maintenance Garage (see Figure.C-12), is chosen as the test vehicle for each of the load tests performed. Wheel load measurements are obtained at the test site by a mobile weigh team with six portable weigh scales for the tests conducted on November 13, 2001 and February 15, 2002; the weigh team was unavailable for the test carried out on March 21, 2002. Typical rear tandem axle weights are approximately 9091kg each, with a total truck weight of 27,273kg. Tables 1 and 2 provide the loading breakdown by tire for the first two field tests and Table 3 provides the overall weight of the test vehicle used in the March 21, 2002 testing. A photograph of the test vehicle along with vehicle dimensions is presented in Figure C-12.

Table 1 Test Vehicle Axle Loads (Test 1, 11-13-2001)

	Axle 1 (kg)	Axle 2 (kg)	Axle 3 (kg)
Left Side	3,409	4,273	4,136
Right Side	4,273	4,727	4,750
Total	7,682	9,000	8,886

Table 2 Test Vehicle Axle Loads (Test 2, 02-15-2002)

	Axle 1 (kg)	Axle 2 (kg)	Axle 3 (kg)
Left Side	3,409	5,818	5,750
Right Side	3,773	5,386	5,455
Total	7,182	11,204	11,205

Table 3 Test Vehicle Axle Loads (Test 3, 03-21-2002)

	Axle 1 (kg)	Axle 2 (kg)	Axle 3 (kg)
Left Side	-	-	-
Right Side	-	-	-
Total Vehicle	24,155		

3.2.2 Load Positions

Three passes of the truck are made, and correspondingly, load positions A, B and C, are chosen so as to situate the test vehicle over the three interior beams, beams 2, 3 and 4, as shown in Figure 4. In addition, the testing procedure requires the test vehicle's wheelbase centerline to be situated directly over the centerline of these three beams.

Position markings are placed on the bridge's asphalt overlay with chalk lines so as to assist in the positioning of the test vehicle as shown in Figure C-8.

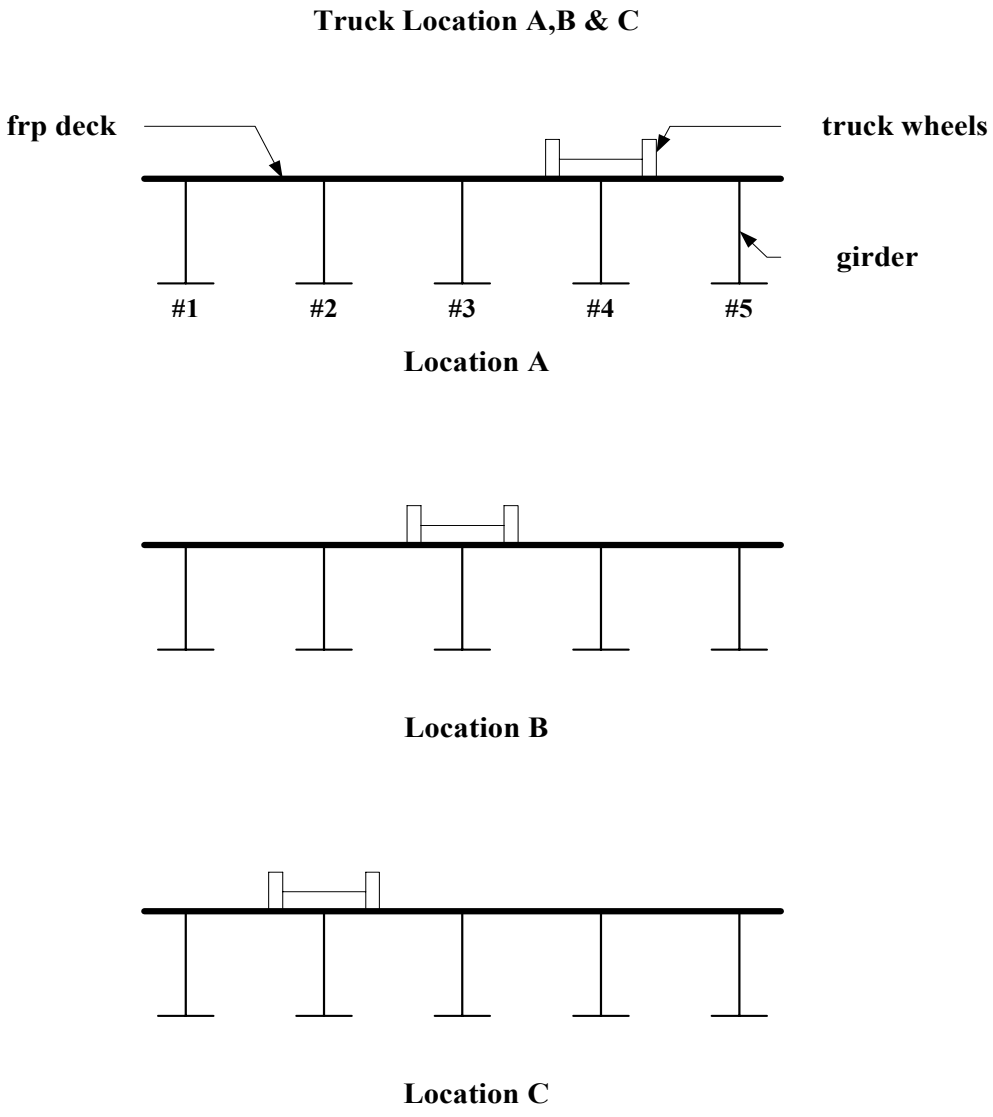

Figure 4 Schematic of the Three Truck Positions Used in the Field Testing

3.2.3 Test Procedure

At the very beginning, an “unstrained” state measurement, which is also called as “the zero measurement”, is performed by using the portable data acquisition system with the test vehicle located off the structure. Following that, the test vehicle is driven forward into position from the forward (eastern) abutment and aligned with the position markings. The vehicle is placed so that the entire tire contact area associated with the front axle is just off the bridge deck and hence bears completely on the adjacent road surface.

Once the truck stops at a required location, the engine is shutdown to reduce electromagnetic interference, the distance between the rear axle and the forward (eastern) abutment is then double checked and the readings from the strain gages are stored automatically on the laptop computer.

Right after the strain measurements, the test vehicle is backed off the bridge, beyond the rear (western) abutment. With the engine shutoff, another set of zero measurements is performed and stored. The same procedure is followed for Positions B and C.

When the test vehicle is backed out of the last position, Position C, the process of testing all three positions is then repeated twice, each time performing a zero measurement between loadings.

The whole procedure is also illustrated in Figure 5.

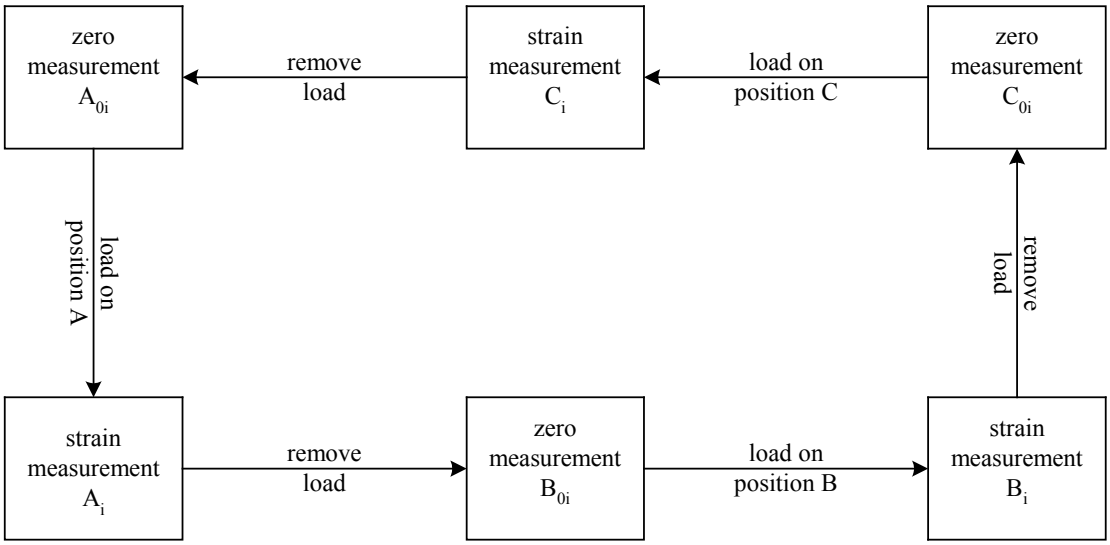

Figure 5 Testing Procedure (i = 1, 2, 3)

4.0 ANALYSIS AND DISCUSSION OF FIELD DATA

4.1 Neutral Axis Location

4.1.1 Theoretical Configurations for Conventional Connections

Composite bending action between the FRP deck and the steel beams is similar to conventional concrete-slab-on-steel-beam connections in which three different cross-sectional strain distributions are possible:

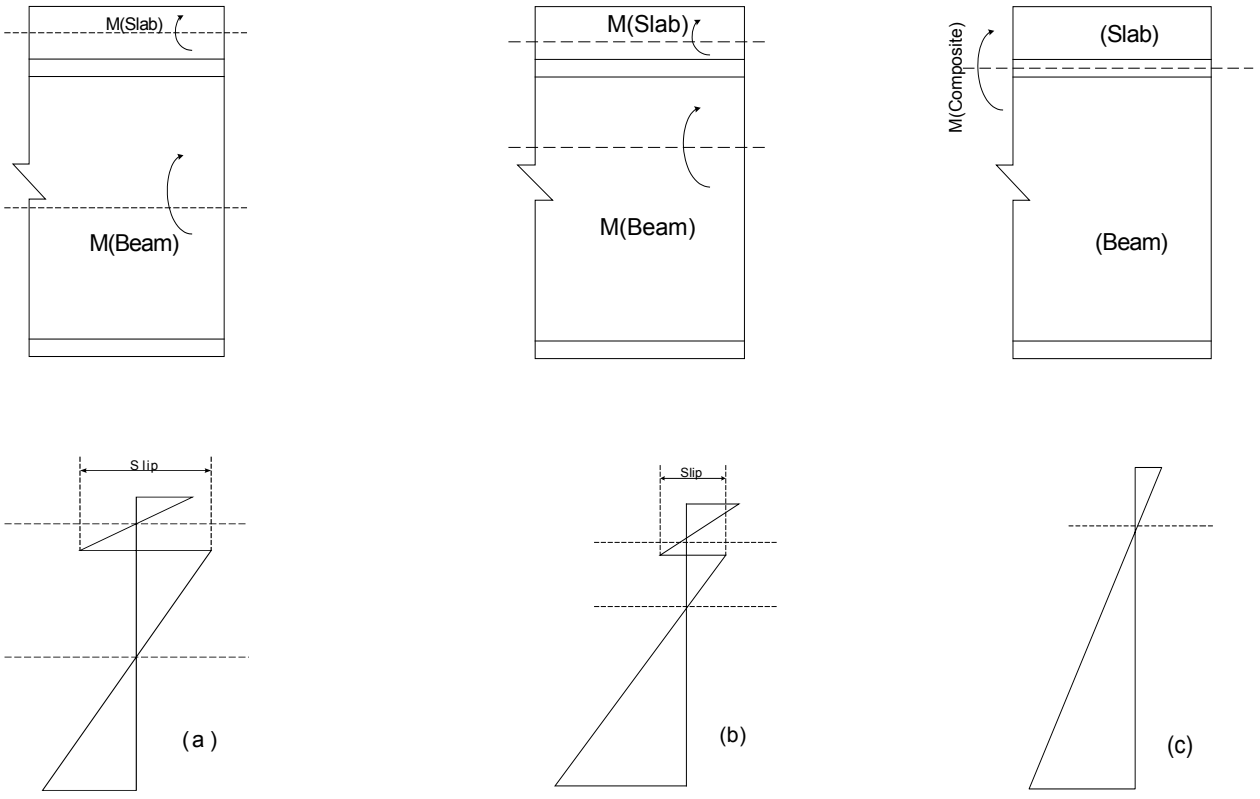

Figure 6 Strain Variation in Composite Beams

a) Slab & beam behave independently from one another. The neutral axis for slab & beam occur at their respective centroids.
b) Slab & Beam are interacting; thus the neutral axes begin to migrate towards one another.
c) Slab & Beam act as one. There is a single neutral axis.

As we can see from Figure 6, the level of compositeness increases from case (a) to (c), and finally reaches 100% for case (c).

4.1.2 Reduction of Field Data

The field data obtained from all 27 load tests is separately analyzed to demonstrate reproducibility and theoretical soundness. Figure 7 illustrates some of the typical **ε–h** plots derived from the field data, where **ε** is the longitudinal strain through the cross-sectional depth **h**. The square of the linear correlation coefficient (R^2) indicates the high degree of linearity of strain as a function of the height of the web. An R^2 =1 indicates perfect linearity; a value < 1.0 indicates a less favorable linearity. Based on these R^2 values, the field data is seen to produce longitudinal strain distributions through the depth with a high degree of linearity as is expected from Navier's plane section hypothesis. This type of analysis is also quite useful for detecting faulty strain gauge installations. Several faulty instruments were identified and ignored in the data collection process associated with the field testing of the Boyer Bridge.

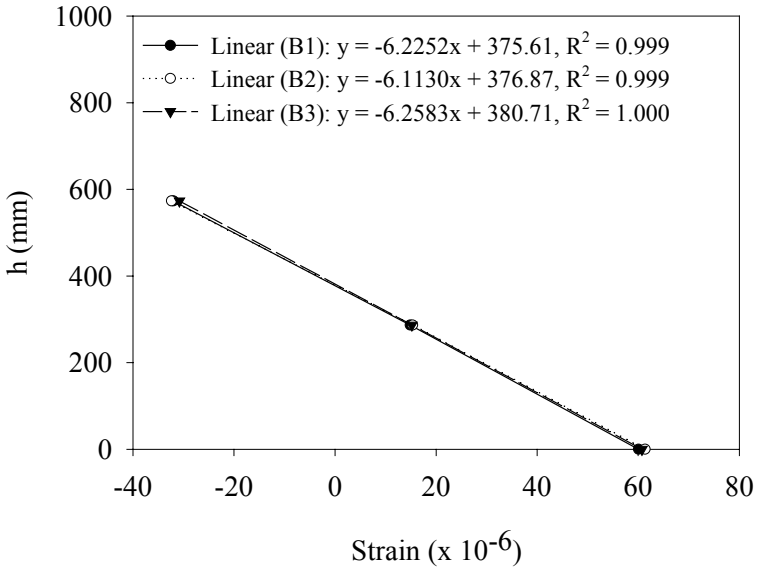

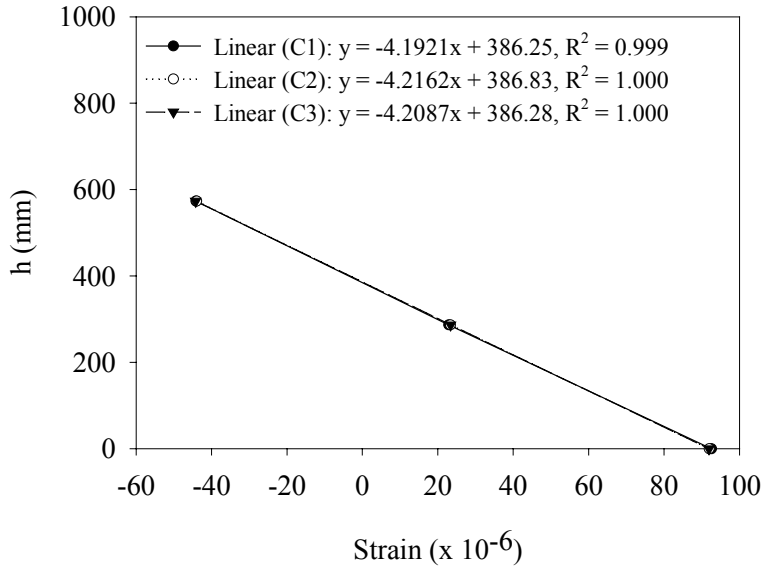

Figure 7 Typical Strain Profiles

4.1.3 Discussion of Results

Measured strains listed in Table D-1 to Table D-39 in Appendix D are used to calculate the location of the neutral axis for the cross section. Most available experimental results reveal a strong linear relationship between longitudinal strain distributions through the cross-sectional depth (see figures in Appendix E). This substantiates the validity of the strain readings obtained during the course of field testing. Table D-40 to Table D-42 present the field measured neutral axis locations for the exterior beams of the Boyer Bridge (broken down by the test designations assigned to each of the three truck positions employed). In addition, Table D-43 to Table D-45 present similar field measured neutral axis locations within the interior beams of the Boyer Bridge (similarly broken down by test designation).

For the five steel beams, the neutral axis is calculated to be an average **356.78** mm above the bottom strain gage, which is placed on the top of the bottom flange of steel beam. This corresponds to an average **216.24** mm below the top strain gage, which is placed on the bottom of the top flange of the steel beam. Since the neutral axis is not in the middle of the beam and the beam is a symmetric section, the FRP deck is assisting the steel beam in resisting applied moments and hence causes a shift in the neutral axis position, relative to the bare steel position.

Based on the upward shift in the measured steel beam neutral axis location it is possible to compute the level of assistance the FRP deck provides in resisting the internal moments needed to equilibrate the truck loadings. Consequently, it is then possible to back calculate the FRP effective compression flange width using standard transformed section properties related to the modular ratio of steel to FRP as well as steel to grout, as is described later.

4.2 Calculation of Effective Width

4.2.1 Assumptions Employed

In applying the field data as the basis for the service load effective compression flange width calculations, standard transformed section methods are employed in conjunction with several approximating assumptions as follows:

Assumption 1:

The analysis for effective width involved theory of elasticity applied to plates, using an infinitely long continuous beam on equidistant supports, with an infinitely wide flange having a small thickness compared to the beam depth. Therefore, all assumptions for elastic plate analysis are applied herein.

Assumption 2:

Only a portion of the FRP cross-section is effective in resisting the compressive stresses that develop during the formation of the internal equilibrating moment of the composite cross-section.

The two "face sheets" of the FRP deck (see Figure 1), each 16.76mm thick, are the portions of the pultruded deck located farthest away from the deck centroid and are the only portion of the FRP system that is continuous over the entire span of the steel beam. This last point may be understood when considering the FRP deck as being made from hollow square tubes bonded together and oriented such that the tubes are perpendicular with the steel beam longitudinal axis. As a result of this, it can be assumed that, due to the voids present inside the

tubes, it is only the top and bottom tube walls that are in continuous contact across tube interfaces and thus represent the only contiguous elements within the FRP system considered.

Assumption 3:

Since the deck is designed to be fully composite, the neutral axis (**N-A**) obtained from the field testing is considered as that of the whole composite cross-section, rather than that of the steel section only. This measured **N-A** location is then used as a basis for determining the effective compression flange width in the FRP deck system at service load. Further justification for the foregoing is given below.

A series of push-off tests incorporating the same deck profile used in the current research were conducted at the University of South Carolina (Turner and Harries 2002) and the University of Delaware (Moon et al. 2002) where it was observed that the shear stiffness of an individual shear plane was 236kN/mm (in a three stud configuration) and 140 KN/mm (in a two stud configuration), respectively; with each stud having a diameter of 22mm and a height of 150mm. Both the Delaware and South Carolina tests employed shear stud sizes that are identical to what is in the subject bridge of the present field study. In addition, the shear studs tested at the University of Delaware and the University of South Carolina were welded to beam flanges with a thickness consistent with the flange thickness in the bridge used in the current field study (the subject bridge uses the two stud configuration across the flange). It is observed from the foregoing that the shear stiffness values for the FRP-steel interface are consistent with concrete-steel composite connection shear stiffness where metal decking is employed; a study by Jaya and Hossain (1987) measured stiffness values on the order of 50kN/mm in a two stud configuration with a shear stud size and spacing consistent with the earlier referenced FRP tests (Moon et al.

2002, Turner and Harries 2002). Based on this last point, it is concluded that full composite action may be considered at service loads in the FRP-steel composite installation under investigation. As a result, the current experimental testing program, focused on the field measurement of the neutral axis location, provides a sufficient basis to make recommendations on the effective compression flange width present in steel beam-FRP deck composite beam designs at service condition.

4.2.2 Discussion of Transformed Section Calculations

Table 4 lists the section and material properties, which are based on the information provided by Martin Marietta Composite for their FRP deck.

Table 4 Material Properties

Steel Beams (mm)	flange thickness (t_f) =	19.05
	b_f =	323.85
	t_w =	12.70
	spacing =	1752.60
FRP Deck (mm)	haunch thickness (t_{haunch}) =	12.70
	FRP flange thickness (t_{top}, t_{btm}) =	16.76
	deck thickness (t_d) =	194.56
Modulus of Elasticity (MPa)	E_{steel} =	200000.00
	E_{grout} =	31841.70
	E_{frp} =	17241.40

For a fully composite section, despite the fact that there is continuity in strains through the depth, the stresses are discontinuous (see Figure 8). This is due to the different modulus of elasticity of the composite materials. For the same strain, high stresses develop in the material with the higher modulus. This is advantageous in many cases as some structural materials are

inexpensive but have certain strength shortcomings. With composites, large quantities of the higher-modulus material can be used in the higher-stress areas.

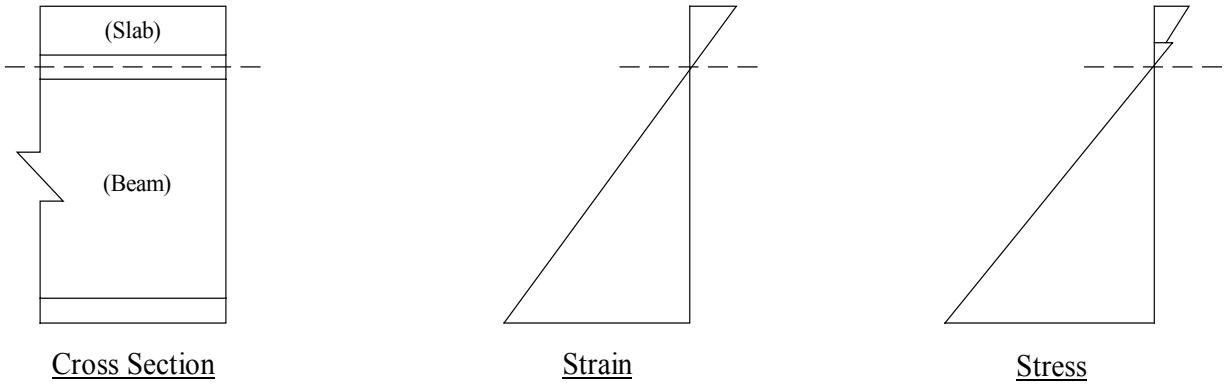

Figure 8 Distribution of Strains and Stresses in Composite Beams

Therefore, when computing section properties, it is necessary to transform the composite section to a cross section of only one material, which is called the **equivalent cross section.** The modular ratio η_1 and η_2 will be used here (using Eq. (1) and Eq. (2)). The total compression force carried by the equivalent system must be the same as that carried by the real system.

$$\eta_1 = \frac{E_{st}}{E_{frp}} = 11.60 \tag{1}$$

$$\eta_2 = \frac{E_{st}}{E_{grout}} = 6.28 \tag{2}$$

Figure 9 depicts a schematic of the cross-sectional idealization. An elementary approach for determining the centroids of composite areas is applied herein for obtaining effective widths. The essential feature of this method is that cross-sectional area is divided into parts whose centroids are known. This information is then used to arrive at the composite cross-section's centroid by using the following expressions:

$$\bar{x} = \frac{\sum_i \bar{x}_i A_i}{\sum_i A_i} \tag{3}$$

$$\bar{y} = \frac{\sum_i \bar{y}_i A_i}{\sum_i A_i} \tag{4}$$

$\bar{x}$, $\bar{y}$ = Coordinates of x and y of the centroid for the composite areas, respectively.

For the convenience of calculation, the cross section is divided into six elements, the top (①) and bottom (②) facesheets of the FRP deck, the top (③) and bottom (⑤) flanges of the steel beam, the steel web (④) and the haunch (⑥) between the deck and the steel beam.

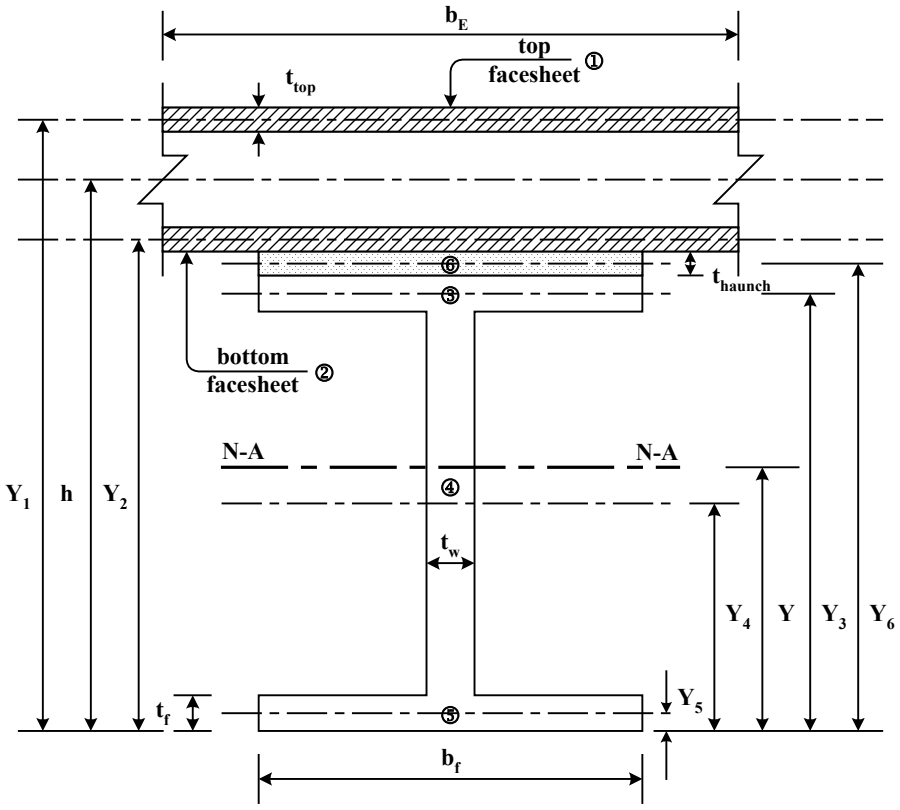

Figure 9 Schematic of the Cross-sectional Idealization for Calculations of B_E

$\mathbf{Y_i}$ = the distance from bottom of element ⑤ to any of the six tabulated NA locations.

Y = the distance from bottom of element ⑤ to the NA of the cross section

The location of **N-A** is obtained from field data.

Among these elements, element ⑤ and the steel web beneath the measured steel beam neutral axis (**N-A**) are subjected to tensile stresses, while elements ①,②,⑥,③ as well as the steel web above the measured steel beam neutral axis (**N-A**), are subjected to compressive stresses.

Based on the transformed area ($\mathbf{A_i}$) and the corresponding moment arm $\mathbf{Y_i}$ of each element, $\mathbf{A_iY_i}$ produced by the steel section elements are calculated while the area of FRP elements is unknown because the width needs to be calculated. By equating the sum of $\mathbf{A_iY_i}$ from

each element to that of the whole section, the effective width of the FRP section is calculated. A detailed discussion of the transformed section calculations incorporating the field data may be found in Table 5.

Table 5 Transformed Section Calculations

Element #	Area (mm^2)	Y_i (mm)	AY_i (mm^3)
1	16.76 B_E / η_1	810.01	13579.08 B_E / η_1
2	16.76 B_E / η_1	632.21	10598.30 B_E / η_1
3	6169.34	601.60	3711470.28
4	7277.40	305.56	2223698.37
5	6169.34	9.53	58762.99
6	4112.90 / η_2 = 654.90	617.47	404383.72
Total	20270.99 + 33.53 B_E / η_1		6398315.35 + 24177.38 B_E / η_1
Equilibrium Equation	(20270.99 + 33.53 B_E / η_1)*Y = 6398315.35 + 24177.38 B_E / η_1		

Table 6 Results of B_E for Exterior Beams (mm)

Test 1	Test 2	Test 3	Average	Theoretical B_E	% Difference Between Calculated B_E & Theoretical B_E
1350	1160	916	1142	1257.3	9.17

Table 7 Results of B_E for Interior Beams (mm)

Test 1	Test 2	Test 3	Average	Theoretical B_E	% Difference Between Calculated B_E & Theoretical B_E
1223	1326	1378	1309	1752.6	25.31

4.2.3 Results from Field Tests

When considering the field data, delineation between exterior and interior beam locations is adopted. Using the exterior beam neutral axis locations presented in Table D-40 to Table D-42 in conjunction with the transformed section calculations outlined in Table 5, an effective service load compression flange width for the exterior beam installations is observed to be **1142**mm.

Similarly, using the exterior beam neutral axis locations presented in Table D-43 to Table D-45 in conjunction with the transformed section calculations outlined in Table 5, an effective service load compression flange width for the interior beam installations is observed to be **1309**mm.

Results of B_E are shown in Table 6 and Table 7 for exterior beams and interior beams, respectively.

4.2.4 Design Assumptions from LRFD and AASHTO

The design assumptions of B_E applied in the Boyer Bridge are obtained by using related specifications in LRFD and AASHTO for the case of a composite steel beam with a concrete

deck. Therefore according to 1998 LRFD Specification section I3.1, the effective width of the slab on each side of the beam centerline ($B_E/2$) shall not exceed:

- One-eighth of the beam span, center to center, of supports;

$$\frac{12954}{8} = 1619.25mm$$

- One-half the distance to the centerline of the adjacent beams;

$$\frac{1752.6}{2} = 876.3mm$$

- The distance to the edge of the slab.

Thus, for interior beams, B_E = 1752.6mm controls, while for exterior beams, B_E = 762mm controls.

However, the 1998 AASHTO uses the following criteria for the effective flange width in this case:

For interior beams, the effective flange width may be taken as the least of:

- One-quarter of the effective span length;

$$\frac{12954}{4} = 3238.5mm$$

- 12.0 times the average thickness of the slab, plus the greater of web thickness or one-half the width of the top flange of the beam;

$$12 \times 194.6 + \frac{323.85}{2} = 2497.125mm$$

- The average spacing of adjacent beams, which is 1752.6mm in our case.

Therefore, B_E = 1752.6mm controls for interior beams.

For exterior beams, the effective flange width may be taken as one-half the effective width of the adjacent interior beam, plus the least of:

- One-eighth of the effective span length;

$$\frac{12954}{8} = 1619.25mm$$

- 6.0 times the average thickness of the slab, plus the greater of half the web thickness or one-quarter of the width of the flange of the basic beam;

$$6 \times 194.6 + \frac{323.85}{4} = 1248.56mm$$

- The width of the overhang, which is 381mm in our case.

Therefore, $B_E = \frac{1752.6}{2} + 381 = 1257.3mm$ controls for exterior beams.

4.2.5 Discussion of the Results

It is seen from Figure 10 that the measured interior effective width is not exactly equal to the center-to-center spacing of the beams; rather, it is somewhat less than the actual center-to-center spacing of the beams (labeled as "design assumption" in the figure), which is based on the corresponding AASHTO specifications for a composite steel beam with a concrete deck. The measured interior effective width is approximately **75%** of the center-to-center beam spacing.

Furthermore, it is pointed out that the percentage of the center-to-center beam spacing is quite different for exterior beams (see Figure 10). The measured exterior effective width is approximately **90%** of the design assumption, which is given by AASHTO to be one-half the actual center-to-center spacing of the beams plus the deck overhang. Therefore, in contrast to the interior beam installations, the exterior beams enjoy a more efficient response.

It is noted that the foregoing percentages are based on conservative material properties published by Martin-Marietta Composites. Based on material testing on DuraSpan deck carried out at the University of Pittsburgh, it appears that the actual modular ratios will result in effective widths somewhat larger than the foregoing percentages.

Exterior Girders:

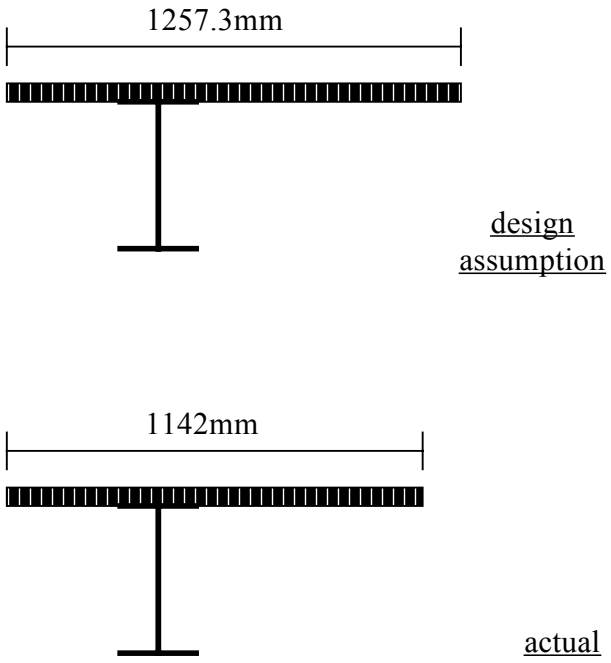

Interior Girders:

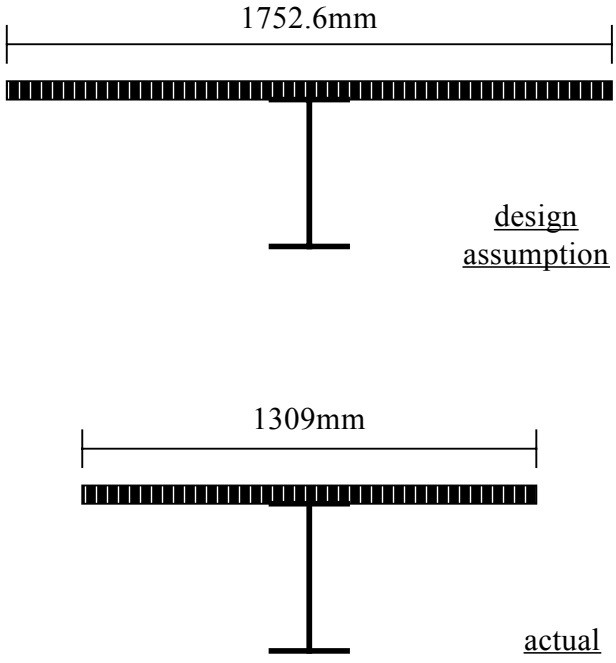

Figure 10 Comparison of Design Assumptions and Actual Values of B_E

4.3 Calculation of Distribution Factors (DF)

4.3.1 Results from Field Tests

There are many ways to assess the distribution of live loads on a bridge. It can be expressed either through the percentage of moments or shears, in the form of a fraction of wheel load distributed to each beam, or as a fraction of live load per lane resisted by each beam. Calculated distribution factors can be very different depending on which of these various points of view is adopted. The distribution factor (DF) considered herein is the distribution of live load per lane in terms of moment; which can be calculated for interior and exterior beams using Eq. (5) and Eq. (6) in conjunction with results from load tests in the field.

For interior beams:

$$DF = \frac{Max(M_2, M_3, M_4)}{\sum_{i=1}^{5} M_i} \tag{5}$$

For exterior beams:

$$DF = \frac{Max(M_1, M_5)}{\sum_{i=1}^{5} M_i} \tag{6}$$

in which:

M_i = the moment computed using the strain at point P on the top of the bottom flange of beam number (i) (i = 1, 2, 3, 4, 5). Location P corresponds with one of the strain gage locations (see Figure 11). The cross-sectional moment can be computed from the strain at point P as:

$$M = \frac{\sigma I}{c} = \varepsilon E s \tag{7}$$

where:

$$I_x = \sum_{i=1}^{4} I_{x(i)} + \sum_{i=1}^{4} A_i d_i^2 \tag{8}$$

$$\sigma = \varepsilon E \tag{9}$$

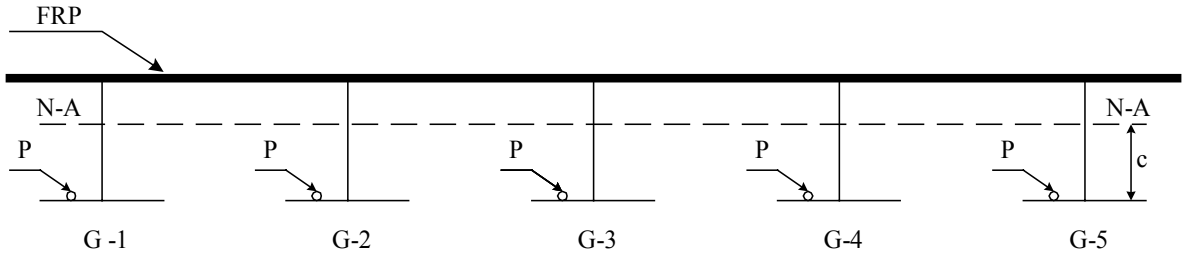

Figure 11 Location of the Point P for Each Beam

Despite the redundancy in strain gage installation, strain gage failures resulted in an incomplete set of strain readings in Beam 1 during the March 21, 2002 field test. Similarly, the gages on Beam 5 were only intermittently functioning during the early load testing. Therefore, it was not possible to compute distribution factors for the exterior beams.

The calculation of the cross section properties is illustrated in Figure 12 as well as Tables 8, 9, and 10. The moments for interior beams in each test are listed in Tables D-46, D-47 and D-48. While the results of DFs are presented in Table 11, 12, and 13. The maximum DF is ultimately picked as the DF for each given test.

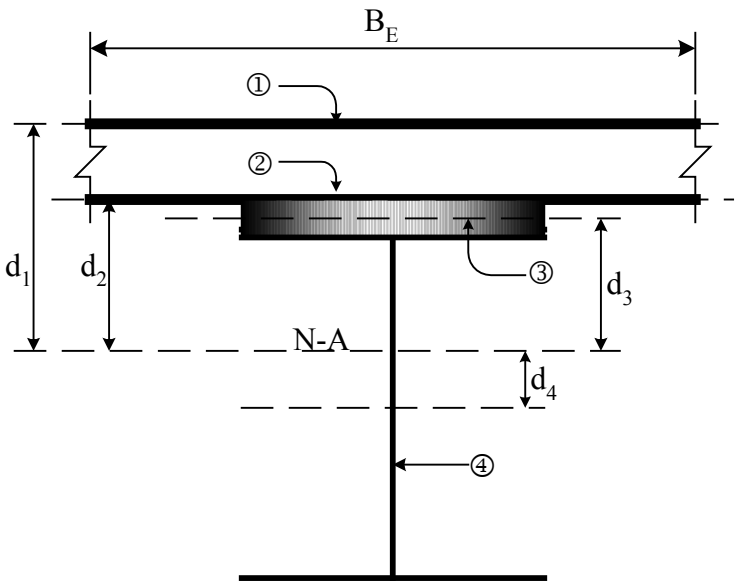

Figure 12 Schematic of the Cross-sectional Idealization for Inertia Moment Calculations

B_E = the service load effective compression flange width

① = the top facesheet of the FRP bridge deck with a width of B_E

② = the bottom facesheet of the FRP bridge deck with a width of B_E

③ = the cross section of the haunch between the deck and the steel beam

④ = the cross section of the steel beam

Table 8 Calculation of Inertia Moment for Interior Sections

INTERIOR BEAM-SLAB CROSS SECTION				
Part #	1	2	3	4
b (in)	51.5	51.5	12.75	
h (in)	0.66	0.66	0.50	
$bh^3/12$ (in^4)	1.23	1.23	0.13	3100

Table 9 Calculation of Inertia Moment for Exterior Sections

EXTERIOR BEAM-SLAB CROSS SECTION				
Part #	1	2	3	4
b (in)	44.96	44.96	12.75	
h (in)	0.66	0.66	0.50	
$bh^3/12$ (in^4)	1.08	1.08	0.13	3100

Table 10 Calculation of Cross Section Properties

INTERIOR BEAM-SLAB CROSS SECTION PROPERTIES							
Part #	1	2	3	4	SUM	I (in4)	S = I/c (in3) (c = 14.05 in)
I (in^4)	1.23	1.23	0.13	3100.00	3102.59		
A (in^2)	33.99	33.99	6.38	30.60		17301.79	1231.44
d (in)	17.09	10.09	9.51	2.77	14199.20		
$A*d^2$ (in^4)	9927.39	3460.46	576.56	234.79			
EXTERIOR BEAM-SLAB CROSS SECTION PROPERTIES							
Part #	1	2	3	4	SUM	I (in4)	S = I/c (in3) (c = 14.05 in)
I (in^4)	1.08	1.08	0.13	3100.00	3102.29		
A (in^2)	29.67	29.67	6.38	30.60		15599.94	1110.32
d (in)	17.09	10.09	9.51	2.77	12497.65		
$A*d^2$ (in^4)	8665.66	3020.65	576.56	234.79			

Table 11 Calculations of DFs in Test 1

DF (A_1)	-
DF (A_2)	0.351
DF (A_3)	0.336
DF (B_1)	0.336
DF (B_2)	0.317
DF (B_3)	0.328
DF (C_1)	0.387
DF (C_2)	0.400
DF (C_3)	0.407

Table 12 Calculations of DFs in Test 2

DF (A_1)	0.384
DF (A_2)	0.388
DF (A_3)	0.393
DF (B_1)	0.426
DF (B_2)	0.389
DF (B_3)	0.389
DF (C_1)	0.411
DF (C_2)	0.407
DF (C_3)	0.415

Table 13 Calculations of DFs in Test 3

DF (A_1)	0.360
DF (A_2)	0.369
DF (A_3)	0.382
DF (B_1)	0.406
DF (B_2)	0.393
DF (B_3)	0.402
DF (C_1)	0.428
DF (C_2)	0.421
DF (C_3)	-

4.3.2 Design Assumption of DF from AASHTO

The live load distribution per lane for moment in interior beams may be determined by applying the formulae in the 1998 AASHTO LRFD (Table 4.6.2.2.2b-1). For our case, we can consider the type of beams as "Concrete Deck, Filled Grid, or Partially Filled Grid on Steel or Concrete Beams; Concrete T-Beams, T-and Double T-Sections" (see Table 14)

Table 14 Distributions of Live Loads per Lane for Moment in Interior Longitudinal Beams

(AASHTO 1998, Table 4.6.2.2.2b-1)

TYPE OF BEAMS	APPLICABLE CROSS-SECTION FROM TABLE 4.6.2.2.1-1	DISTRIBUTION FACTORS	RANGE OF APPLICABILITY
Concrete Deck, Filled Grid, or Partially Filled Grid on Steel or Concrete Beams; Concrete T-Beams, T- and Double T-Sections	a, e, k and also i, j if sufficiently connected to act as a unit	One Design Lane Loaded: $0.06+(\frac{S}{14})^{0.4}(\frac{S}{L})^{0.3}(\frac{K_g}{12.0Lt_s^3})^{0.1}$ Two or More Design Lanes Loaded: $0.075+(\frac{S}{9.5})^{0.6}(\frac{S}{L})^{0.2}(\frac{K_g}{12.0Lt_s^3})^{0.1}$	$3.5 \le S \le 16.0$ $4.5 \le t_s \le 12.0$ $20 \le L \le 240$ $N_b \ge 4$
		use lesser of the values obtaining from the equation above with $N_b = 3$ or the lever rule	$N_b = 3$

in which:

K_g = longitudinal stiffness parameter (IN^4)

L = span of beam (FT) = 42.5

N_b = number of beams, stringers or girders = 5

S = spacing of beams or webs (FT) = 5.75

t_S = depth of concrete slab (IN) = 7.66

And according to the definition of AASHTO LRFD (1998), longitudinal stiffness parameter, K_g, shall be taken as:

$$K_g = n(1 + Ae_g^2) \tag{10}$$

in which:

$$n = \frac{E_B}{E_D} \tag{11}$$

where:

A = area of stringer, beam or girder (IN^2) = 30.60

E_B = modulus of elasticity of beam material (KSI) = 29000

E_D = modulus of elasticity of deck material (KSI) = 2500

I = moment of inertia of beam (IN^4) = 3100

e_g = distance between the centers of gravity of the basic beam and deck (IN)

= 16.36

The design assumption of interior DF in this case is calculated to be 0.412.

4.3.3 Discussion of the Results

The distribution factors obtained from the field data are compared with the one calculated by AASHTO formula (see Table 14) in Table 15. The maximum interior DF is 0.428 for tested results. Compared to 0.412 for the AASHTO (1998), it can be observed that using AASHTO formulae results in DF only 3.7% less than tested results. The average interior DF of all three tests is 0.420, which presents an even smaller difference, 2.0%.

Table 15 Comparison of DFs from Tests and AASHTO

	TESTED RESULTS	AASHTO	% DIFFERENCE
Test 1	0.407	0.412	1.2
Test 2	0.426	0.412	3.2
Test 3	0.428	0.412	3.7
Average	0.420	0.412	2.0

5.0 CONCLUSIONS AND RECOMMENDATIONS

5.1 Summary and Conclusions

The present study reports on the field study of a steel beam-FRP deck composite bridge in Pennsylvania. The objective of the study is to assess the composite response of the FRP deck system when acting with underlying steel beams at service conditions.

The research results reported herein support the notion of employing a design approach for FRP composite systems that is consistent with current practice related to steel beams acting compositely with concrete decking. Based on the current results the following conclusions can be drawn:

1. There is an upward shift in the measured steel beam neutral axis location. For the five steel beams, the neutral axis is calculated to be an average **356.78** mm above the bottom strain gage, which is approximately **60%** of the web height of the steel beam. Since the neutral axis is not in the middle of the beam and the beam is a symmetric section, the FRP deck does act compositely with the steel beams to some extent and hence assist the steel beam in resisting applied moments.
2. FRP decks and floors acting compositely with underlying steel beams exhibit an effective width, at service condition, of approximately **75%** of the beam spacing for interior beam installations and **90%** of the total distance, made up of one-half the beam spacing added to the deck overhang, for the case of exterior beams. Based on the test results, some preliminary recommendations are presented herein for the calculation of the effective flange width:

For interior beams, the effective flange width may be conservatively taken as 0.75 times the average spacing of adjacent beams.

For exterior beams, the effective flange width may be conservatively taken as 0.9 times the sum of one-half the effective width of the adjacent interior beam and the width of the overhang.

Further study is recommended to obtain the precise coefficients with actual FRP material properties.

3. The live load distribution per lane for moment in interior longitudinal beams is calculated for each test and then compared to the AASHTO criteria for the case of concrete decks on steel or concrete beams. It is shown in Table 15 that the interior distribution factor (0.412) using the AASHTO (1998) formulas is only 3.7% less than the maximum interior DF (0.428) and 2.0% less than the average distribution factor (0.420) obtained from the field test results. Based on this slight difference, it appears that the AASHTO LRFD (1998) formulas may be applicable for FRP decks on steel beams in a short span simply supported bridge with small beam spacing.

5.2 Recommendations

Since the conclusions presented above are based on testing conducted when some of the strain gages did not work efficiently, further research is required to verify the tested results through investigating the long-term performance of the steel-supported FRP deck bridges and bridge deck panels, both in-situ and in the laboratory.

In addition to the field-testing and lab work, developing a three-dimensional finite element model is also a good way to validate the tested results. This mathematical analysis may allow for the complicated behavior observed during the field-testing to be studied in detail.

APPENDICES

Appendix A

The Boyer Bridge Drawings

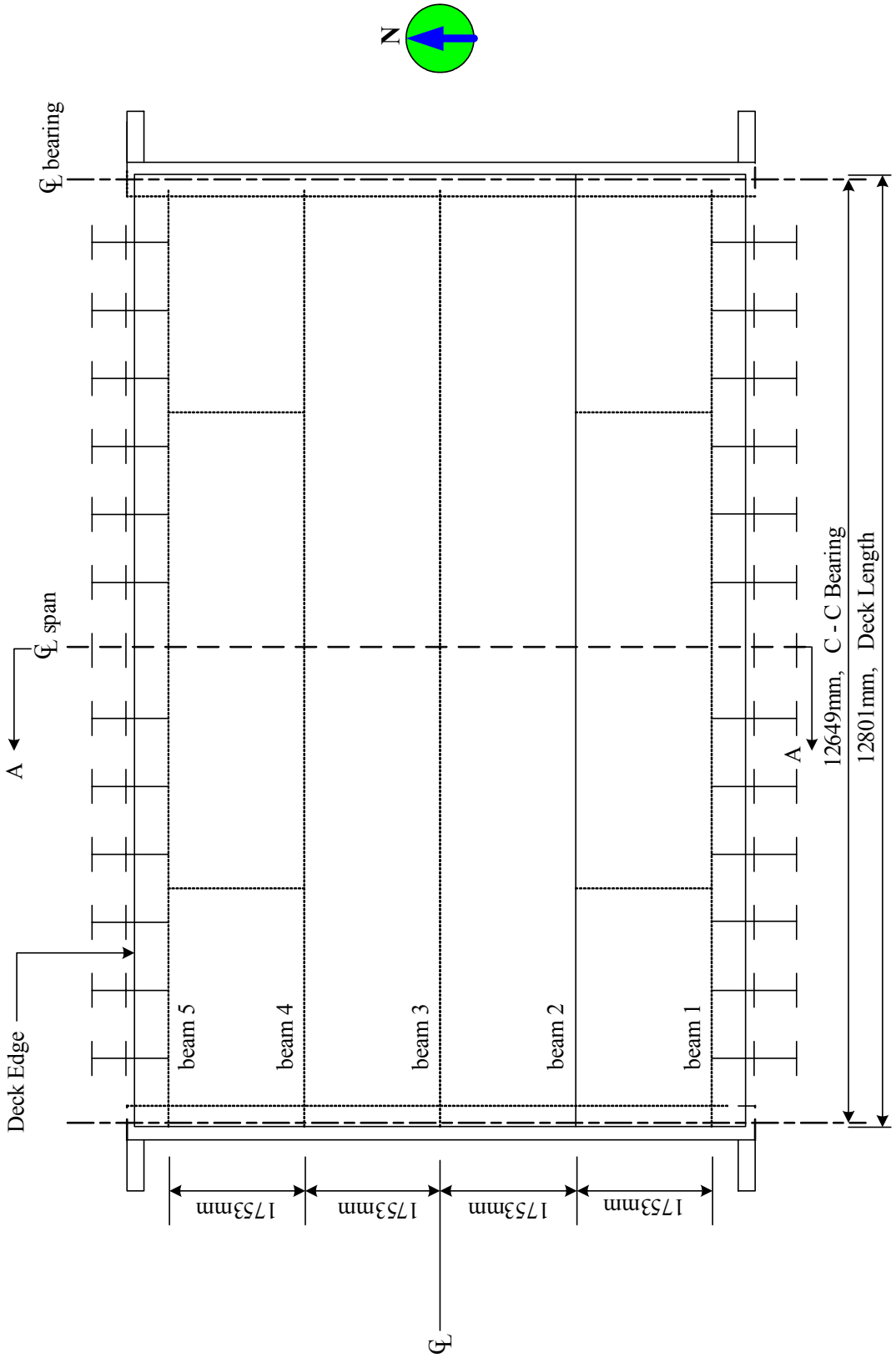

Figure A-1 Plan View of the Boyer Bridge

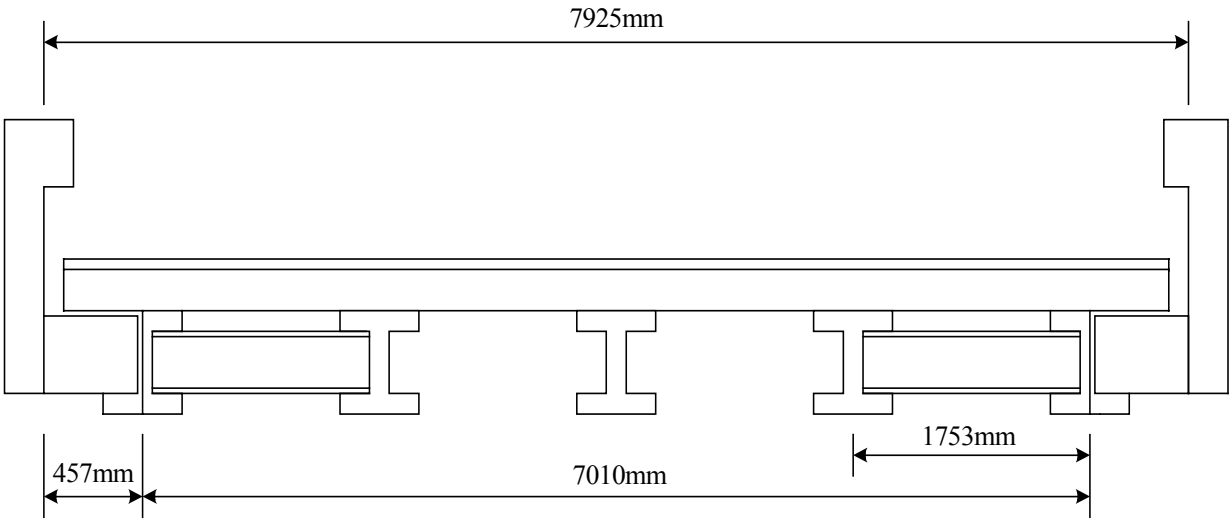

Figure A-2 Typical Section A-A (not to scale)

Appendix B

The Loading Test Setup

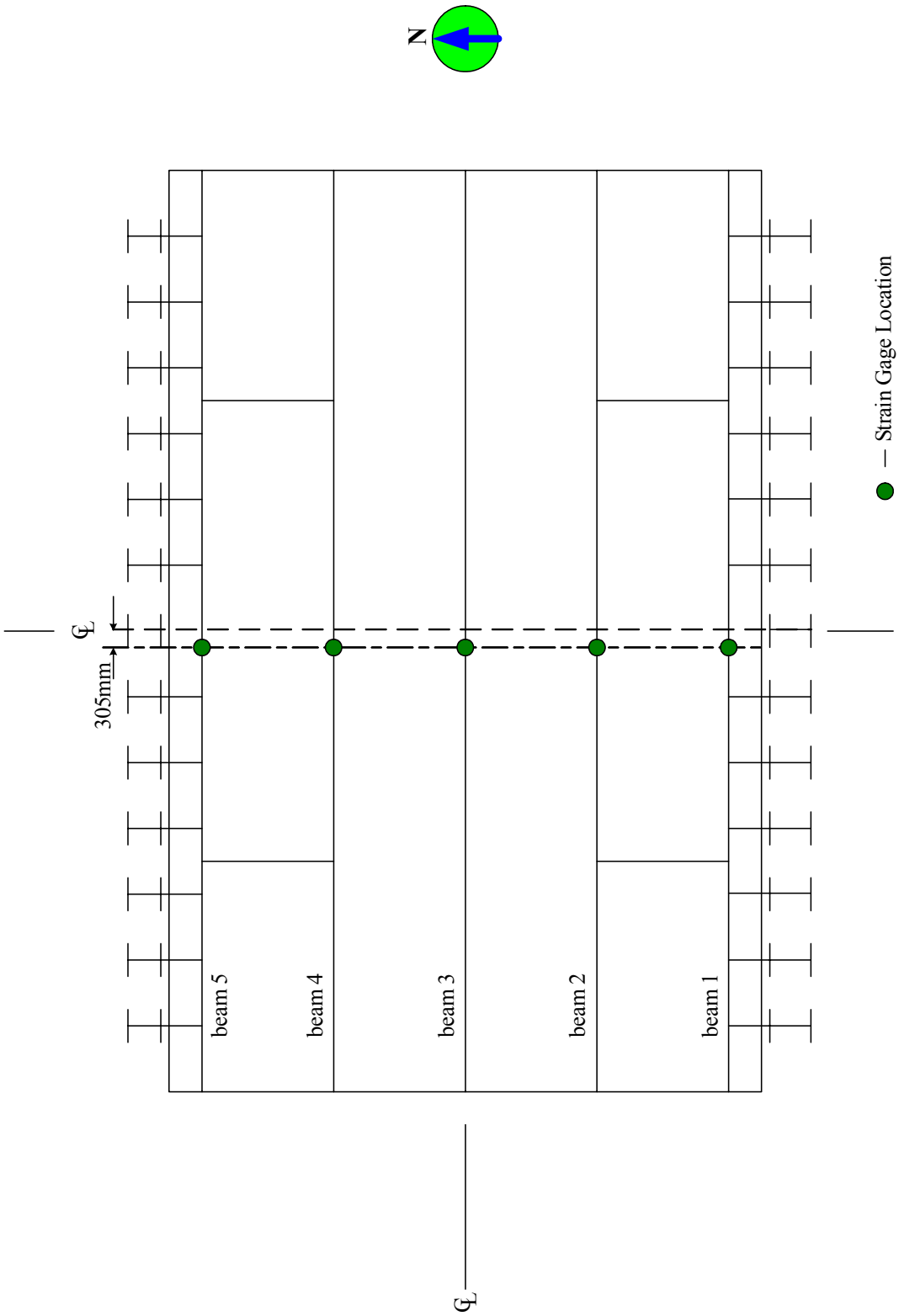

Figure B-1 Strain Gage Layout Plan

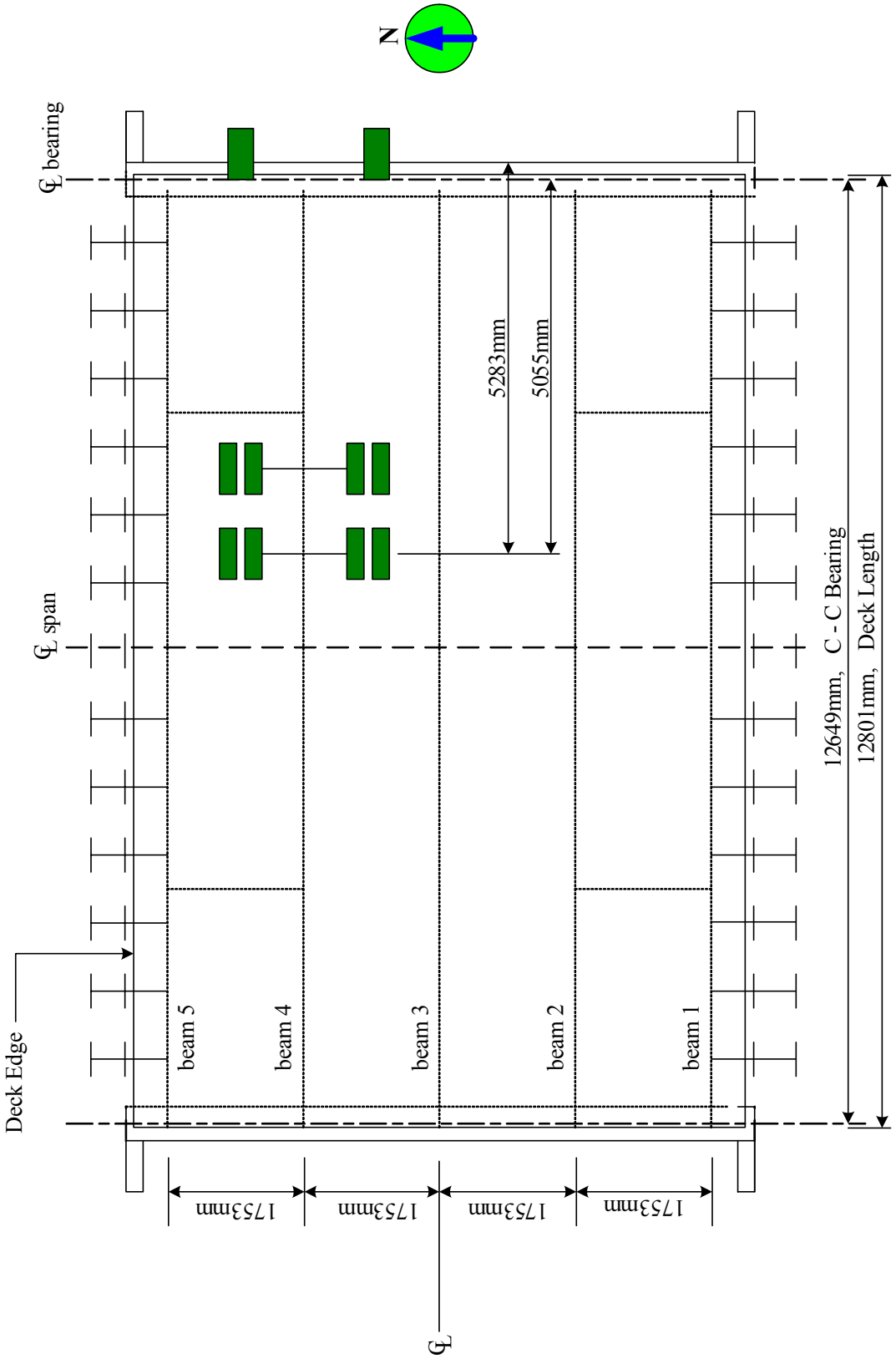

Figure B-2 Truck Load at Position A

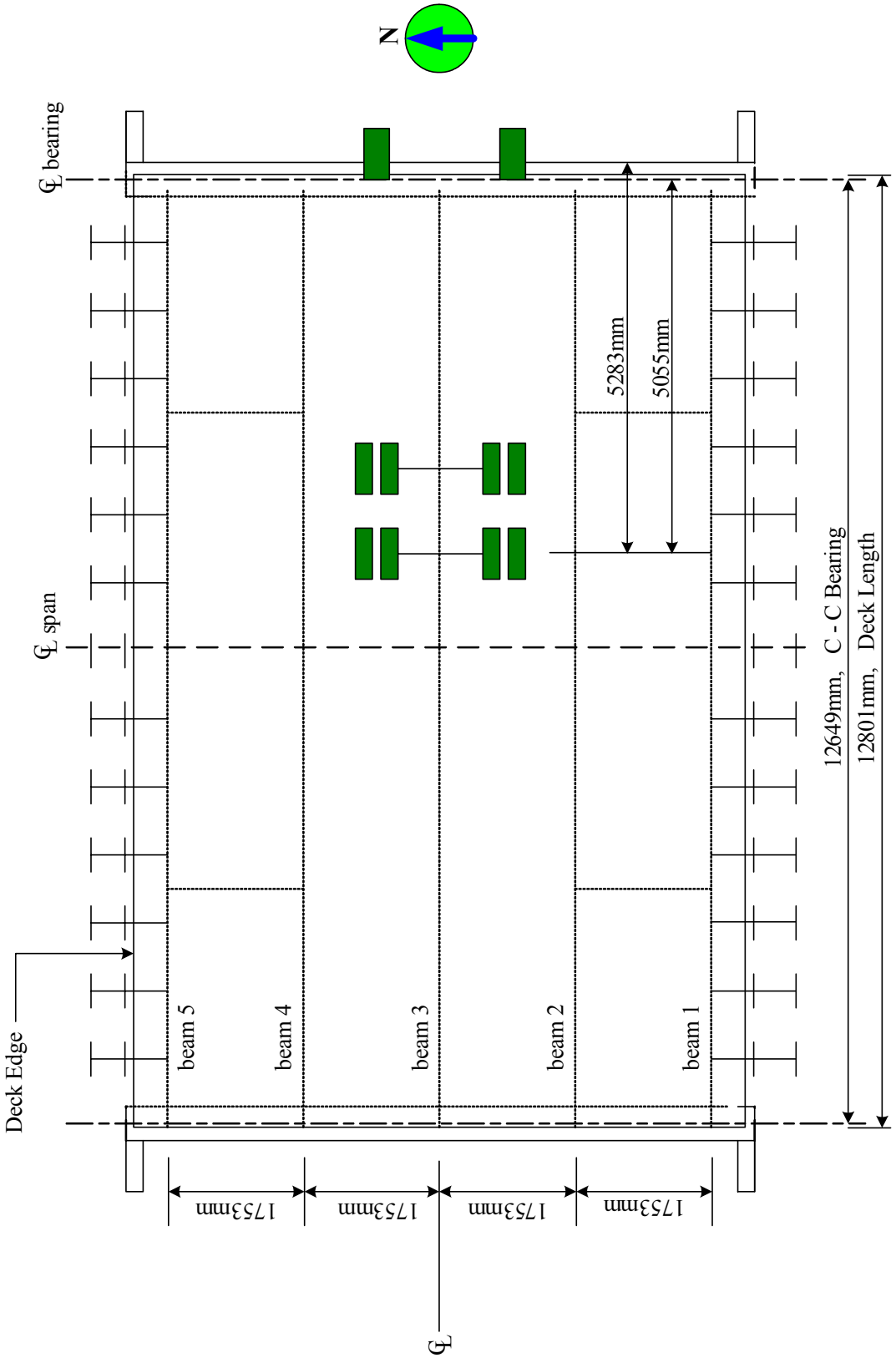

Figure B-3 Truck Load at Position B

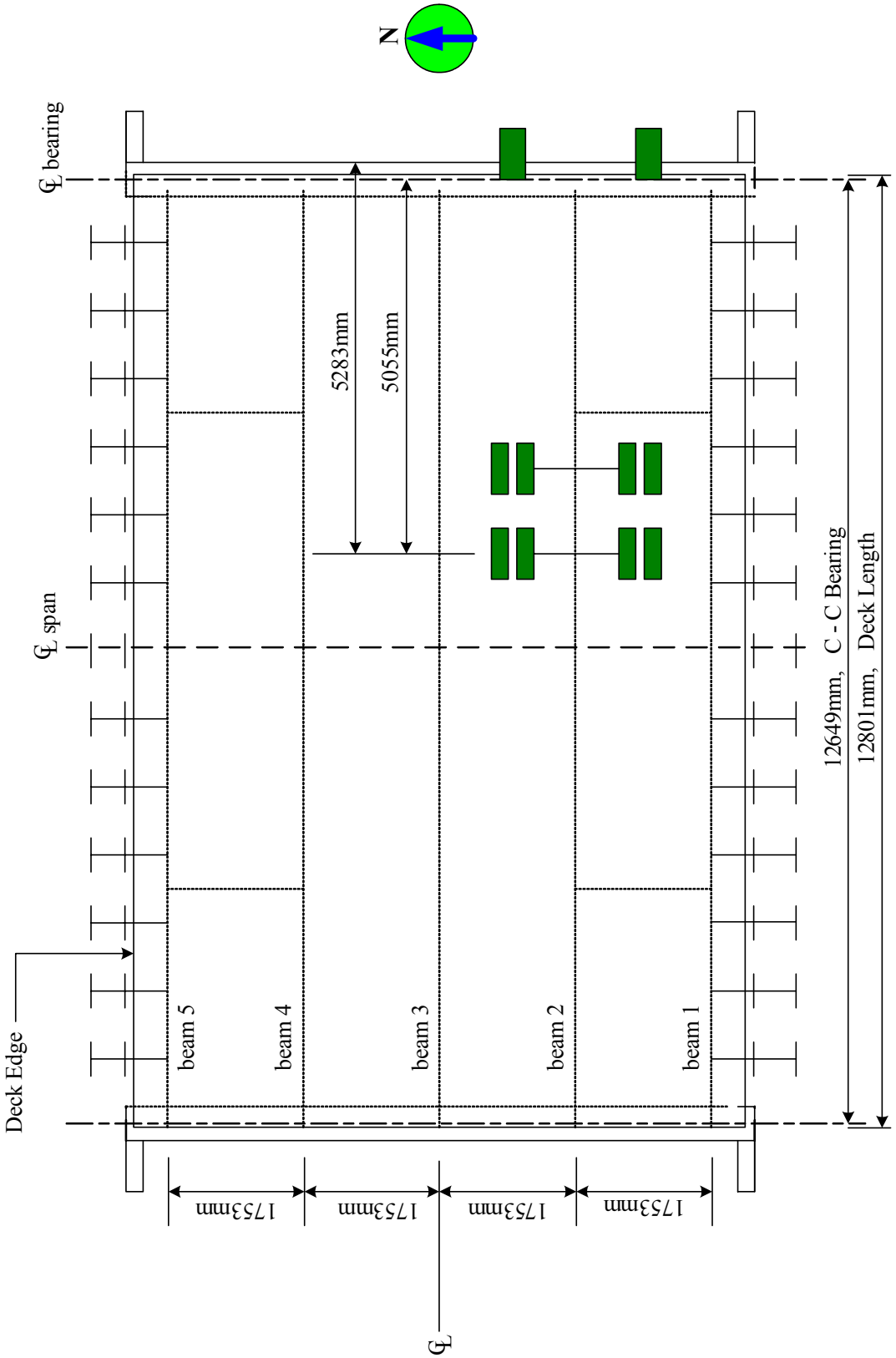

Figure B-4 Truck Load at Position C

Appendix C

Photographs

Figure C-1 Strain Gage Installation at the Boyer Bridge

Figure C-2 Strain Gage Installations

Figure C-3 Strain Gage Wire Arrangement

Figure C-4 Framing Plan View (Facing East)

Figure C-5 Framing Plan View (Facing West)

Figure C-6 Abutment Details

Figure C-7 Installation of Deck Panels

Figure C-8 Finished Boyer Bridge

Figure C-9 Midspan Test Layout Points

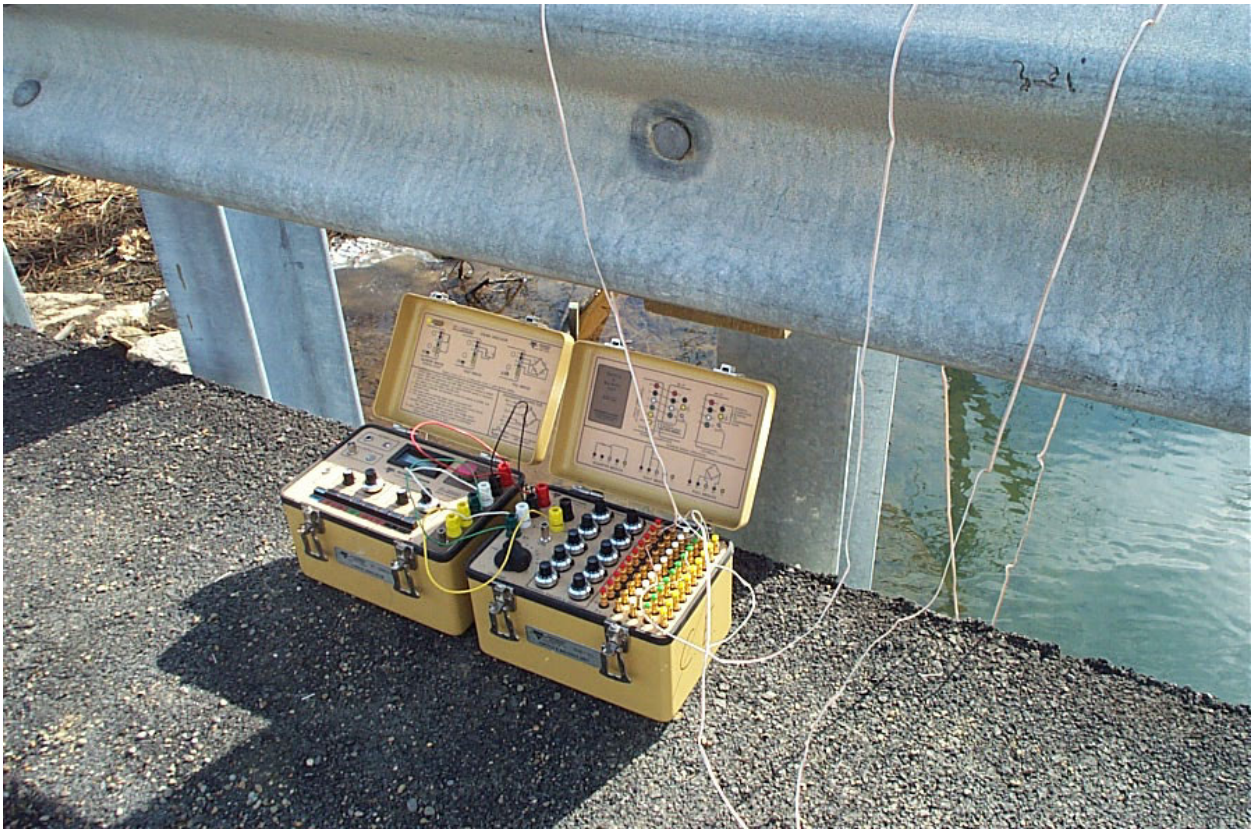

Figure C-10 P3500 Strain Indicators

Figure C-11 Field Data Acquisition System

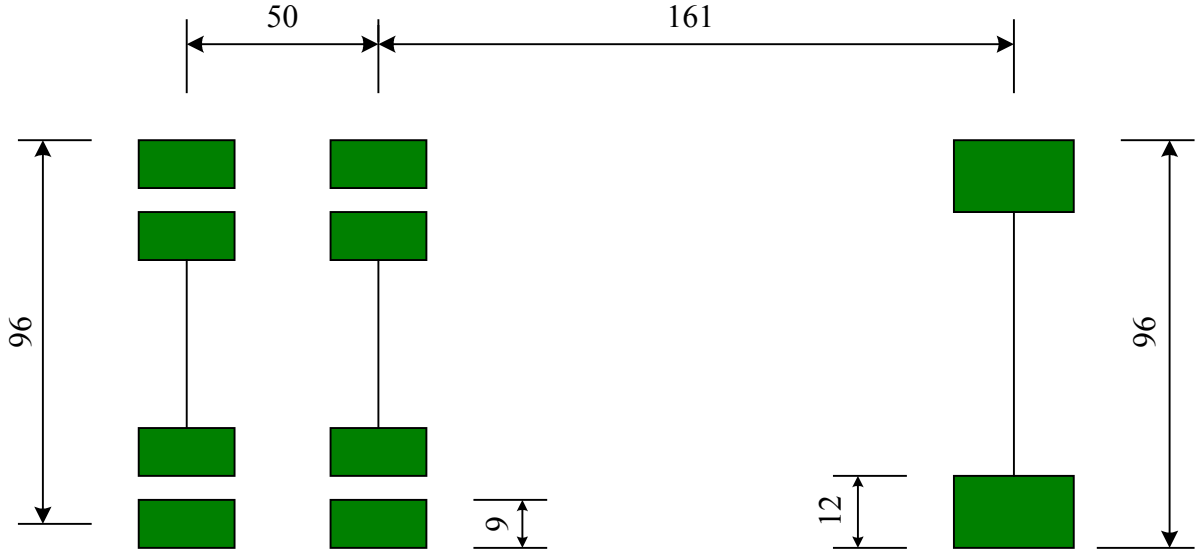

Figure C-12 Photograph and Dimensions of Test Vehicle (units are inches)

Figure C-13 Truck Load Approaching Position A

Figure C-14 Truck Load at Position B

Figure C-15 Truck Load at Position C

Appendix D

Tables

The following notation and definitions shall apply to Tables (D-1) to (D-39):

- **B-i (L) / B-i (R)** - the left/right side of beam **i**. (**i** = 1, 2 … 5)
- **A_j-zero / B_j-zero / C_j-zero** - the reading recorded just before the truck went to Location A / B / C (**j** = 1, 2 or 3, which means the (**j**)th record at each location.)
- **A_j /B_j /C_j** - the reading recorded when the truck stopped at Location A / B / C.
- **$\varepsilon(A_j/B_j/C_j)$** - the micro-strain transformed from the strain gage reading at Location A / B / C in the (**j**)th record. It shall be taken as:

$$\varepsilon = \frac{4000 * \Delta}{2.14 * (1 - 0.002 * \Delta)} (10^{-6}) strain$$

$\Delta = A_j - (A_j\text{-zero})$

- **Ave-zero** - In test 1, we recorded the ZERO-readings only at the beginning and the end of the whole test, therefore, here we use the average values for approximation.
- In Test 2 & 3, the readings of strain gage number 1, 2 and 3 were recorded manually. Most of them were not good compared with other results.
- **"-"** - the result is either bad or unavailable.

Table D-1 Measured Strains at Position A, Beam 1 (test 1)

BEAM #	B-1(L)			B-1(R)		
Strain Gage #	1	2	3	4	5	6
A_1-zero	-0.71	-	-0.614	-0.464	-	-
C_3-zero	-0.700	-	-0.612	-0.457	-	-
Ave-zero	-0.705	-	-0.613	-0.46	-	-
A_1	0.212	-	-0.489	-1.150	-	-
ε (A_1)	-	-	-	-	-	-
A_2	-0.703	-	-0.613	-0.46	-	-
ε (A_2)	-	-	-	-	-	-
A_3	-0.699	-	-0.612	-0.457	-	-
ε (A_3)	-	-	-	-	-	-

Table D-2 Measured Strains at Position A, Beam 2 (test 1)

BEAM #	B-2 (L)			B-2 (R)		
Strain Gage #	7	8	9	10	11	12
A_1-zero	0.490	-1.033	-	0.108	0.347	-0.741
C_3-zero	0.498	-1.025	-	0.118	0.356	-0.717
Ave-zero	0.494	-1.029	-	0.113	0.352	-0.729
A_1	-0.077	-0.426	-	-0.2405	-0.2975	-0.836
ε (A_1)	-1066.072	1128.464	-	-	-	-
A_2	0.488	-1.021	-	0.106	0.357	-0.71
ε (A_2)	-11.215	14.954	-	-13.084	9.346	35.515
A_3	0.489	-1.021	-	0.108	0.358	-0.707
ε (A_3)	-9.346	14.954	-	-9.346	11.215	42.058

Table D-3 Measured Strains at Position A, Beam 3 (test 1)

BEAM #	B-3 (L)			B-3 (R)		
Strain Gage #	**13**	**14**	**15**	**16**	**17**	**18**
A_1-zero	-	-	-	-	0.227	-0.393
C_3-zero	-	-	-0.222	-0.048	0.6215	-0.3905
Ave-zero	-	-	-0.222	-0.048	0.424	-0.392
A_1	-	-	-	-	-0.708	-
ε (A_1)	-	-	-	-	-	-
A_2	-	-	-0.191	-0.075	0.456	-0.36
ε (A_2)	-	-	57.948	-50.465	-	59.817
A_3	-	-	-0.1905	-0.074	0.492	-0.359
ε (A_3)	-	-	58.882	-48.596	-	61.686

Table D-4 Measured Strains at Position A, Beam 4 (test 1)

BEAM #	B-4 (L)			B-4 (R)		
Strain Gage #	**19**	**20**	**21**	**22**	**23**	**24**
A_1-zero	-0.460	-1.159	-0.926	-	-0.084	-0.471
C_3-zero	-0.459	-1.154	-0.9265	-	-0.081	-0.470
Ave-zero	-0.459	-1.156	-0.926	-	-0.082	-0.471
A_1	-0.6135	-0.462	-	-	0.485	-1.028
ε (A_1)	-	-	-	-	-	-
A_2	-0.494	-1.147	-0.881	-	-0.076	-0.423
ε (A_2)	-65.416	16.823	84.120	-	11.215	89.728
A_3	-0.498	-1.147	-0.881	-	-0.076	-0.423
ε (A_3)	-71.957	16.823	84.120	-	12.150	89.728

Table D-5 Measured Strains at Position A, Beam 5 (test 1)

BEAM #	B-5 (L)			B-5 (R)		
Strain Gage #	**25**	**26**	**27**	**28**	**29**	**30**
A_1-zero [2]	-1.337		-0.339	-0.812	-0.1915	-0.531
C_3-zero	-1.332	-0.242	-0.334	-0.808	-0.1875	-0.526
		-0.245	-0.336	-0.81	-0.19	-0.528
		0.103	0.353	-0.723	-	-
ε (A_1) [4]	-		-	-	-	-
A_2	-1.363	-0.239		-0.835	-0.181	-0.49
ε (A_2)	-52.334	11.215		-46.727	16.823	71.033
A_3	-1.362	-0.238	-0.294	-0.834	-0.181	-0.488
ε (A_3)	-50.465	13.084	78.511	-44.858	17.757	75.707

Table D-6 Measured Strains at Position B, Beam 1 (test 1)

BEAM #	B-1 (L)			B-1 (R)		
Strain Gage #	**1**	**2**	**3**	**4**	**5**	**6**
A_1-zero	-0.71	-	-0.614	-0.464	-	-
C_3-zero	-0.700	-	-0.612	-0.457	-	-
Ave-zero	-0.705	-	-0.613	-0.46	-	-
B_1	-0.712	-	-0.604	-0.467	-	-
ε (B_1)	-13.084	-	16.823	-13.084	-	-
B_2	-0.709	-	-0.603	-0.467	-	-
ε (B_2)	-7.477	-	18.692	-13.084	-	-
B_3	-0.705	-	-0.602	-0.463	-	-
ε (B_3)	-	-	-	-	-	-

Table D-7 Measured Strains at Position B, Beam 2 (test 1)

BEAM #	B-2 (L)			B-2 (R)		
Strain Gage #	**7**	**8**	**9**	**10**	**11**	**12**
A_1-zero	0.490	-1.033	-	0.108	0.347	-0.741
C_3-zero	0.498	-1.025	-	0.118	0.356	-0.717
Ave-zero	0.494	-1.029	-	0.113	0.352	-0.729
B_1	0.479	-1.017	-	0.099	0.361	-0.697
ε (B_1)	-28.037	22.430	-	-26.167	16.823	59.817
B_2	0.480	-1.016	-	0.099	0.362	-0.690
ε (B_2)	-27.102	25.234	-	-26.167	18.692	73.838
B_3	0.4815	-1.016	-	0.102	0.364	-0.687
ε (B_3)	-23.364	24.300	-	-20.560	22.430	79.446

Table D-8 Measured Strains at Position B, Beam 3 (test 1)

BEAM #	B-3 (L)			B-3 (R)		
Strain Gage #	**13**	**14**	**15**	**16**	**17**	**18**
A_1-zero	-	-	-	-	0.227	-0.393
C_3-zero	-	-	-0.222	-0.048	0.6215	-0.3905
Ave-zero	-	-	-0.222	-0.048	0.424	-0.392
B_1	-	-	-0.18	-0.085	0.237	-0.349
ε (B_1)	-	-	78.511	-69.154	-	80.381
B_2	-	-	-0.18	-0.086	0.457	-0.3485
ε (B_2)	-	-	78.511	-70.088	-	81.315
B_3	-	-	-0.180	-0.0795	0.4925	-0.348
ε (B_3)	-	-	79.446	-58.875	-	82.250

Table D-9 Measured Strains at Position B, Beam 4 (test 1)

BEAM #	B-4 (L)			B-4 (R)		
Strain Gage #	**19**	**20**	**21**	**22**	**23**	**24**
A_1-zero	-0.460	-1.159	-0.926	-	-0.084	-0.471
C_3-zero	-0.459	-1.154	-0.9265	-	-0.081	-0.470
Ave-zero	-0.459	-1.156	-0.926	-	-0.082	-0.471
B_1	-0.481	-1.15	-0.894	-	-0.077	-0.435
ε (B_1)	-41.120	11.215	59.817	-	9.346	67.295
B_2	-0.485	-1.15	-0.895	-	-0.077	-0.4355
ε (B_2)	-48.596	11.215	57.948	-	9.346	66.360
B_3	-0.483	-1.1485	-0.894	-	-0.077	-0.435
ε (B_3)	-44.858	14.019	59.817	-	10.280	68.229

Table D-10 Measured Strains at Position B, Beam 5 (test 1)

BEAM #	B-5 (L)			B-5 (R)		
Strain Gage #	**25**	**26**	**27**	**28**	**29**	**30**
A_1-zero	-1.337	-0.247	-0.339	-0.812	-0.1915	-0.531
C_3-zero	-1.332	-0.242	-0.334	-0.808	-0.1875	-0.526
Ave-zero	-1.335	-0.245	-0.336	-0.81	-0.19	-0.528
B_1	-1.342	-0.242	-0.326	-0.815	-0.185	-0.516
ε (B_1)	-13.084	5.608	18.692	-9.346	9.346	22.430
B_2	-1.342	-0.243	-0.325	-0.815	-0.186	-0.516
ε (B_2)	-13.084	4.673	20.561	-9.346	8.411	22.430
B_3	-1.341	-0.241	-0.324	-0.814	-0.185	-0.514
ε (B_3)	-11.215	7.477	23.365	-7.477	10.280	26.169

Table D-11 Measured Strains at Position C, Beam 1 (test 1)

BEAM #	B-1 (L)			B-1 (R)		
Strain Gage #	**1**	**2**	**3**	**4**	**5**	**6**
A_1-zero	-0.710	-	-0.614	-0.464	-	-
C_3-zero	-0.700	-	-0.612	-0.457	-	-
Ave-zero	-0.705	-	-0.613	-0.46	-	-
C_1	-0.735	-	-0.573	-0.489	-	-
ε (C_1)	-56.071	-	74.772	-54.202	-	-
C_2	-0.730	-	-0.571	-0.486	-	-
ε (C_2)	-46.727	-	78.511	-47.661	-	-
C_3	-0.728	-	-0.57	-0.484	-	-
ε (C_3)	-42.989	-	80.381	-44.858	-	-

Table D-12 Measured Strains at Position C, Beam 2 (test 1)

BEAM #	B-2 (L)			B-2 (R)		
Strain Gage #	**7**	**8**	**9**	**10**	**11**	**12**
A_1-zero	0.490	-1.033	-	0.108	0.347	-0.741
C_3-zero	0.498	-1.025	-	0.118	0.356	-0.717
Ave-zero	0.494	-1.029	-	0.113	0.352	-0.729
C_1	0.471	-1.015	-	0.092	0.365	-0.681
ε (C_1)	-42.989	26.169	-	-39.251	24.300	89.728
C_2	0.474	-1.012	-	0.0945	0.366	-0.675
ε (C_2)	-37.382	31.777	-	-34.578	26.169	100.945
C_3	0.475	-1.014	-	0.0965	0.367	-0.673
ε (C_3)	-35.513	28.038	-	-30.840	28.038	105.619

Table D-13 Measured Strains at Position C, Beam 3 (test 1)

BEAM #	B-3 (L)			B-3 (R)		
Strain Gage #	**13**	**14**	**15**	**16**	**17**	**18**
A_1-zero	-	-	-	-	0.227	-0.393
C_3-zero	-	-	-0.222	-0.048	0.6215	-0.3905
Ave-zero	-	-	-0.222	-0.048	0.424	-0.392
C_1	-	-	-0.197	-0.076	0.291	-0.362
ε (C_1)	-	-	46.731	-52.334	-	56.078
C_2	-	-	-0.196	-0.074	0.494	-0.360
ε (C_2)	-	-	48.601	-48.596	-	59.817
C_3	-	-	-0.195	-0.0685	0.490	-0.360
ε (C_3)	-	-	50.470	-38.316	-	59.817

Table D-14 Measured Strains at Position C, Beam 4 (test 1)

BEAM #	B-4 (L)			B-4(R)		
Strain Gage #	**19**	**20**	**21**	**22**	**23**	**24**
A_1-zero	-0.460	-1.159	-0.926	-	-0.084	-0.471
C_3-zero	-0.459	-1.154	-0.9265	-	-0.081	-0.470
Ave-zero	-0.459	-1.156	-0.926	-	-0.082	-0.471
C_1	-0.469	-1.154	-0.915	-	-0.079	-0.457
ε (C_1)	-18.691	3.738	20.561	-	5.608	26.169
C_2	-0.471	-1.152	-0.914	-	-0.078	-0.455
ε (C_2)	-22.429	7.477	22.430	-	7.477	29.907
C_3	-0.467	-1.152	-0.914	-	-0.077	-0.455
ε (C_3)	-14.018	7.477	22.430	-	9.346	29.907

Table D-15 Measured Strains at Position C, Beam 5 (test 1)

BEAM #	B-5 (L)			B-5 (R)		
Strain Gage #	**25**	**26**	**27**	**28**	**29**	**30**
A_1-zero	-1.337	-0.247	-0.339	-0.812	-0.192	-0.531
C_3-zero	-1.332	-0.242	-0.334	-0.808	-0.188	-0.526
Ave-zero	-1.335	-0.245	-0.336	-0.810	-0.190	-0.528
C_1	-1.335	-0.244	-0.337	-0.810	-0.188	-0.527
ε (C_1)	-	-	-	-	-	-
C_2	-1.333	-0.242	-0.334	-0.808	-0.186	-0.525
ε (C_2)	-	-	-	-	-	-
C_3	-1.331	-0.241	-0.333	-0.807	-0.186	-0.524
ε (C_3)	-	-	-	-	-	-

Table D-16 Measured Strains at Position A, Beam 2 (test 2)

BEAM #	B-2 (L)			B-2 (R)		
Strain Gage #	**7**	**8**	**9**	**10**	**11**	**12**
A_1-zero	-	-	-0.697	0.046	0.304	-0.797
A_1	-	-	-0.689	0.036	0.307	-0.783
ε (A_1)	-	-	14.738	-18.103	5.776	25.692
A_2-zero	-	-	-0.699	0.045	0.304	-0.798
A_2	-	-	-0.689	0.036	0.307	-0.784
ε (A_2)	-	-	19.187	-17.121	6.243	26.299
A_3-ZERO	-	-	-0.697	0.043	0.305	-0.796
A_3	-	-	-0.689	0.035	0.308	-0.784
ε (A_3)	-	-	14.000	-15.346	5.093	22.561

Table D-17 Measured Strains at Position A, Beam 3 (test 2)

BEAM #	B-3 (L)			B-3 (R)		
Strain Gage #	**13**	**14**	**15**	**16**	**17**	**18**
A_1-zero	-	-0.918	-	-0.172	0.692	-0.367
A_1	-	-0.911	-	-0.192	0.684	-0.334
ε (A_1)	-	13.972	-	-38.000	-14.822	62.065
A_2- zero	-	-0.918	-	-0.177	0.657	-0.366
A_2	-	-0.911	-	-0.196	0.654	-0.333
ε (A_2)	-	14.112	-	-36.458	-5.019	62.290
A_3- zero	-	-0.916	-	-0.176	0.643	-0.363
A_3	-	-0.909	-	-0.195	0.644	-0.333
ε (A_3)	-	12.916	-	-34.234	3.336	56.570

Table D-18 Measured Strains at Position A, Beam 4 (test 2)

BEAM #	B-4 (L)			B-4 (R)		
Strain Gage #	**19**	**20**	**21**	**22**	**23**	**24**
A_1-zero [2]	-	-1.093	-	-	-0.106	-0.452
A_1 [3]	-	-1.081	-	-	-0.095	-0.402
ε (A_1) [4]	-	22.617	-	-	19.037	93.290
A_2-zero	-	-1.093	-	-	-0.106	-0.451
A_2	-	-1.081	-	-	-0.095	-0.400
ε (A_2)	-	23.551	-	-	19.131	94.991
A_3-zero	-	-1.091	-	-	-0.104	-0.448
A_3	-	-1.079	-	-	-0.094	-0.398
ε (A_3)	-	23.084	-	-	18.112	92.813

Table D-19 Measured Strains at Position A, Beam 5 (test 2)

BEAM #	B-5 (L)			B-5 (R)		
Strain Gage #	**25**	**26**	**27**	**28**	**29**	**30**
A_1-zero	-1.889	-0.778	-	-0.908	-0.241	-0.192
A_1	-1.918	-0.756	-	-0.927	-0.231	-0.152
ε (A_1)	-54.579	42.187	-	-34.439	17.355	74.551
A_2-zero	-1.904	-0.743	-	-0.898	-0.239	-0.196
A_2	-1.931	-0.735	-	-0.920	-0.230	-0.157
ε (A_2)	-50.280	15.187	-	-40.542	16.112	71.607
A_3-zero	-1.902	-0.738	-	-0.891	-0.237	-0.199
A_3	-1.930	-0.732	-	-0.912	-0.229	-0.159
ε (A_3)	-51.869	12.542	-	-39.972	16.411	76.084

Table D-20 Measured Strains at Position B, Beam 2 (test 2)

BEAM #	B-2 (L)			B-2 (R)		
Strain Gage #	**7**	**8**	**9**	**10**	**11**	**12**
B_1-zero	-	-	-0.698	0.045	0.304	-0.798
B_1	-	-	-0.681	0.028	0.312	-0.766
ε (B_1)	-	-	30.981	-31.991	14.879	60.047
B_2-zero	-	-	-0.698	0.045	0.304	-0.799
B_2	-	-	-0.681	0.028	0.312	-0.766
ε (B_2)	-	-	32.215	-32.364	15.346	61.364
B_3-zero	-	-	-0.698	0.043	0.305	-0.798
B_3	-	-	-0.682	0.027	0.313	-0.765
ε (B_3)	-	-	30.402	-30.804	15.202	60.757

Table D-21 Measured Strains at Position B, Beam 3 (test 2)

BEAM #	B-3 (L)			B-3 (R)		
Strain Gage#	**13**	**14**	**15**	**16**	**17**	**18**
B_1-zero	-	-0.918	-	-0.173	0.677	-0.367
B_1	-	-0.909	-	-0.202	0.675	-0.320
ε (B_1)	-	18.028	-	-54.271	-3.542	88.336
B_2-zero	-	-0.918	-	-0.176	0.649	-0.366
B_2	-	-0.908	-	-0.204	0.654	-0.319
ε (B_2)	-	19.112	-	-51.654	9.178	87.804
B_3-zero	-	-0.917	-	-0.177	0.635	-0.365
B_3	-	-0.907	-	-0.204	0.645	-0.318
ε (B_3)	-	18.692	-	-51.402	17.782	87.153

Table D-22 Measured Strains at Position B, Beam 4 (test 2)

BEAM #	B-4 (L)			B-4 (R)		
Strain Gage #	**19**	**20**	**21**	**22**	**23**	**24**
B_1-zero	-	-1.093	-	-	-0.105	-0.451
B_1	-	-1.084	-	-	-0.097	-0.411
ε (B_1)	-	18.037	-	-	15.495	73.692
B_2-zero	-	-1.093	-	-	-0.105	-0.449
B_2	-	-1.084	-	-	-0.097	-0.411
ε (B_2)	-	17.290	-	-	15.729	72.000
B_3-zero	-	-1.091	-	-	-0.104	-0.446
B_3	-	-1.082	-	-	-0.096	-0.407
ε (B_3)	-	17.726	-	-	16.255	72.299

Table D-23 Measured Strains at Position B, Beam 5 (test 2)

BEAM #	B-5 (L)			B-5 (R)		
Strain Gage #	**25**	**26**	**27**	**28**	**29**	**30**
B_1-zero	-1.894	-0.745	-	-0.904	-0.240	-0.192
B_1	-1.910	-0.743	-	-0.908	-0.237	-0.179
ε (B_1)	-29.159	3.766	-	-	-	-
B_2-zero	-1.904	-0.740	-	-0.896	-0.238	-0.198
B_2	-1.913	-0.739	-	-0.901	-0.236	-0.187
ε (B_2)	-16.168	3.318	-	-8.645	3.850	20.963
B_3-zero	-1.904	-0.738	-	-0.889	-0.237	-0.199
B_3	-1.912	-0.736	-	-0.894	-0.235	-0.188
ε (B_3)	-15.452	2.950	-	-9.860	3.794	20.891

Table D-24 Measured Strains at Position C, Beam 2 (test 2)

BEAM #	B-2 (L)			B-2 (R)		
Strain Gage #	**7**	**8**	**9**	**10**	**11**	**12**
C_1-zero	-	-	-0.698	0.045	0.304	-0.799
	-	-	-0.676	0.021		-0.749
	-	-	42.402		22.888	92.579
	-	-	-0.698		0.304	-0.799
C_2	-		-0.675		0.316	
ε (C_2)	-	-		-43.944	23.364	91.963
	-	-		0.044	0.305	-0.798
C_3		-		0.021		-0.749
ε (C_3)	-		42.051	-44.220	23.402	91.930

Table D-25 Measured Strains at Position C, Beam 3 (test 2)

BEAM #				B-3 (R)		
Strain Gage #	**13**	**14**		**16**	**17**	**18**
C_1-zero		-0.918		-0.176		-0.366
C_1	-		-	-0.198	0.664	-0.329
ε (C)	-		-		-3.551	69.234
C_2-zero	-	-0.918	-	-0.176	0.642	-0.366
C_2	-		-	-0.197	0.650	-0.330
ε (C_2)		14.252	-	-37.925	15.271	67.757
C_3-zero	-	-0.917	-	-0.176	0.635	-0.365
C_3	-	-0.909	-	-0.197	0.643	-0.328
ε (C_3)	-	14.262	-	-40.364		69.005

Table D-26 Measured Strains at Position C, Beam 4 (test 2)

BEAM #	B-4 (L)			B-4 (R)		
Strain Gage #	19	20	21	22	23	24
C_1-zero	-	-1.093	-	-	-0.106	-0.451
C_1	-	-1.090	-	-	-0.101	-0.433
ε (C_1)	-	5.514	-	-	7.636	31.916
C_2-zero	-	-1.092	-	-	-0.105	-0.449
C_2	-	-1.089	-	-	-0.101	-0.432
ε (C_2)	-	6.729	-	-	8.019	31.290
C_3-zero	-	-1.091	-	-	-0.104	-0.446
C_3	-	-1.087	-	-	-0.100	-0.430
ε (C_3)	-	6.121	-	-	7.715	30.224

Table D-27 Measured Strains at Position C, Beam 5 (test 2)

BEAM #	B-5 (L)			B-5 (R)		
Strain Gage #	25	26	27	28	29	30
C_1-zero	-1.906	-0.744	-	-0.901	-0.240	-0.193
C_1	-1.906	-0.743	-	-0.899	-0.239	-0.192
ε (C_1)	-	-	-	-	-	-
C_2-zero	-1.903	-0.739	-	-0.893	-0.238	-0.199
C_2	-1.903	-0.738	-	-0.893	-0.237	-0.196
ε (C_2)	-	-	-	-	-	-
C_3-zero	-1.902	-0.737	-	-0.885	-0.236	-0.200
C_3	-1.903	-0.736	-	-0.885	-0.236	-0.197
ε (C_3)	-	-	-	-	-	-

Table D-28 Measured Strains at Position A, Beam 2 (test 3)

BEAM #	B-2 (L)			B-2 (R)		
Strain Gage #	**7**	**8**	**9**	**10**	**11**	**12**
A_1 -zero	-	-	-0.582	-	0.378	-0.759
A_1	-	-	-0.575	-	0.381	-0.747
ε (A_1)	-	-	13.047	-	5.589	22.814
A_2- zero	-	-	-0.583	-	0.378	-0.756
A_2	-	-	-0.575	-	0.382	-0.745
ε (A_2)	-	-	16.337	-	-	-
A_3- zero	-	-	-0.584	-	0.380	-0.759
A_3	-	-	-0.577	-	0.382	-0.748
ε (A_3)	-	-	11.832	-	4.430	20.842

Table D-29 Measured Strains at Position A, Beam 3 (test 3)

BEAM #	B-3 (L)			B-3 (R)		
Strain Gage #	**13**	**14**	**15**	**16**	**17**	**18**
A_1 -zero	-	-0.689	-	0.250	-	-3.047
A_1	-	-0.682	-	0.226	-	-3.013
ε (A_1)	-	11.720	-	-44.755	-	62.621
A_2-zero		-0.689	-	0.225	-	
A_2	-	-0.682	-	0.205	-	-2.998
ε (A_2)	-	12.692	-	-36.223	-	58.134
A_3-zero	-	-0.688	-	0.216	-	-3.021
A_3	-	-0.683	-	0.198	-	-2.993
ε (A_3)	-	10.355	-	-32.831	-	52.246

Table D-30 Measured Strains at Position A, Beam 4 (test 3)

BEAM #	B-4 (L)			B-4 (R)		
Strain Gage #	**19**	**20**	**21**	**22**	**23**	**24**
A_1 -zero	-	-1.151	-	-	-0.227	-1.084
A_1	-	-1.140	-	-	-0.218	-1.042
ε (A_1)	-	19.533	-	-	15.851	78.792
A_2-zero	-	-1.149	-	-	-0.226	-1.080
A_2	-	-1.140	-	-	-0.217	-1.037
ε (A_2)	-	17.384	-	-	15.785	79.913
A_3-zero	-	-1.149	-	-	-0.225	-1.075
A_3	-	-1.140	-	-	-0.217	-1.034
ε (A_3)	-	16.636	-	-	15.168	75.894

Table D-31 Measured Strains at Position A, Beam 5 (test 3)

BEAM #	B-5 (L)			B-5 (R)		
Strain Gage #	**25**	**26**	**27**	**28**	**29**	**30**
A_1 -zero	-1.352		-		-0.454	
A	-1.374	-0.365	-	-	-0.453	-0.778
ε (A_1)	-41.120	9.122	-	-	2.028	66.126
A	-1.352	-0.368	-	-	-0.455	-0.809
A_2	-1.374	-0.364	-	-	-0.454	-0.772
ε (A_2)	-40.279		-	-		68.977
A_3-zero	-1.353		-	-	-0.461	
A_3	-1.375	-0.362		-		-0.765
ε (A_3)	-41.400	7.991	-	-	7.290	

Table D-32 Measured Strains at Position B, Beam 2 (test 3)

BEAM #	B-2 (L)			B-2 (R)		
Strain Gage #	7	8	9		11	12
B_1 -zero	-	-		-	0.378	-0.759
B_1	-	-		-	0.385	-0.731
ε (B_1)	-	-	25.290	-	12.851	52.171
B_2-zero	-	-	-0.582	-	0.379	-0.758
B_2	-	-	-0.569	-	0.386	-0.731
ε (B_2)	-	-		-	12.614	
B_3-zero	-	-		-	0.378	-0.760
B_3	-	-		-	0.385	-0.728
	-	-	29.861	-	13.841	60.004

Table D-33 Measured Strains at Position B, Beam 3 (test 3)

BEAM #	B-3 (L)			B-3 (R)		
Strain Gage#	13	14		16	17	18
B_1 -zero	-	-0.689	-	0.239	-	-3.038
B_1	-		-	0.213	-	-2.998
ε (B_1)	-		-	-48.988	-	76.361
B_2-zero	-	-0.688		0.221	-	
B_2		-0.680	-	0.197	-	-2.987
ε (B_2)	-		-	-44.842	-	74.430
B_3-zero	-		-	0.212	-	-3.019
B_3	-		-	0.185	-	-2.972
ε (B_3)	-	20.057		-49.941	-	87.298

Table D-34 Measured Strains at Position B, Beam 4 (test 3)

BEAM #	B-4 (L)			B-4 (R)		
Strain Gage #	19	20	21		23	
B_1 -zero	-		-	-	-0.226	-1.081
B_1	-	-1.143	-	-	-0.220	-1.051
ε (B_1)	-	12.804	-	-	12.458	55.704
B_2-zero	-	-1.149	-	-	-0.226	-1.078
B	-	-1.142	-	-		-1.047
ε (B_2)	-	13.022	-	-	11.826	58.010
B_3-zero	-	-1.149		-		-1.073
	-	-1.141	-	-	-0.217	-1.038
ε (B_3)	-	15.234	-	-	15.626	65.986

Table D-35 Measured Strains at Position B, Beam 5 (test 3)

BEAM #	B-5 (L)			B-5 (R)		
	25	26	27	28	29	30
B_1 -zero	-1.353	-0.369	-	-	-0.456	-0.809
B_1	-1.360	-0.368	-		-0.457	-0.799
ε (B_1)	-13.084	2.178	-	-	-2.907	19.019
	-1.353	-0.368	-	-	-0.456	-0.802
B_2	-1.360	-0.366	-	-	-0.455	-0.791
	-12.710	2.520	-	-	0.636	21.029
B_3-zero	-1.354	-0.366	-	-	-0.463	-0.797
	-1.362	-0.365	-	-	-0.462	-0.786
ε (B_3)	-14.299	1.430	-		1.879	20.888

Table D-36 Measured Strains at Position C, Beam 2 (test 3)

BEAM #	B-2(L)			B-2(R)		
Strain Gage #	**7**	**8**	**9**	**10**	**11**	**12**
C_1 -zero	-	-	-0.582	-	0.379	-0.759
C_1	-	-	-0.565	-	0.388	-0.720
ε (C_1)	-	-	32.581	-	17.898	72.959
C_2-zero	-	-	-0.583	-	0.380	-0.758
C_2	-	-	-0.565	-	0.389	-0.718
ε (C_2)	-	-	33.067	-	17.739	75.006
C_3-zero	-	-	-0.589	-	0.374	-0.766
C	-	-	-0.577	-	0.359	-0.742
ε (C_3)	-	-	23.888	-	-	-

Table D-37 Measured Strains at Position C, Beam 3 (test 3)

BEAM #	B-3 (L)			B-3 (R)		
	13	**14**	**15**	**16**	**17**	**18**
C_1 -zero	-	-0.688	-	0.233	-	-3.035
C	-	-0.683	-	0.211	-	
ε (C_1)	-	10.365	-	-41.232	-	56.732
C_2-zero	-	-0.688	-	0.218		-3.023
C_2	-	-0.683	-	0.200	-	
ε (C_2)	-	10.458	-	-32.989	-	57.574
C_3-zero	-	-0.693	-	0.206	-	-3.020
C_3	-	-0.692	-	0.184	-	-3.028
ε (C_3)	-	0.748	-	-	-	-

Table D-38 Measured Strains at Position C, Beam 4 (test 3)

BEAM #	B-4 (L)			B-4 (R)		
Strain Gage #	19		21	22	23	24
C_1 -zero	-	-1.150	-	-	-0.226	-1.080
C_1	-	-1.147	-	-	-0.223	
ε (C_1)	-	4.579	-	-	5.224	
C_2-zero	-	-1.149	-	-	-0.225	-1.076
C_2	-	-1.147	-	-	-0.223	-1.063
ε (C_2)	-	3.458	-	-	5.075	25.047
C_3-zero	-	-1.151	-	-	-0.228	-1.075
C_3	-	-1.186	-	-	-0.263	-1.101
ε (C_3)	-	-64.668	-	-	-	-

Table D-39 Measured Strains at Position C, Beam 5 (test 3)

BEAM #	B-5 (L)			B-5 (R)		
	25	26	27		29	30
C_1 -zero	-1.353	-0.368	-		-0.459	-0.808
C_1	-1.353	-0.368	-		-0.456	-0.806
ε (C_1)	-1.215	0.981	-	-		-
C_2-zero	-1.352	-0.367	-		-0.454	-0.798
C_2	-1.353	-0.366	-	-	-0.456	-0.795
ε (C_2)	-1.963	1.224	-		-	-
C_3-zero	-1.357	-0.369	-	-	-0.461	-0.798
C_3	-1.395	-0.404	-	-	-0.510	-0.831
ε (C_3)	-	-	-	-	-	-

The following apply to Tables (D-40) to (D-45):

- **N-A** Location = the height from top face of the bottom flange, mm
- Since each test was repeated three times, $\mathbf{A_i}$, $\mathbf{B_i}$ or $\mathbf{C_i}$ (**i** = 1, 2 or 3) references the neutral axis location obtained from the (**i**)th record at location A, B or C, respectively.
- The complete set of raw data from both sides of the web is available only in Beam 5.
- **"-"** implies result unavailable.

Table D-40 Results of Neutral Axis Location for Exterior Beams
(Test 1, 11-13-2001)

BEAM #	B-1	B-5 (R)	B-5 (L)	AVERAGE (1, 5)
A_1	-	-	-	
A_2	-	353.08	339.12	
A_3	-	363.48	347.42	
B_1	322.33	419.96	353.24	
B_2	409.31	415.13	355.42	
B_3	-	450.82		
C_1	327.46	-	-	
C	359.23		-	
C_3	373.35	-	-	
AVERAGE (A)		358.28	343.27	350.78
AVERAGE (B)	365.82	428.64	367.78	
AVERAGE (C)	353.35	-	-	353.35
AVERAGE (A, B, C)	359.58	393.46	355.53	362.05
FINAL			***362.05***	

Table D-41 Results of Neutral Axis Location for Exterior Beams

(Test 2 02-15-2002)

BEAM #		B-5 (R)	B-5 (L)	AVERAGE (1, 5)
A_1	-	387.14		
A_2	-	366.86	352.98	
	-	372.93	342.30	
B	-	-	319.29	
B_2		389.98	335.29	
B_3	-	378.22		
C_1	-	-	-	
	361.74	-	-	
C_3	305.45	-	-	
AVERAGE (A)	-	375.64	368.90	
AVERAGE (B)	-	384.10	329.01	356.56
AVERAGE (C)	333.60	-	-	333.60
AVERAGE (A, B, C)	333.60	379.03		354.14
FINAL			***354.14***	

Table D-42 Results of Neutral Axis Location for Exterior Beams
(Test 3, 03-21-2002)

BEAM #	B-1	B-5 (R)	B-5 (L)	AVERAGE (1, 5)
A	-	295.58	338.53	
	-	289.33	333.57	
A	-	326.01	332.87	
B_1	-		327.39	
B_2	-	295.44	333.92	
B_3	-	314.82	312.56	
	-	-	414.53	
C	-	-	396.58	
C_3	-		-	
AVERAGE (A)	-	303.64	334.99	319.32
AVERAGE (B)	-	286.26	324.62	305.44
AVERAGE (C)		-	405.56	405.56
AVERAGE (A, B, C)	-	294.95		343.44
FINAL			***343.44***	

Table D-43 Results of Neutral Axis Location for Interior Beams

(Test 1, 11-13-2001)

BEAM #	B-2	B-3	B-4	AVERAGE (2-4)
A	433.84	-	-	
A_2	411.16		331.74	
A_3	447.59	320.52		
B_1	398.63	308.02	343.09	
	412.82	307.76	323.20	
B	440.81	333.97	339.12	
C_1	397.24		313.62	
C_2	416.47	316.17		
C_3	429.53	349.29	368.89	
	430.86	315.67	326.75	357.76
AVERAGE (B)	417.42		335.14	356.38
AVERAGE (C)	414.86	320.62	333.24	356.24
AVERAGE (A, B, C)	421.05	317.62	331.71	356.79
FINAL			***356.79***	

Table D-44 Results of Neutral Axis Location for Interior Beams

(Test 2, 02-15-2002)

BEAM #		B-3	B-4	AVERAGE (2-4)
A_1	344.64	-		
A_2	354.22	325.07	358.77	
	348.41	339.99	355.98	
B	375.61	326.29	362.80	
B_2		348.26	366.60	
B_3	380.71	360.31		
C_1	386.25	326.03	376.61	
	386.83	368.03	385.24	
C	386.28	362.60	384.71	
AVERAGE (A)	349.09		358.24	346.62
AVERAGE (B)	377.73	344.95	366.34	363.01
	386.45	352.22	382.19	373.62
AVERAGE (A, B, C)	371.09		368.92	361.08
FINAL			***361.08***	

Table D-45 Results of Neutral Axis Location for Interior Beams

(Test 3, 03-21-2002)

BEAM #	B-2		B-4	AVERAGE (2-4)
A_1	379.47	334.18		
A_2	-	353.05	357.04	
	363.85	351.90	358.08	
B	380.15	349.08	369.05	
B_2	378.93		359.87	
B_3	372.42	364.50		
C_1	379.64	331.85	370.32	
	375.26	364.29	359.31	
C	-	-	-	
AVERAGE (A)	371.66	346.38		358.66
	377.17		368.11	367.45
	377.45	348.07	364.82	363.45
AVERAGE (A,B,C)	375.43		363.62	363.18
FINAL			***363.18***	

The following notation shall apply to Tables (D-46) to (D-48):

- **B-i** - beam # i. (i = 1, 2 … 5)
- **ε (A_j) / (B_j) / (C_j)** - the strain recorded when the truck stopped at Location #A / B / C.

  (**j** = 1, 2 or 3, which means the (**j**)th record at each location.)
- **Mj** - the corresponding moment at point P (see Figure 11) of beam #1 to #5 for each truck location. (**j** = 1, 2 or 3, which means the (**j**)th record at each location.). **M** shall be taken as:

  M = εES

  where:

  E - Young's modulus of steel = 29000 KSI

  S - elastic section modulus, IN^3
- **"-"** - The result is either bad or unavailable.

Table D-46 Moments at Point P for Interior Beams in Test 1

BEAM #	B-1	B-2	B-3	B-4	B-5
1		-	-	-	-
	-		58.883	86.924	73.838
M2=εES	-	1268303.156	2102797.708	3104209.026	2377514.337
		42.058	60.284	86.924	77.109
M3=εES	-	1501965.202	2152847.740		2482854.282
		59.817	79.446	63.556	20.561
M1=εES	541688.487	2136170.348	2837156.485	2269696.619	662049.396
ε (B_2)	18.692	73.838		62.154	21.496
M2=εES	601868.942	2636884.935	2853833.877	2219628.731	
		79.446	80.848	64.023	24.767
M3=εES	-	2837156.485	2887224.372	2286374.010	797479.568
ε (C)		89.728	51.405	23.365	-
M1=εES	2407604.564	3204344.801	1835745.167	834405.272	-
		100.945	54.209	26.169	-
M2=εES	2527997.672	3604923.613	1935898.798	934523.192	-
		105.619	54.994	26.169	-
M3=εES	2588210.326		1963914.674	934523.192	-

Table D-47 Moments at Point P for Interior Beams in Test 2

BEAM #	B-1	B-2	B-3		B-5
ε (A_1)	-	20.215	62.065	93.290	74.551
M1 = εES	-	721913.228	2216450.384	3331550.090	2400488.523
ε (A_2)	-	22.743	62.290	94.991	
M2 = εES	-	812192.558	2224485.530	3392295.794	2305693.843
ε (A_3)	-	18.281	56.570	92.813	76.084
M3 = εES	-	652828.829	2020214.263	3314515.581	
ε (B_1)	-		88.336	73.692	-
	-	1625385.045	3154634.031	2631671.018	-
ε (B_2)	-	46.790	87.804	72.000	20.963
	-	1670935.395	3135635.375	2571246.720	674993.507
	-	45.580	87.153	72.299	20.891
M3 = εES	-	1627724.165	3112387.019	2581924.536	672675.159
	-	67.491	69.234	31.916	-
M1 = εES	-	2410204.538	2472467.992	1139776.532	-
ε (C_2)	-	67.370	67.757	31.290	-
M2 = εES	-	2405883.415	2419721.722	1117420.970	-
ε (C_3)	-	66.991	69.005	30.224	-
M3 = εES		2392348.658	2464289.999	1079352.234	-

Table D-48 Moments at Point P for Interior Beams in Test 3

BEAM #	B-1	B-2	B-3	B-4	B-5
ε (A_1)	-	17.931	62.621	78.792	66.126
M1 = εES	-	640329.713	2236306.123	2813800.994	2129209.589
ε (A_2)	-	16.337	58.134	79.913	68.977
M2 = εES	-	583423.023	2076067.456	2853833.877	2221009.737
ε (A_3)	-	16.337	52.246	75.894	60.163
M3 = εES	-	583423.023	1865796.613	2710308.313	1937205.283
ε (B_1)	-	38.731	76.361	55.704	19.019
M1 = εES	-	1383134.321	2726985.705	1989287.879	612398.106
ε (B_2)	-	38.179	74.430	58.010	21.029
M2 = εES	-	1363439.285	2658026.297	2071639.198	677118.659
ε (B_3)	-	44.933	87.298	65.986	20.888
M3 = εES	-	1604618.656	3117565.224	2356476.195	672578.561
ε (C_1)	-	52.770	56.732	23.085	-
M1 = εES	-	1884509.575	2025999.568	824405.980	-
ε (C_2)	-	54.037	57.574	25.047	-
M2 = εES	-	1929738.519	2056068.870	894472.453	-
ε (C_3)	-	23.888	-	-	-
M3 = εES	-	853082.523	-	-	-

Appendix E

Figures

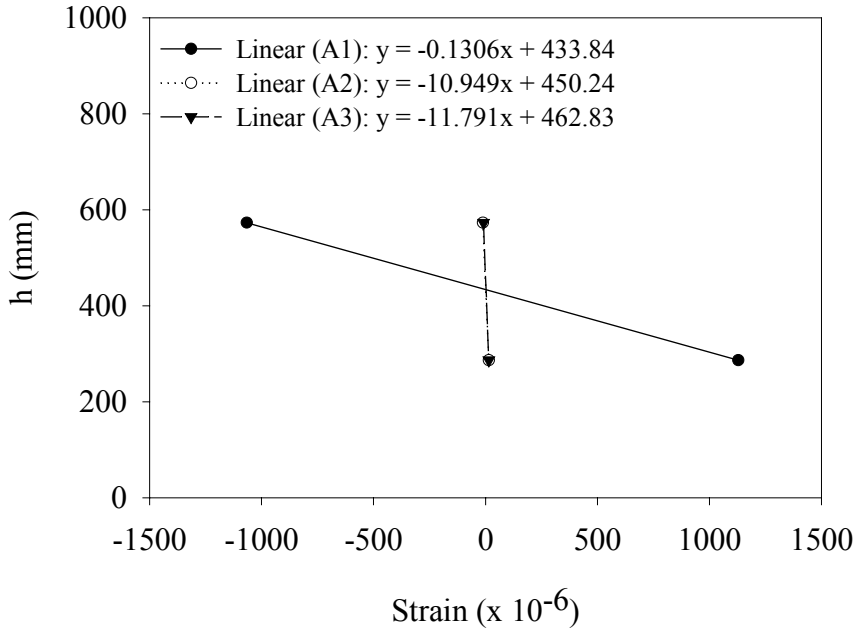

Figure E-1 Web Height (h) vs. Strain, Beam 2 (L), Test 1 (Position A)

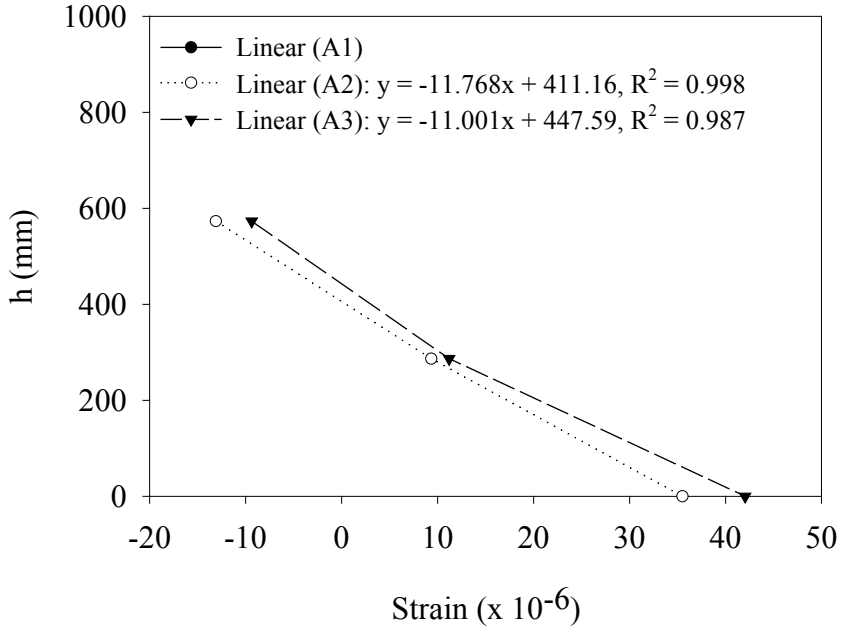

Figure E-2 Web Height (h) vs. Strain, Beam 2 (R), Test 1 (Position A)

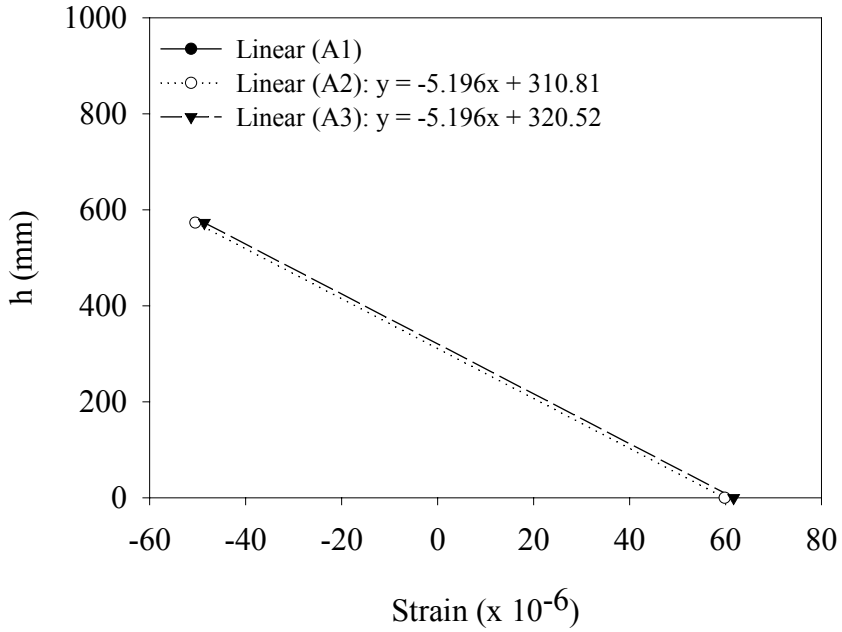

Figure E-3 Web Height (h) vs. Strain, Beam 3 (R), Test 1 (Position A)

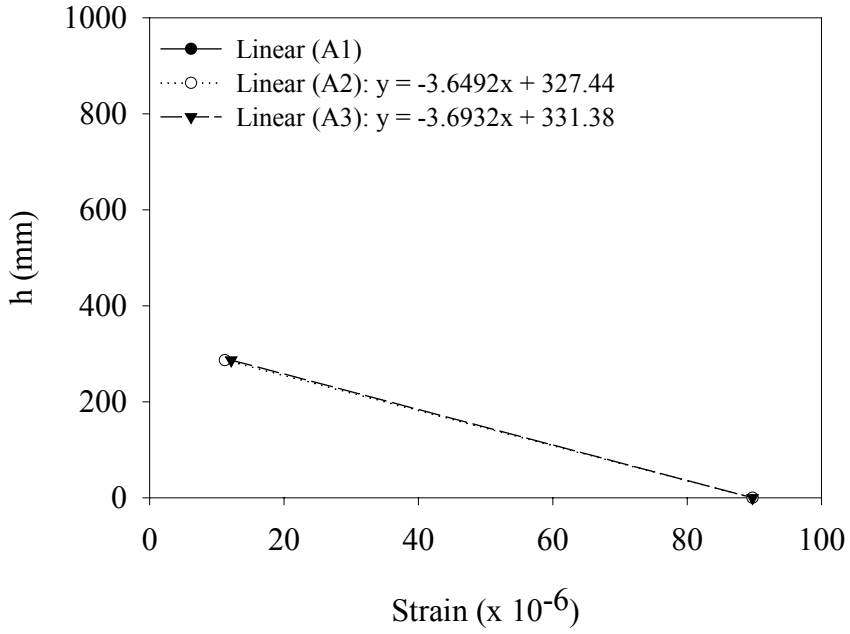

Figure E-4 Web Height (h) vs. Strain, Beam 4 (L), Test 1 (Position A)

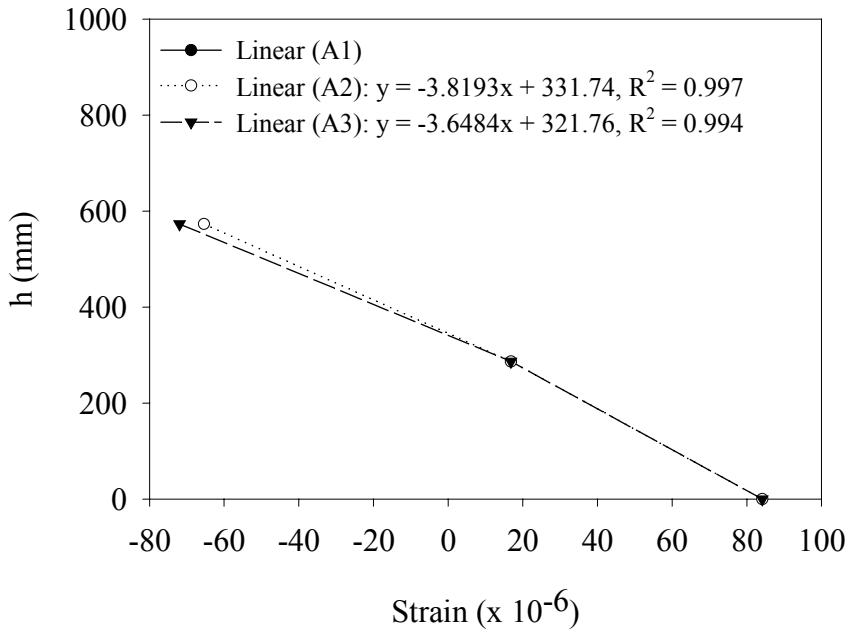

Figure E-5 Web Height (h) vs. Strain, Beam 4 (R), Test 1 (Position A)

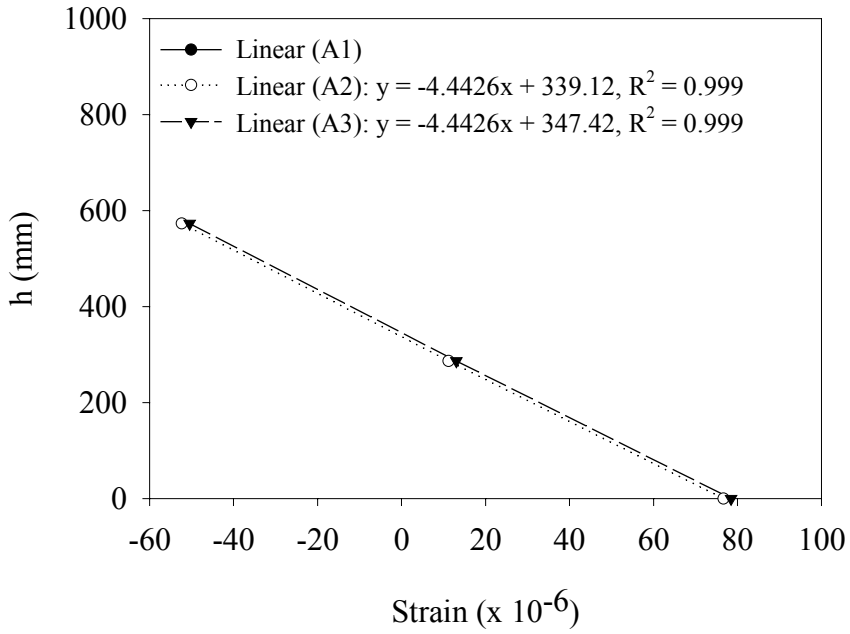

Figure E-6 Web Height (h) vs. Strain, Beam 5 (L), Test 1 (Position A)

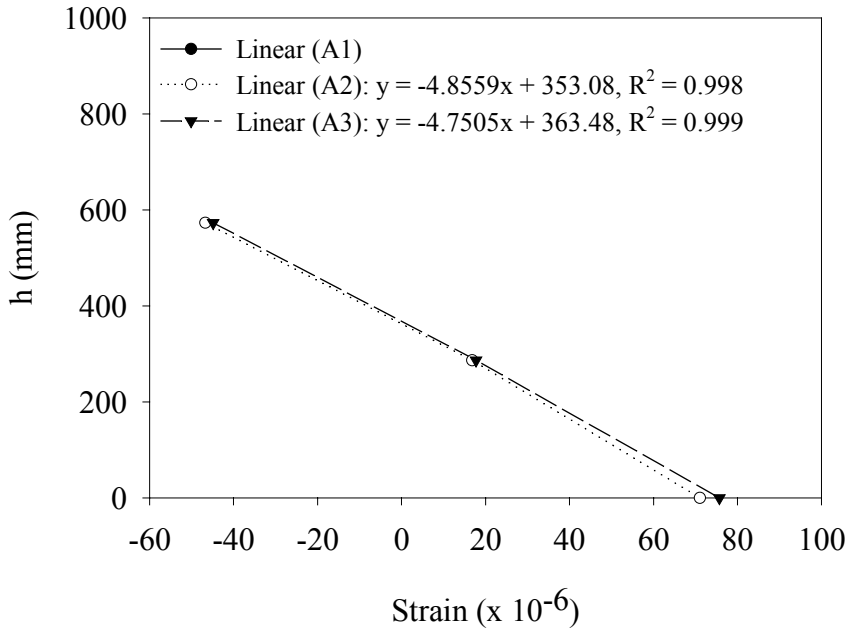

Figure E-7 Web Height (h) vs. Strain, Beam 5 (R), Test 1 (Position A)

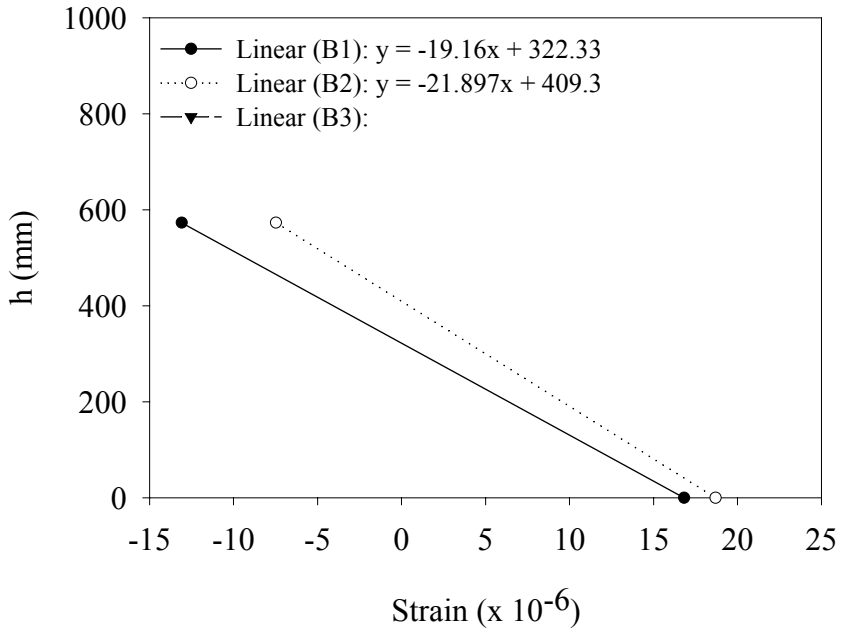

Figure E-8 Web Height (h) vs. Strain, Beam 1 (L), Test 1 (Position B)

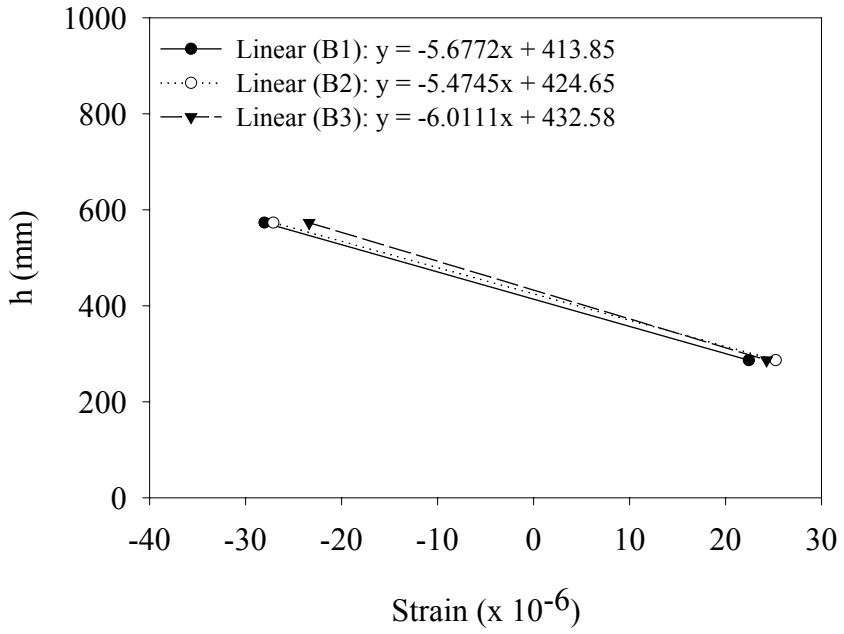

Figure E-9 Web Height (h) vs. Strain, Beam 2 (L), Test 1 (Position B)

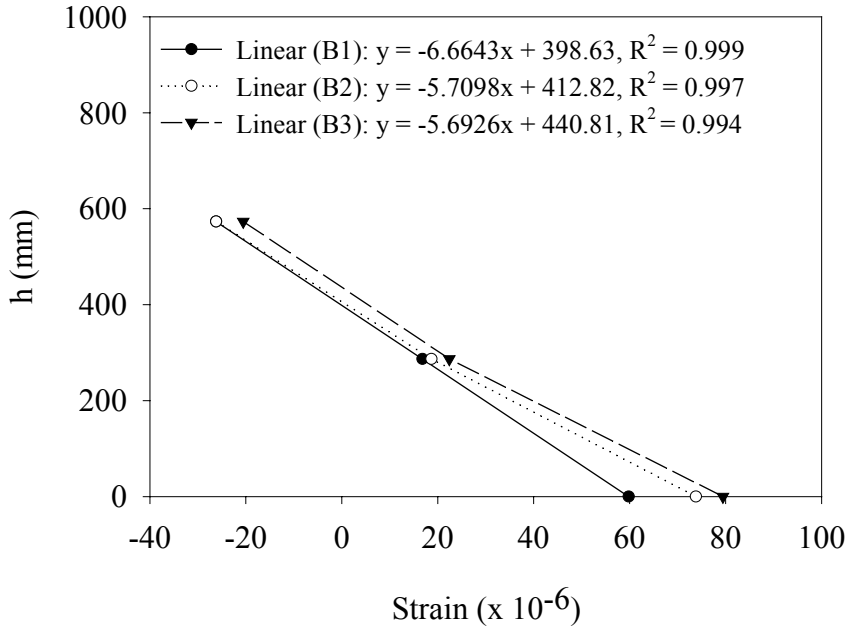

Figure E-10 Web Height (h) vs. Strain, Beam 2 (R), Test 1 (Position B)

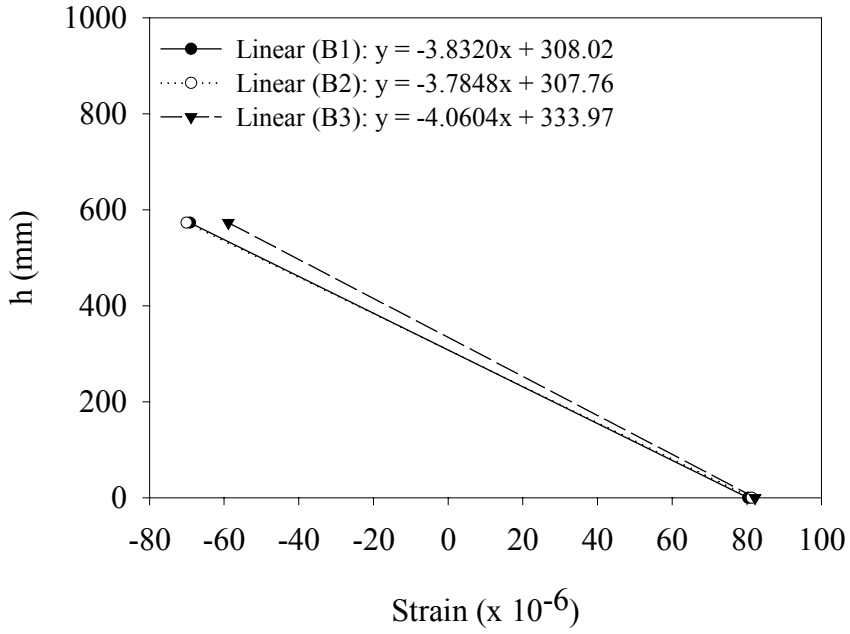

Figure E-11 Web Height (h) vs. Strain, Beam 3 (R), Test 1 (Position B)

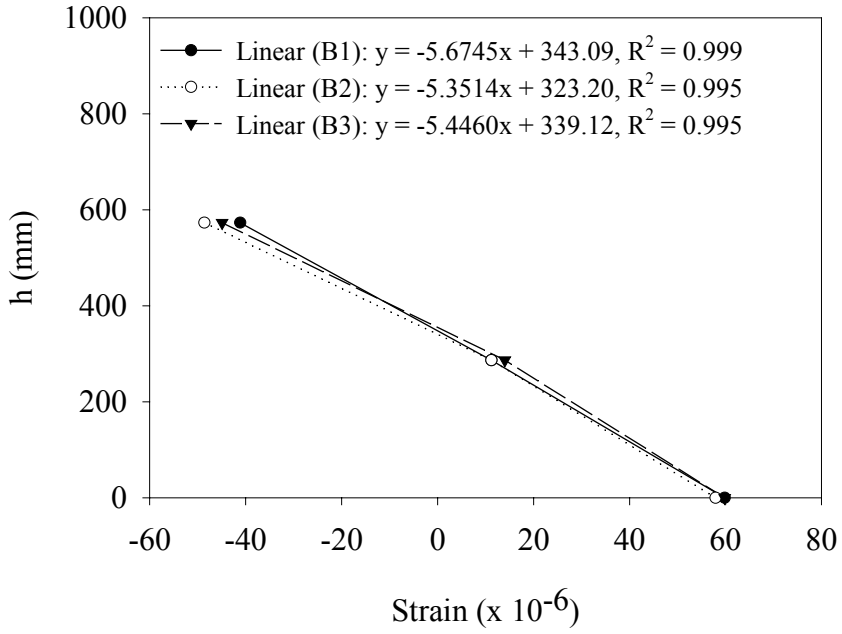

Figure E-12 Web Height (h) vs. Strain, Beam 4 (L), Test 1 (Position B)

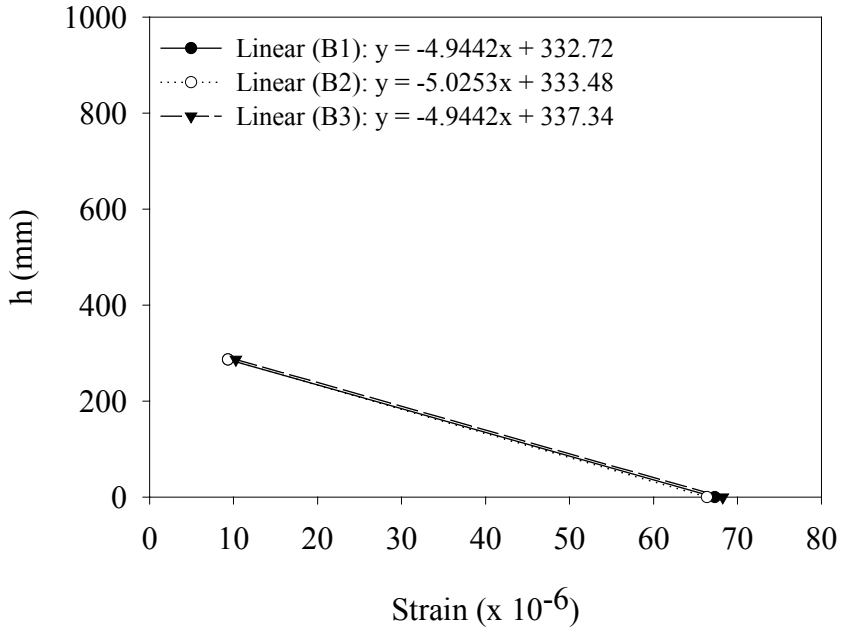

Figure E-13 Web Height (h) vs. Strain, Beam 4 (R), Test 1 (Position B)

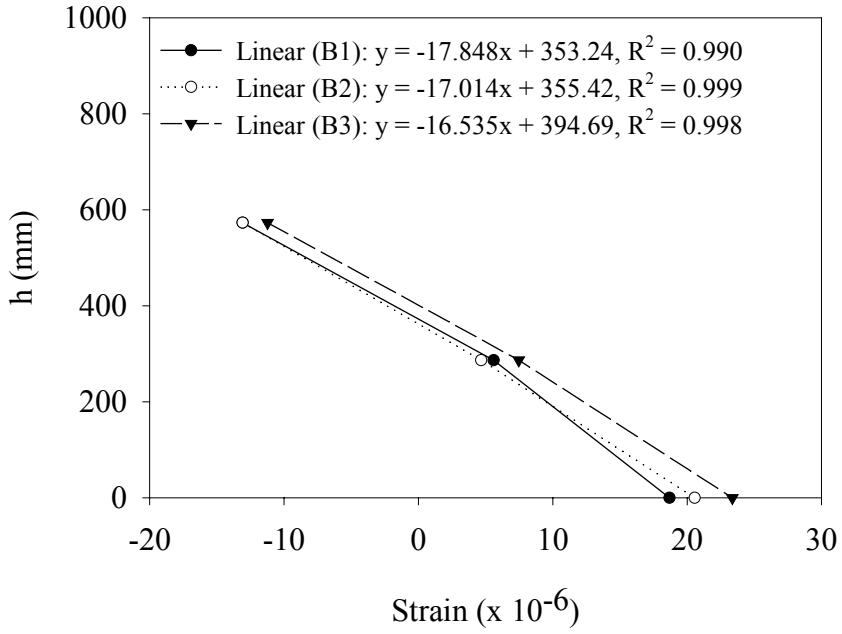

Figure E-14 Web Height (h) vs. Strain, Beam 5 (L), Test 1 (Position B)

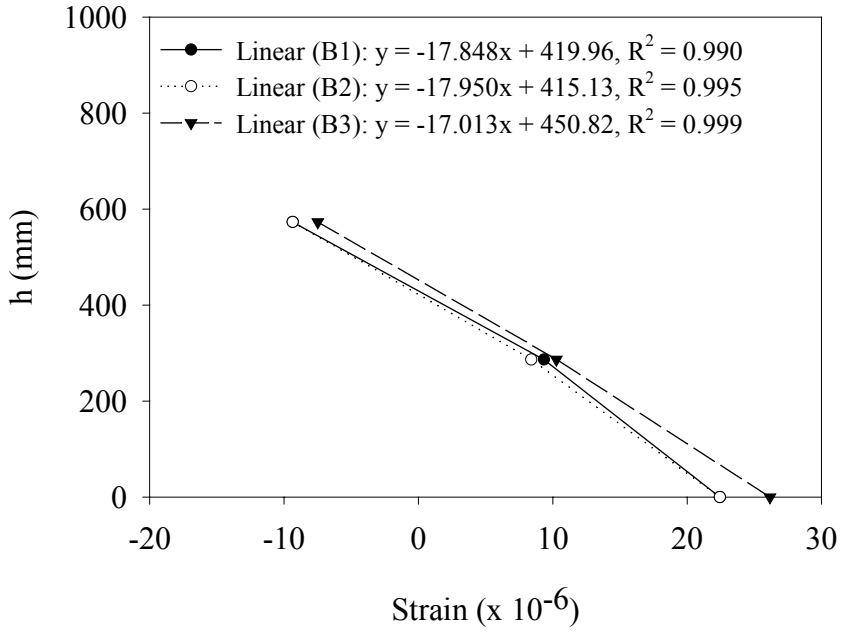

Figure E-15 Web Height (h) vs. Strain, Beam 5 (R), Test 1 (Position B)

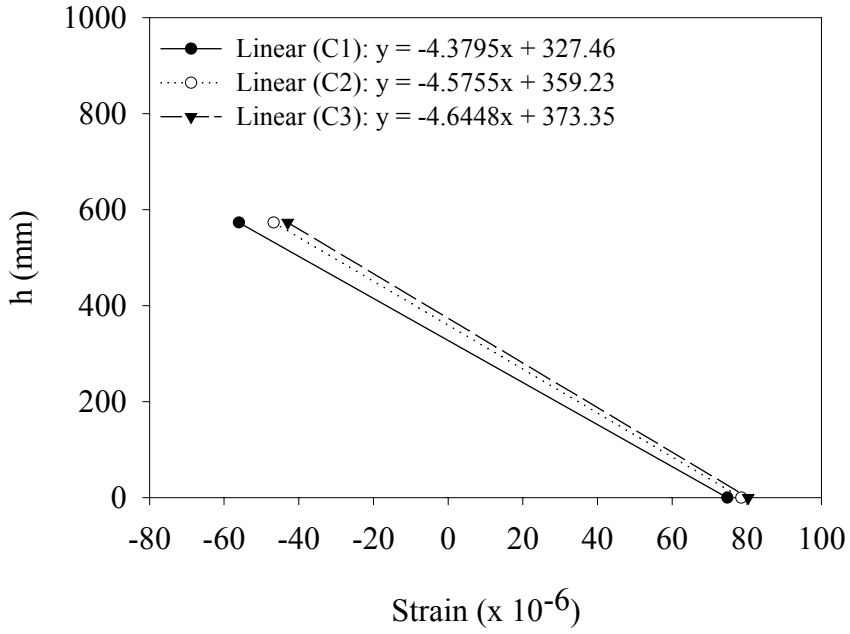

Figure E-16 Web Height (h) vs. Strain, Beam 1 (L), Test 1 (Position C)

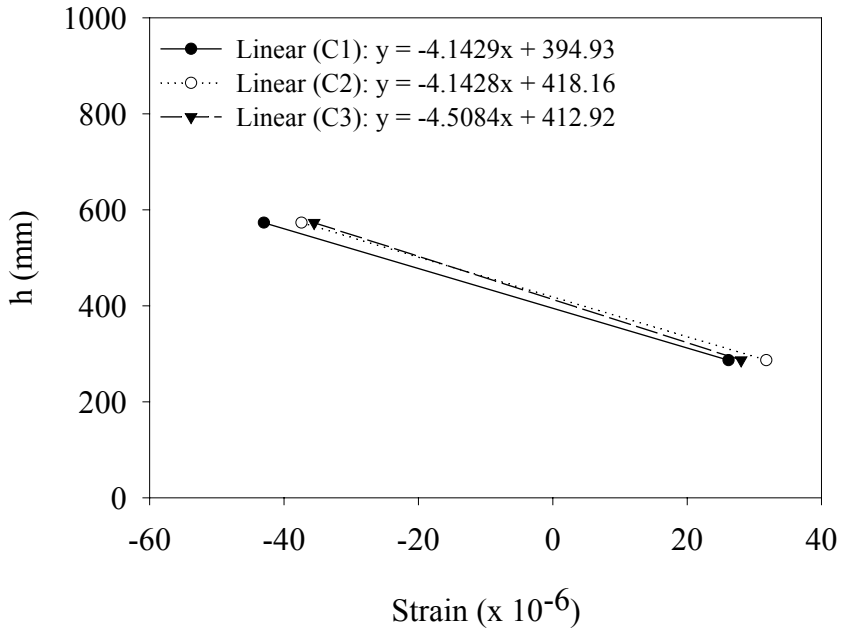

Figure E-17 Web Height (h) vs. Strain, Beam 2 (L), Test 1 (Position C)

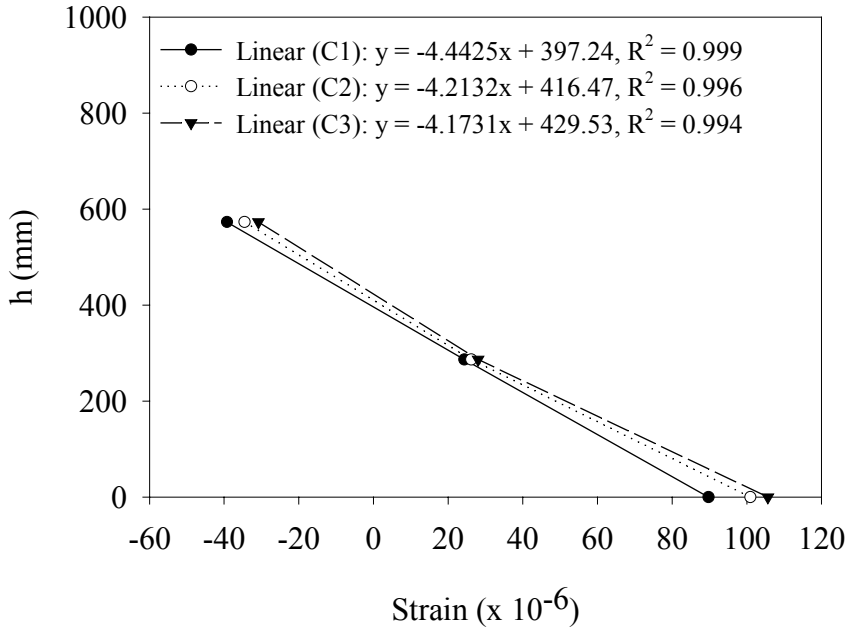

Figure E-18 Web Height (h) vs. Strain, Beam 2 (R), Test 1 (Position C)

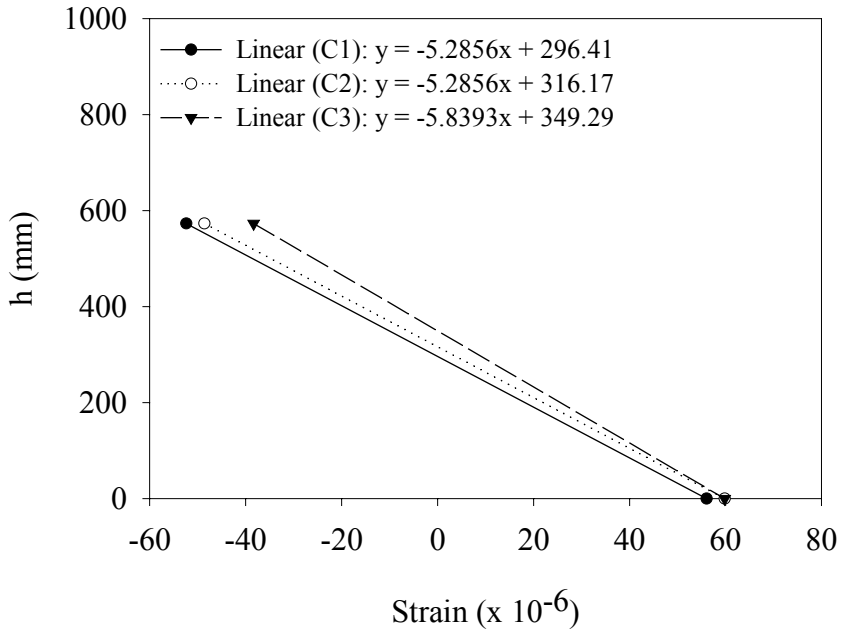

Figure E-19 Web Height (h) vs. Strain, Beam 3 (R), Test 1 (Position C)

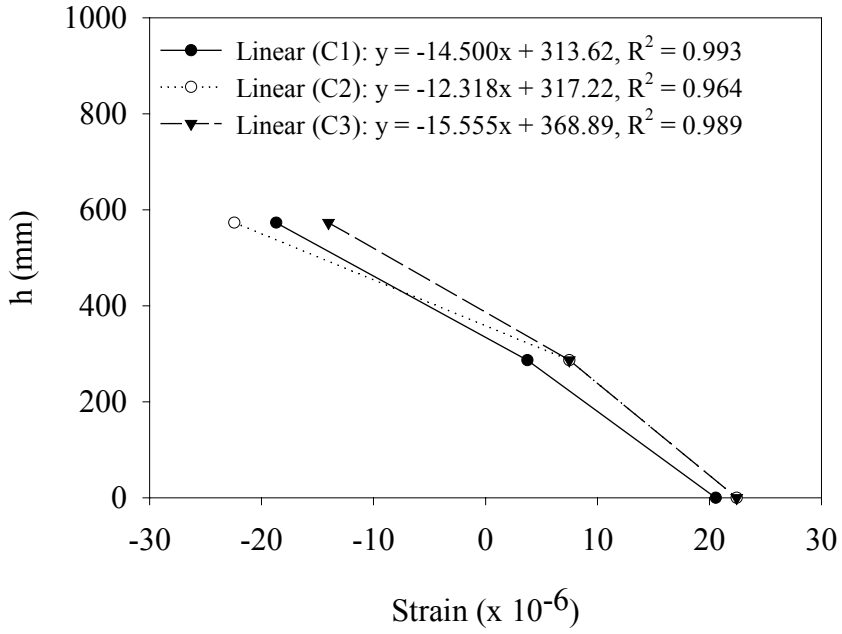

Figure E-20 Web Height (h) vs. Strain, Beam 4 (L), Test 1 (Position C)

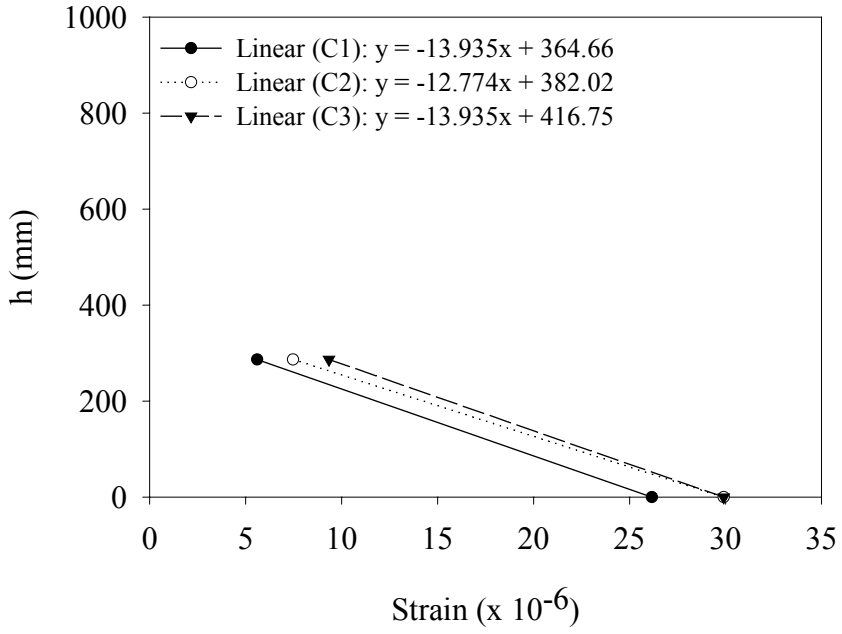

Figure E-21 Web Height (h) vs. Strain, Beam 4 (R), Test 1 (Position C)

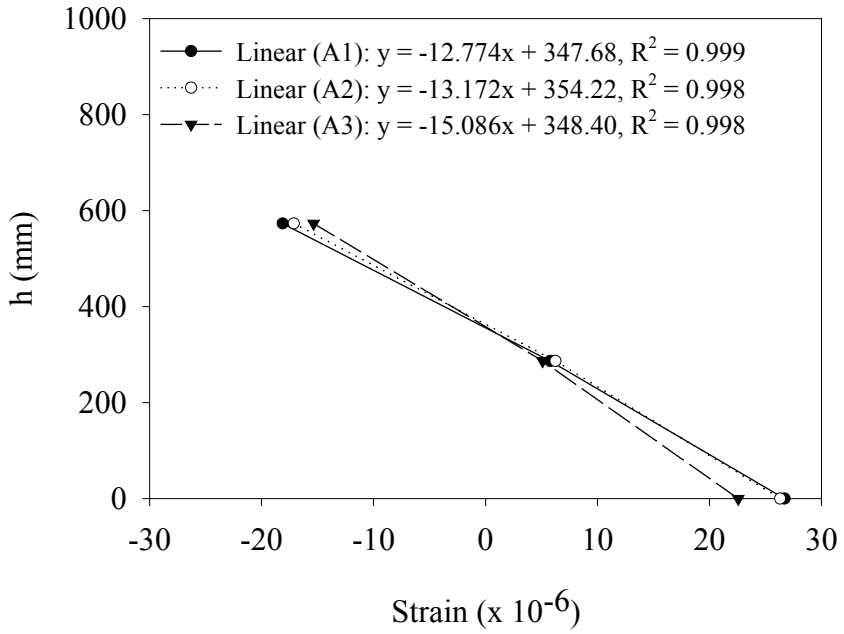

Figure E-22 Web Height (h) vs. Strain, Beam 2 (R), Test 2 (Position A)

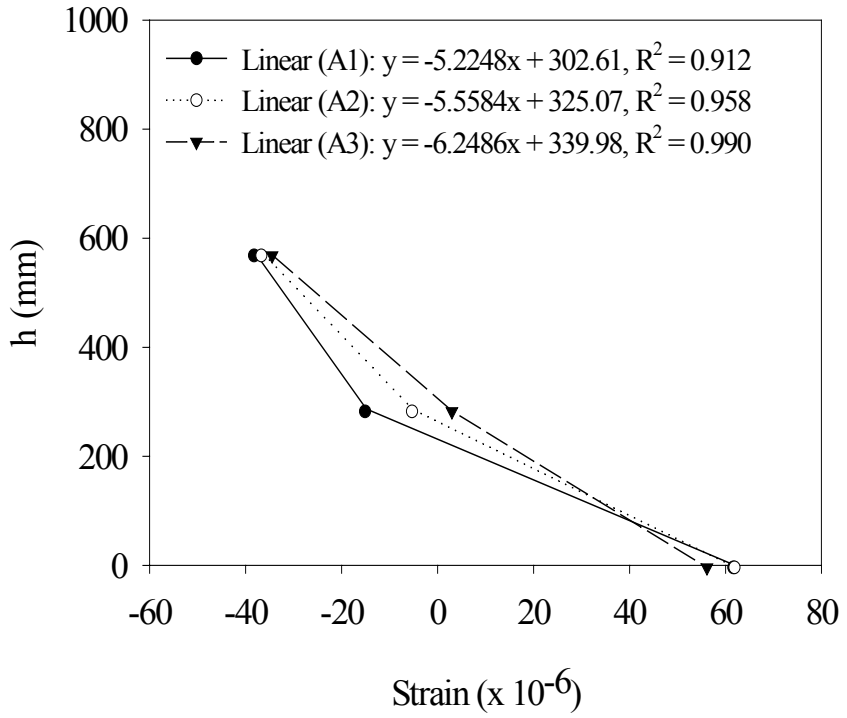

Figure E-23 Web Height (h) vs. Strain, Beam 3 (R), Test 2 (Position A)

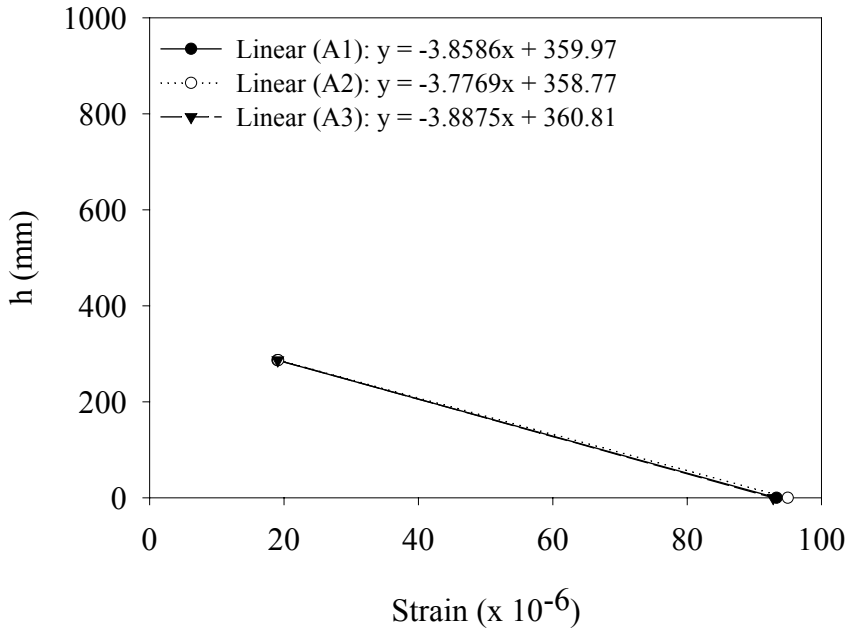

Figure E-24 Web Height (h) vs. Strain, Beam 4 (R), Test 2 (Position A)

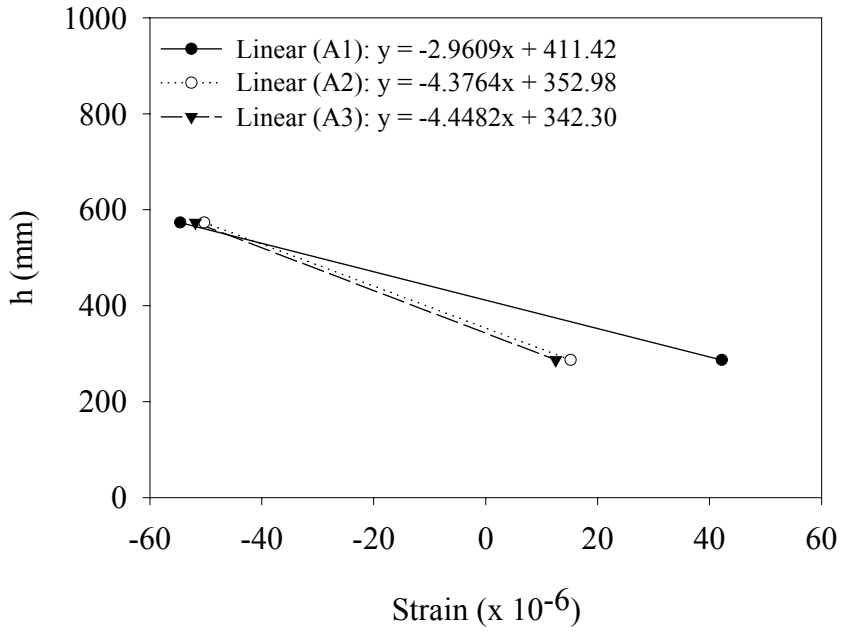

Figure E-25 Web Height (h) vs. Strain, Beam 5 (L), Test 2 (Position A)

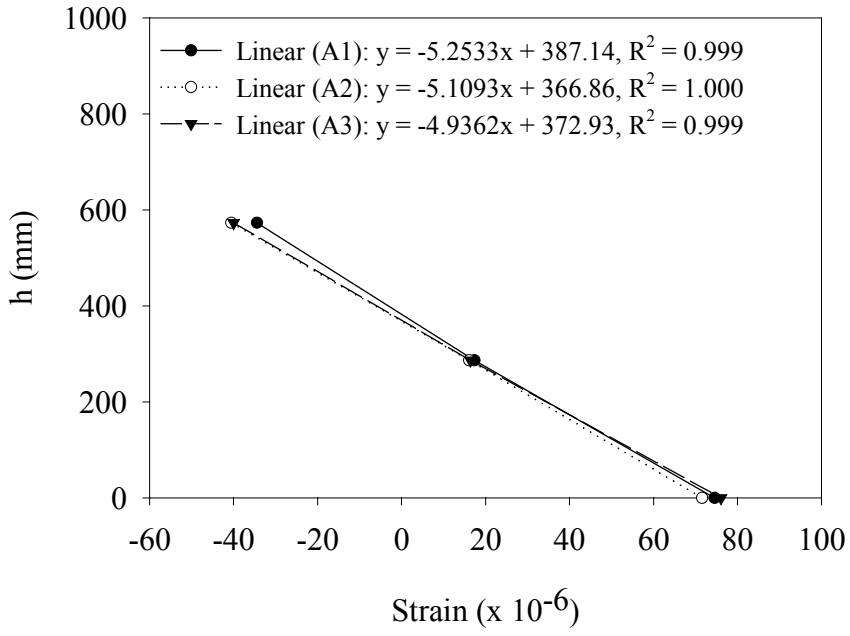

Figure E-26 Web Height (h) vs. Strain, Beam 5 (R), Test 2 (Position A)

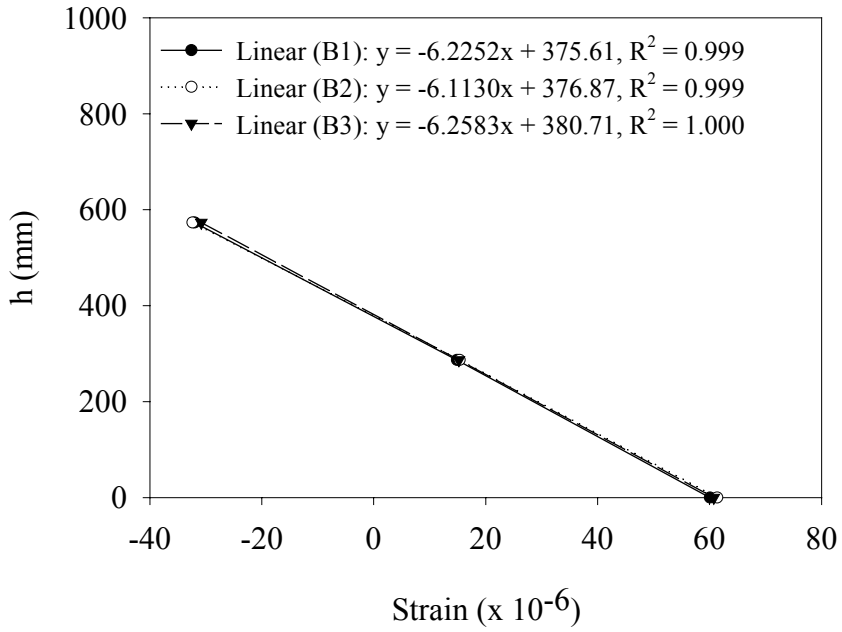

Figure E-27 Web Height (h) vs. Strain, Beam 2 (R), Test 2 (Position B)

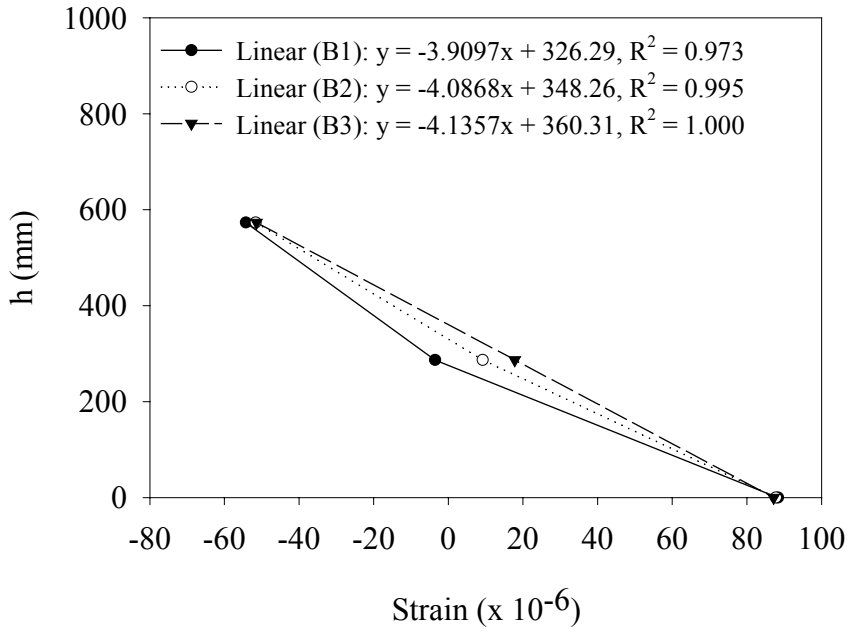

Figure E-28 Web Height (h) vs. Strain, Beam 3 (R), Test 2 (Position B)

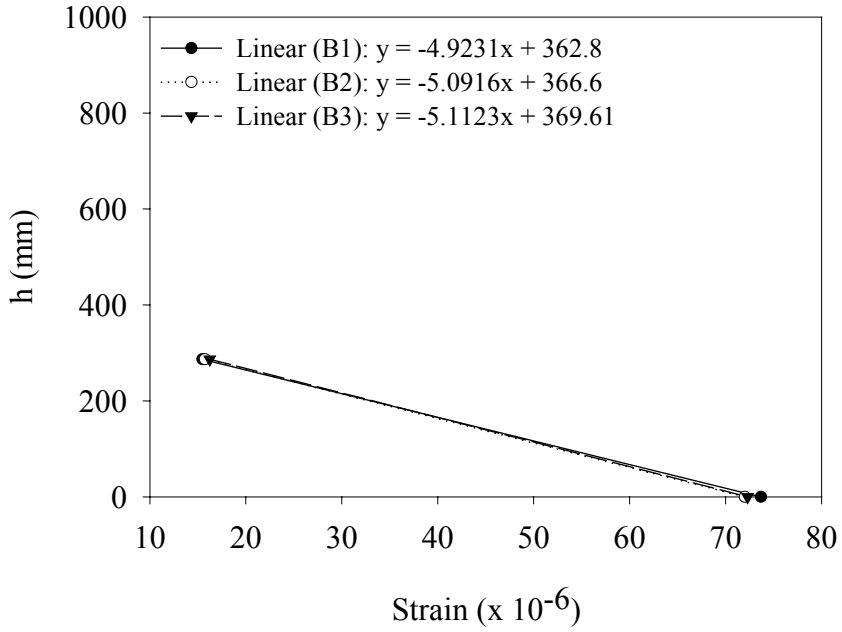

Figure E-29 Web Height (h) vs. Strain, Beam 4 (R), Test 2 (Position B)

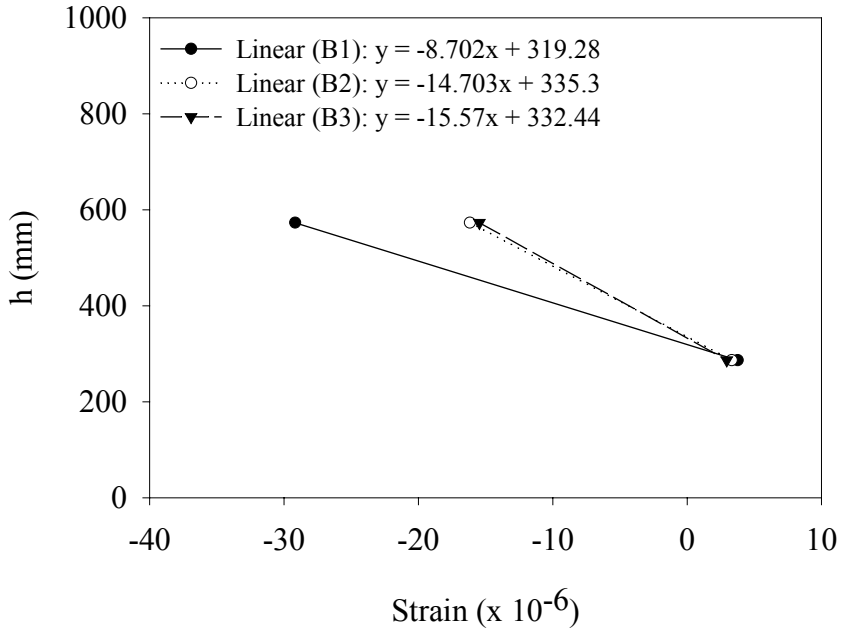

Figure E-30 Web Height (h) vs. Strain, Beam 5 (L), Test 2 (Position B)

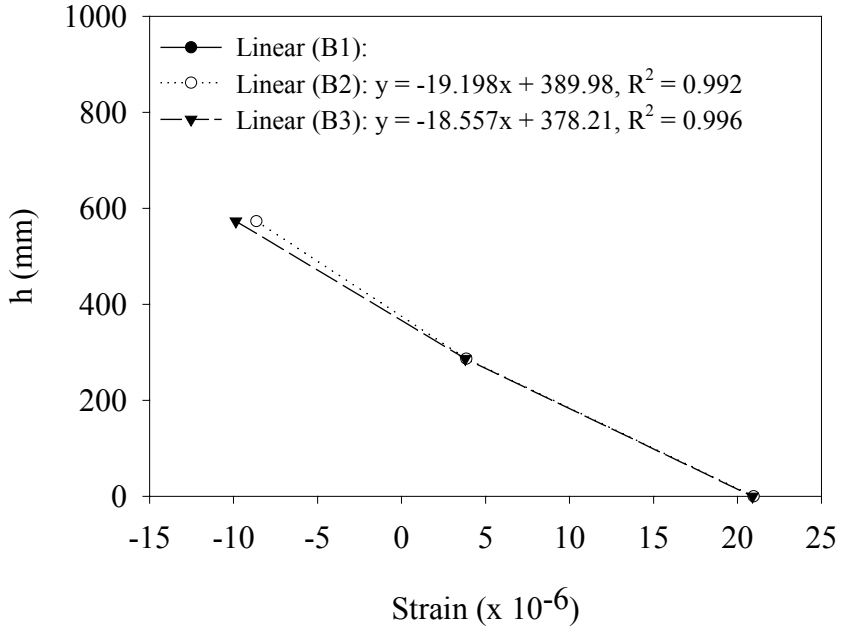

Figure E-31 Web Height (h) vs. Strain, Beam 5 (R), Test 2 (Position B)

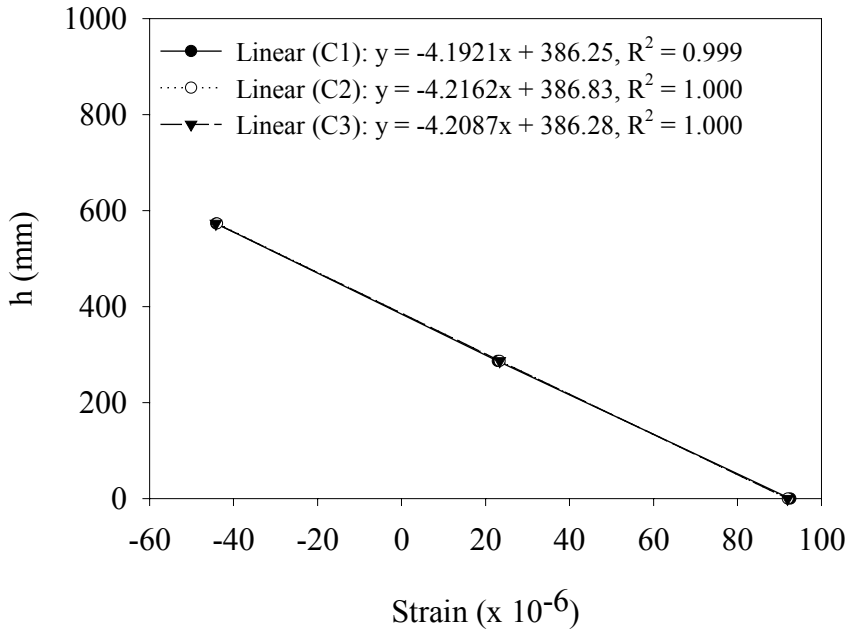

Figure E-32 Web Height (h) vs. Strain, Beam 2 (R), Test 2 (Position C)

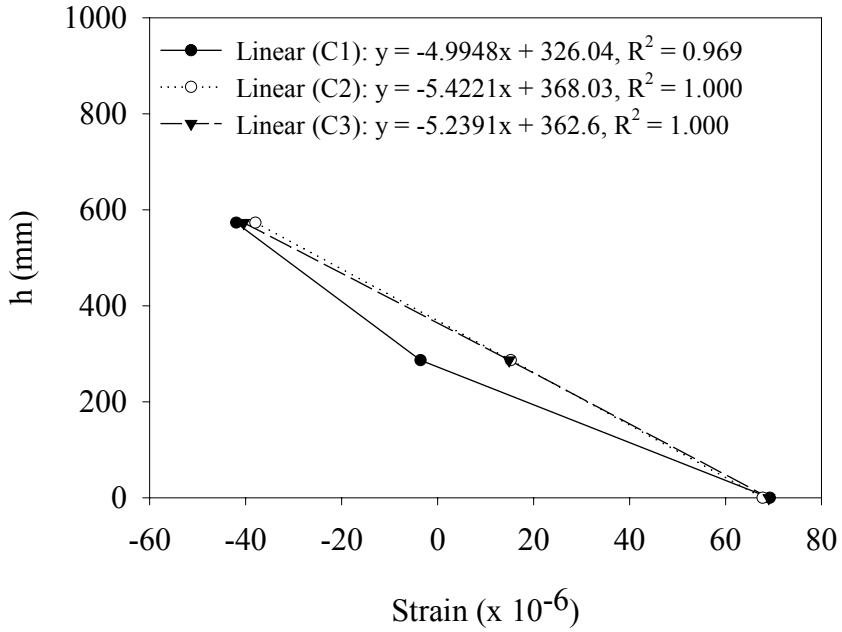

Figure E-33 Web Height (h) vs. Strain, Beam 3 (R), Test 2 (Position C)

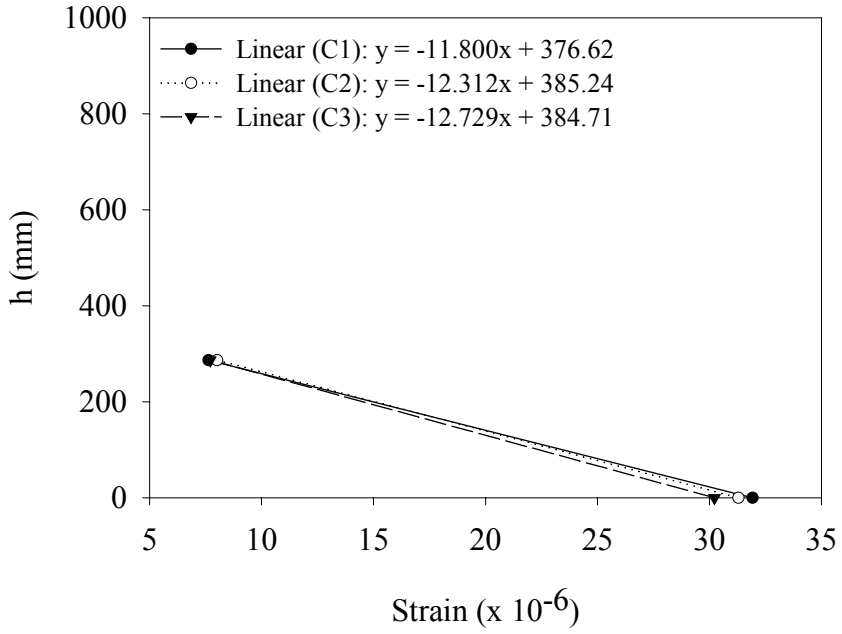

Figure E-34 Web Height (h) vs. Strain, Beam 4 (R), Test 2 (Position C)

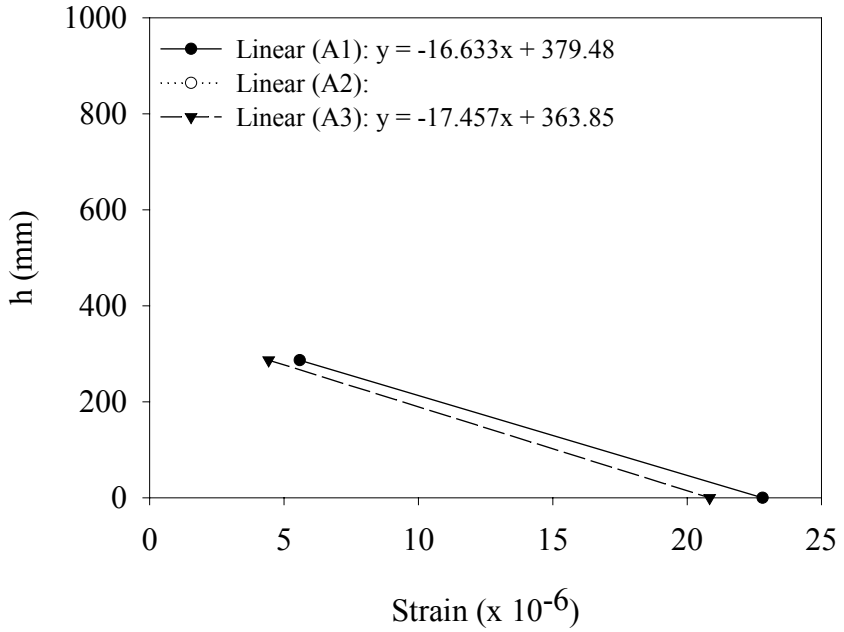

Figure E-35 Web Height (h) vs. Strain, Beam 2 (R), Test 3 (Position A)

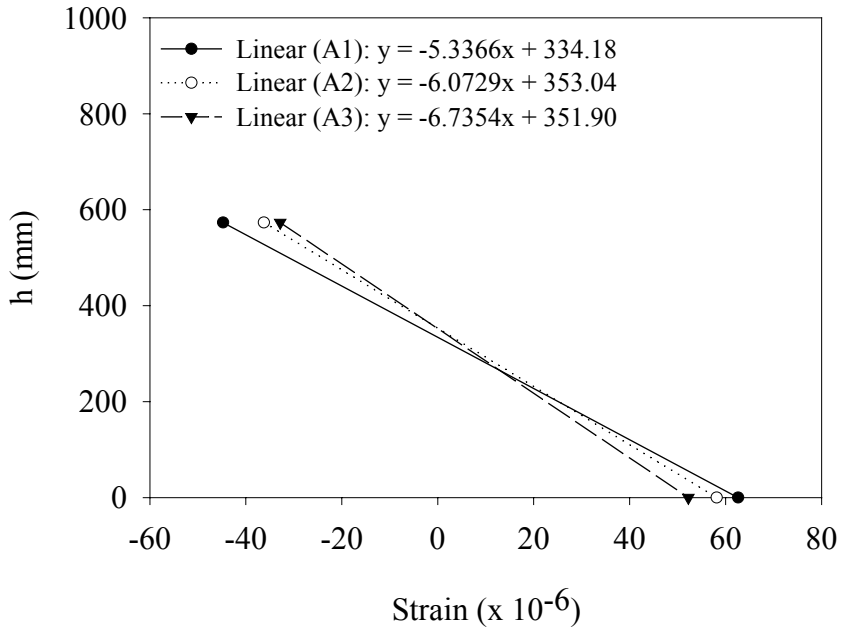

Figure E-36 Web Height (h) vs. Strain, Beam 3 (R), Test 3 (Position A)

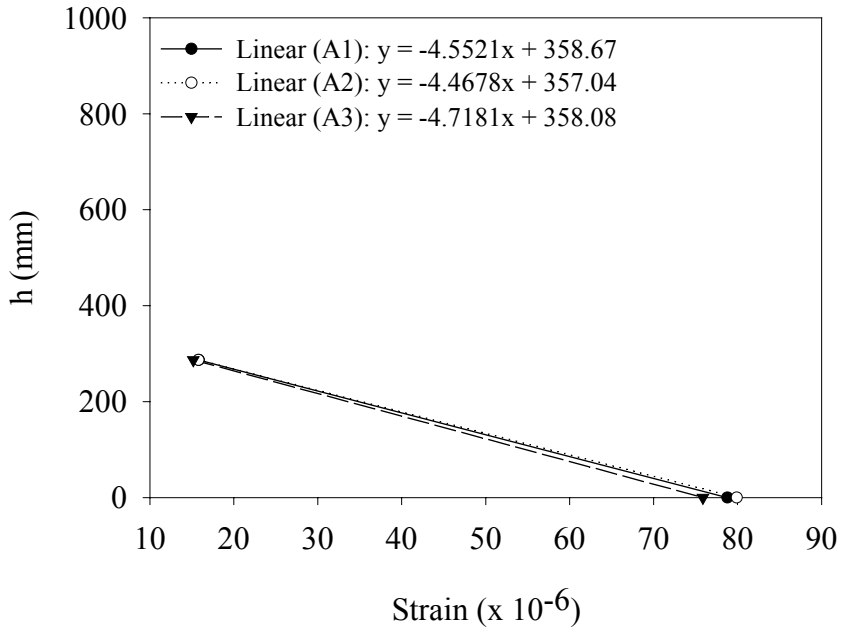

Figure E-37 Web Height (h) vs. Strain, Beam 4 (R), Test 3 (Position A)

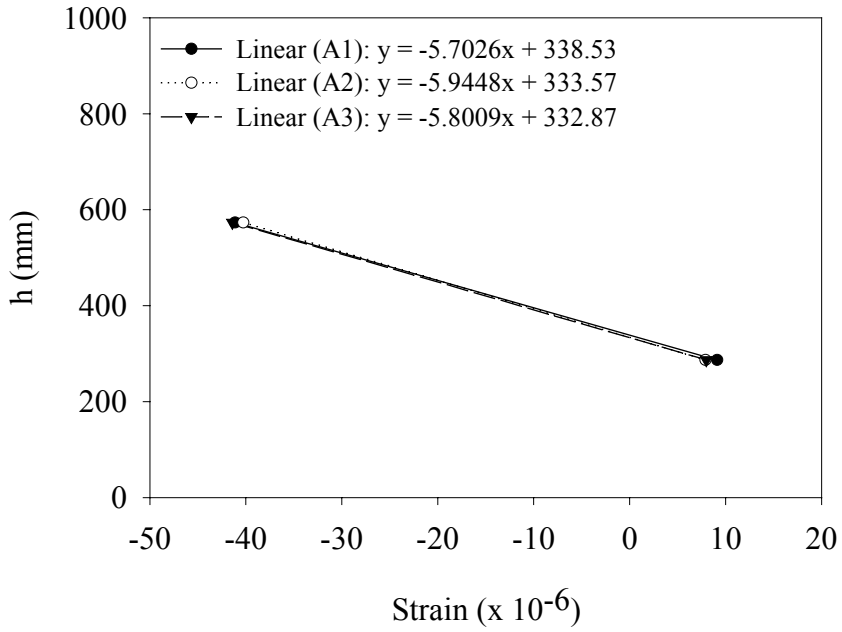

Figure E-38 Web Height (h) vs. Strain, Beam 5 (L), Test 3 (Position A)

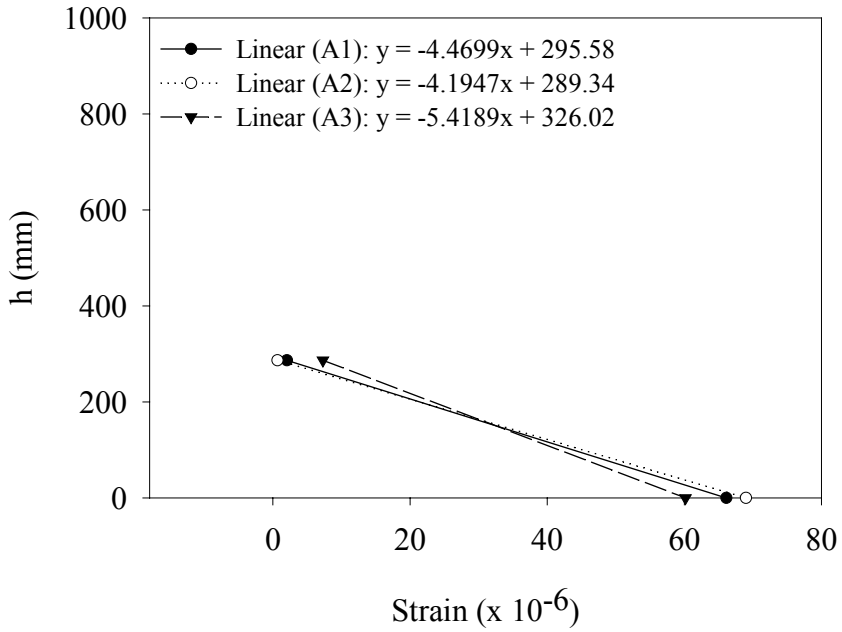

Figure E-39 Web Height (h) vs. Strain, Beam 5 (R), Test 3 (Position A)

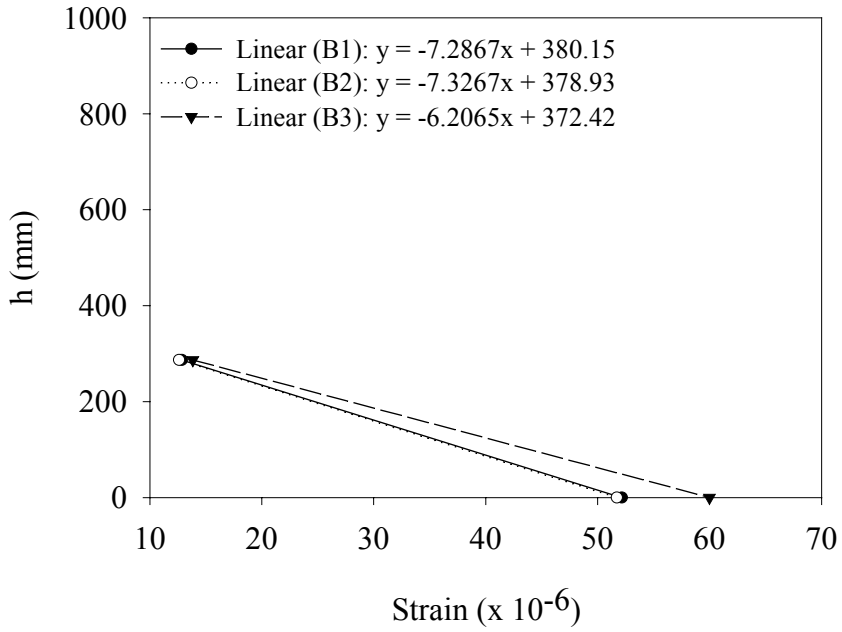

Figure E-40 Web Height (h) vs. Strain, Beam 2 (R), Test 3 (Position B)

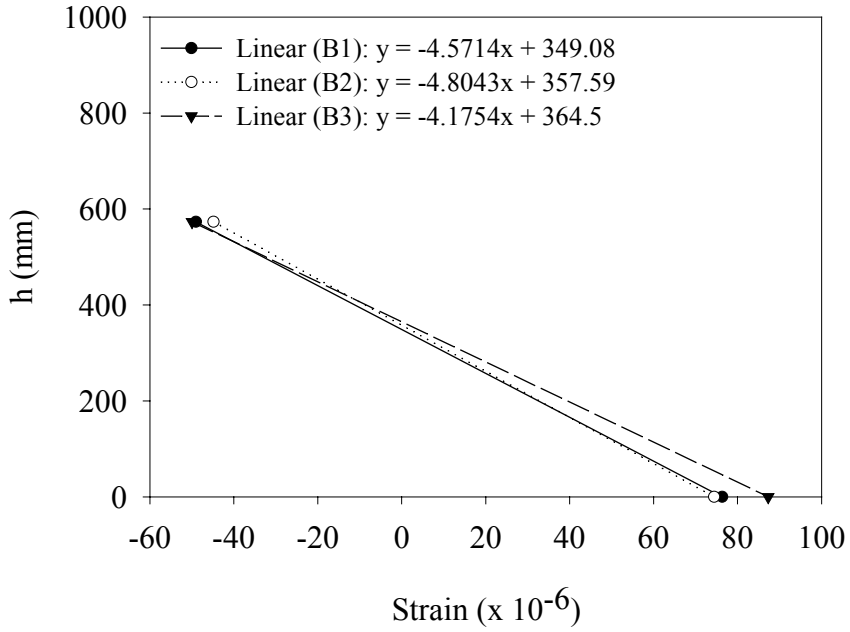

Figure E-41 Web Height (h) vs. Strain, Beam 3 (R), Test 3 (Position B)

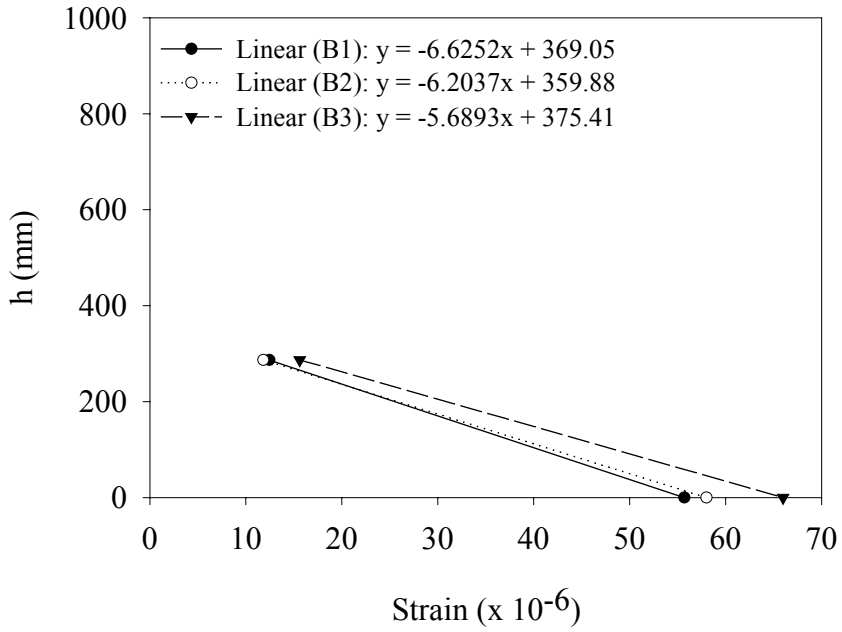

Figure E-42 Web Height (h) vs. Strain, Beam 4 (R), Test 3 (Position B)

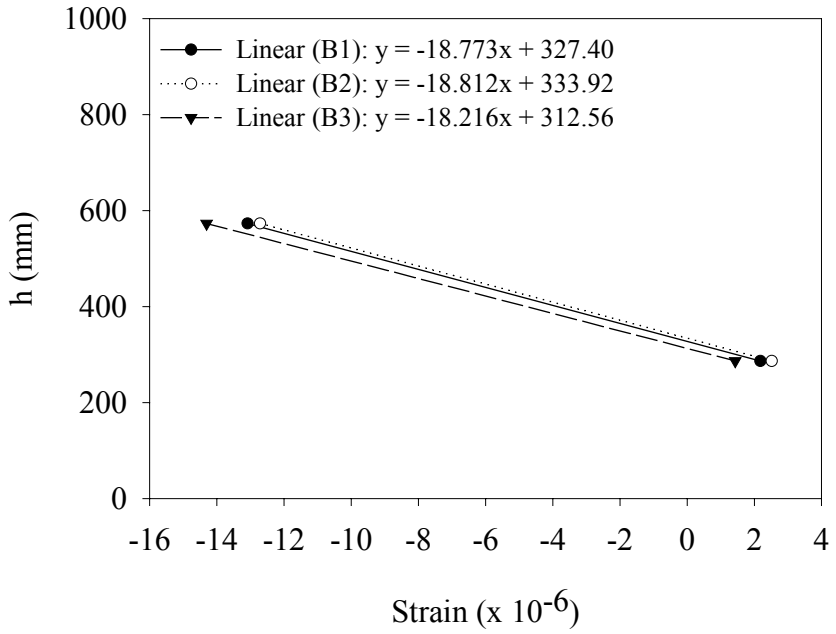

Figure E-43 Web Height (h) vs. Strain, Beam 5 (L), Test 3 (Position B)

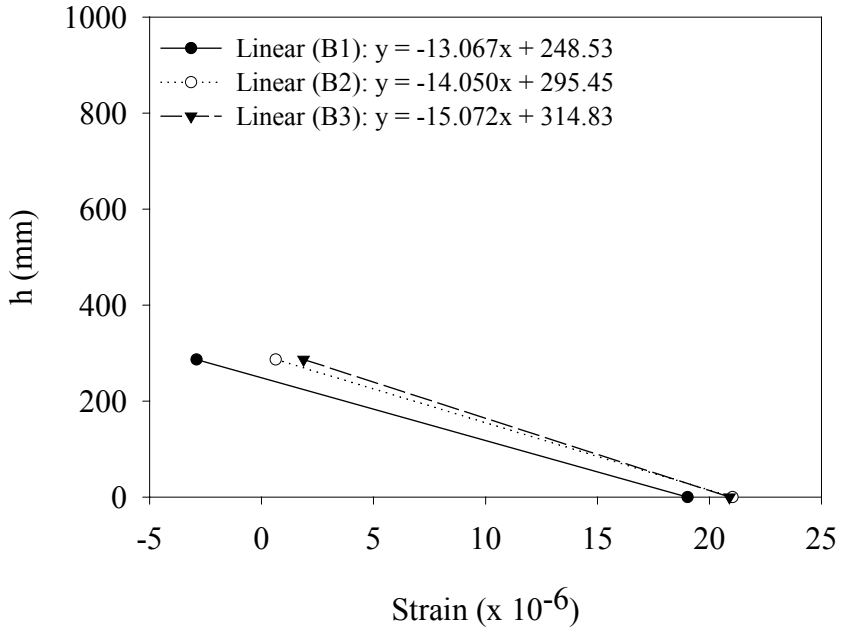

Figure E-44 Web Height (h) vs. Strain, Beam 5 (R), Test 3 (Position B)

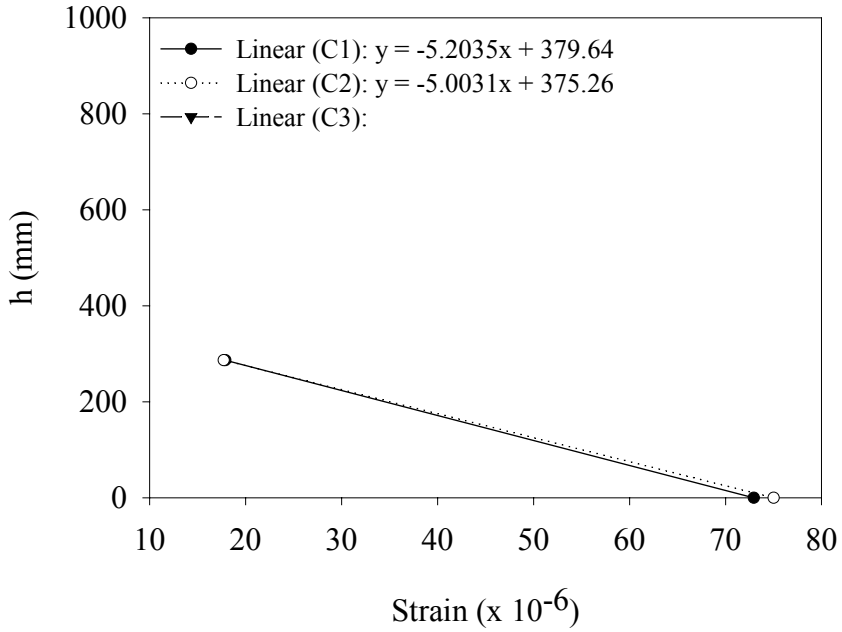

Figure E-45 Web Height (h) vs. Strain, Beam 2 (R), Test 3 (Position C)

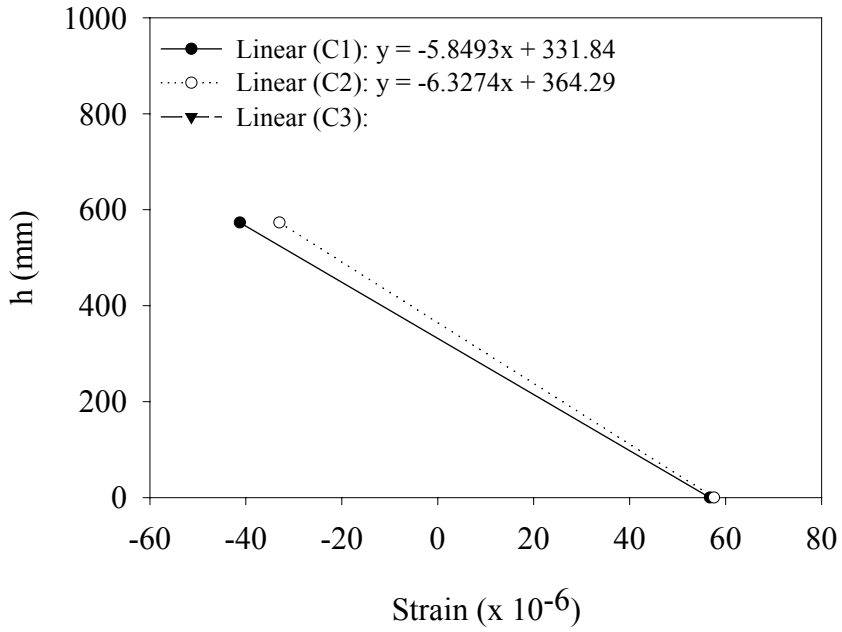

Figure E-46 Web Height (h) vs. Strain, Beam 3 (R), Test 3 (Position C)

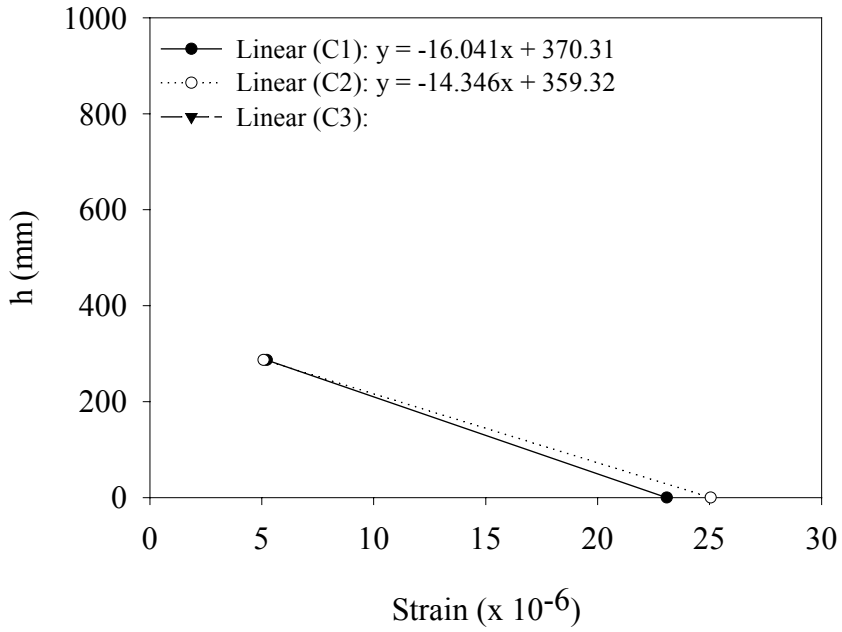

Figure E-47 Web Height (h) vs. Strain, Beam 4 (R), Test 3 (Position C)

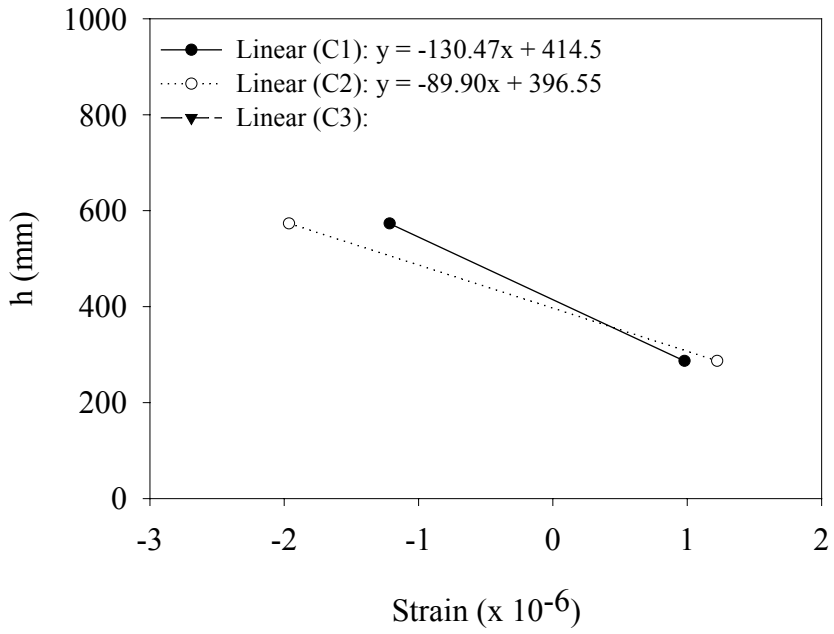

Figure E-48 Web Height (h) vs. Strain, Beam 5 (L), Test 3 (Position C)

BIBLIOGRAPHY

BIBLIOGRAPHY

1. Ahmadi, A. (1996) "Full Scale Test of Half Depth Grid on Upper Buckeye Bridge to Determine Effective Flange Width, Live Load Distribution, and Grid Deck Stresses," *Bridge Grid Flooring Manufacturers Report,* Pittsburgh, Pennsylvania.

2. ASCE (1979) *Structural Design of Tall Steel Buildings*, American Society of Civil Engineering, New York, New York.

3. Jayas, B.S., Hosain, M.U. (1987) "Composite Beams with Perpendicular Ribbed Metal Deck," *Proceedings of Composite Construction in Steel and Concrete*, American Society of Civil Engineers, New York, New York.

4. Keelor, D.C. (2002) "Design, Construction and Deployment of a Compact, Robust Field Data Acquisition System for Structural Field Monitoring," *MS Thesis,* University of Pittsburgh, Pittsburgh, Pennsylvania.

5. Moon II, F.L., Eckel II, D.A., Gillespie Jr., J.W. (2002) "Shear Stud Connection for the Development of Composite Action Between Steel Girders and Fiber-Reinforced Polymer Bridge Decks," *Journal of Structural Engineering,* Vol. 128, No. 6, American Society of Civil Engineers, Reston Virginia, pp. 762-770.

6. Ollgaard, Slutter, R.G., Fisher, J.W. (1971) "Shear Strength of Stud Connectors in Lightweight and Normal-weight Concrete," *Engineering Journal*, American Institute of Steel Construction, Chicago, Illinois, pp. 55-64.

7. Turner, K., Harries, K.A. (2002) "Tests of Shear Stud Connections Between GFRP Bridge Decks and Steel Girders" Draft Final Report, *Report No. ST02-03-LD*, Department of Civil and Environmental Engineering, University of South Carolina, Columbia, South Carolina.

8. AASHTO (1998), AASHTO, LRFD Bridge Design Specifications, Second Edition, Washington, D.C.

9. Manual of Steel Construction, Load & Resistance Factor Design, Structural Members, Specifications, & Codes", Vol.I, Second Edition, AISC.

10. Charles G. Salmon, John E. Johnson (1996) "Steel Structures, Design and Behavior, Emphasizing Load and Resistance Factor Design", Fourth Edition.

11. Jeffrey Robert, Chung C. Fu, Hamed Alayed (2002) “Deck Replacement for the Skewed Truss Bridge on MD 24 Over Deer Creek in Harford County, Maryland utilizing a Fiber-Reinforced Polymer (FRP) Bridge Deck”, IBC-02-56.

12. Benjamin Tang (1997) “Fiber Reinforced Polymer Composites Applications in USA”, *the First Korea/U.S.A. Road Workshop Proceedings.*

13. Antonio Nanni (1999) “Composites: Coming on Strong”, Concrete Construction, vol.44, p.120.

14. Bridge Diagnostics, Inc. (2002) “Load Test and Rating Report Fairground Road Bridge, Greene County, Ohio”, The National Composite Center, OH.